Universidade do Minho
Escola de Ciências

Pedro Miguel Gomes Ribeiro

Disclosing the catalytic mechanism of Xanthine Oxidase by computational means

outubro de 2017

Disclosing the catalytic mechanism of Xanthine Oxidase by computational means
Pedro Miguel Gomes Ribeiro
UMinho | 2017

Universidade do Minho
Escola de Ciências

Pedro Miguel Gomes Ribeiro

Disclosing the catalytic mechanism of Xanthine Oxidase by computational means

Dissertação de Mestrado
Mestrado em Bioquímica Aplicada
Ramo de Biotecnologia

Trabalho realizado sob orientação do
Doutor Professor Nuno M. F. S. A. Cerqueira

outubro de 2017

Declaração

Nome: Pedro Miguel Gomes Ribeiro

Endereço eletrónico: pmiguelgribeiro@gmail.com

Número do cartão de cidadão: 14419285 3 ZW6

Título da dissertação: Disclosing the catalytic mechanism of Xanthine Oxidase by computational means

Orientadores: Doutor Professor Nuno M. F. S. A. Cerqueira

Ano de Conclusão: 2017

Designação do Mestrado: Mestrado em Bioquímica Aplicada – ramo de Biotecnologia

É AUTORIZADA A REPRODUÇÃO INTEGRAL DESTA DISSERTAÇÃO APENAS PARA EFEITOS DE INVESTIGAÇÃO, MEDIANTE DECLARAÇÃO ESCRITA DO INTERESSADO, QUE A TAL SE COMPROMETE

Universidade do Minho, __ de _____ de 2017

*Assinatura:*_____

Esta dissertação foi realizada no UCIBIO-REQUINTE, no grupo de Química e Bioquímica Teórica e Computacional do Departamento do Química e Bioquímica da Faculdade de Ciências da Universidade do Porto, sob a orientação do investigador Nuno Manuel Ferreira de Sousa de Azevedo Cerqueira.

Este projeto teve ainda o apoio financeiro da Fundação para a Ciência e Tecnologia (FCT), através do projeto IF/01310/2013, e dos fundos nacionais e cofinanciamento da FEDER, sob o acordo de parceria PT2020.

Universidade do Minho
Escola de Ciências

U.PORTO
FACULDADE DE CIÊNCIAS
UNIVERSIDADE DO PORTO

INSTITUTO DE CIÊNCIAS BIOMÉDICAS ABEL SALAZAR
UNIVERSIDADE DO PORTO

UCIBIO
@ REQUIMTE

requimte
rede de química e tecnologia

FCT
Fundação para a Ciência e a Tecnologia
MINISTÉRIO DA CIÊNCIA, TECNOLOGIA E ENSINO SUPERIOR

This page was intentionally left blank

Agradecimentos

Esta tese assinala mais um fim de uma etapa do meu percurso académico, e não seria a mesma coisa sem as pessoas que me ajudaram ao longo dos últimos anos.

Em primeiro quero agradecer ao Professor Doutor Nuno Cerqueira, pela oportunidade que me deu em integrar este projeto e a sua confiança que depositou em mim para o realizar. Obrigado por toda a sua simpatia, palavras de apoio, incentivo e ensinamentos, que ao longo deste ano ajudaram a desenvolver como pessoa, a desenvolver o meu olhar crítico e ganhar novas capacidades para o meu futuro.

À Professora Doutora Maria João Ramos, agradeço a possibilidade de me acolher neste excelente grupo de investigação.

Aos elementos do grupo de Química Teórica e Bioquímica Computacional, pela forma amigável e acolhedora como me receberam e que contribuíram para o sucesso deste trabalho. Quero agradecer especialmente ao Henrique, que acompanhou o meu trabalho ao longo do ano, juntamente com o Professor Nuno, e me deu apoio sempre que necessário e ajudou a ultrapassar obstáculos.

Ao Zé Tó e ao Miguel pela amizade durante os diversos anos deste meu percurso, pelos momentos de distração, desde as noites de jogos de tabuleiro até às conversas idiotas e teorias da conspiração.

À Lara, à Daniela, à Laura, que apesar da distância durante o meu mestrado, sempre me ajudaram, se preocupavam comigo e que me ajudaram a crescer ao longo dos últimos anos, tornando-me uma pessoa cada vez melhor. Obrigado pela vossa amizade.

Uma espécie de agradecimento ao Fábio, pela preocupação que demonstra e pela ajuda nos últimos anos, pela sua espécie de amizade com algum ódio, e mais importante um agradecimento à sua prima por todos os momentos de comédia que proporcionou em diversas ocasiões.

Quero agradecer à Sara, ao Hugo, à Mafalda, à Christina, à Joana pela a amizade e pela companhia com que fui recebido neste mestrado e por toda a ajuda que me deram nestes anos.

Ao Rui, ao Areal, ao Brandão e ao Vidal, pela amizade que demonstraram ao longo dos anos e pelos momentos de ajuda e diversão.

À minha irmã, que ao longo da minha vida sempre se esforçou e me ajudou a que os meus sonhos se realizassem e em me tornar hoje no que sou. A ti dedico esta tese.

À minha família, em especial à minha mãe e ao Bruno, por desejarem o melhor para mim e apoiarem ao longo destes anos.

Abstract

Xanthine and uric acid are two important intermediates in the nucleotide degradation pathway. However, there are some diseases associated with it, being the most common the deposition of uric acid in joints, causing lots of pain. To solve these problems, some inhibitors already exist to reduce the enzymatic activity of Xanthine Oxidase. However, in order to develop new and more efficient inhibitors targeting this enzyme, it is necessary to gather a better understanding about its catalytic mechanism. In this thesis, theoretical and computational means are used to unravel all the steps that are required for the oxidation of hypoxanthine to uric acid. To this end, QM/MM methodologies were applied having as reference the X-ray structure with the pdb code: 3AMZ. The QM part was calculated using DFT (B3LYP) with the 6-31G(d) basis set, whereas the MM part was considered under MM approach using GAFF and ff99SB force fields amongst other parameters determined by us.

The new proposal for the catalytic mechanism of XO is composed by three main stages. The first one involves the coordination of xanthine to the Mo ion, the second one involves the release of uric acid and the third one the oxidation of the Moco, and subsequent enzymatic turnover.

The first part consists in a nucleophilic attack from xanthine to the molybdenum cofactor, followed by a hydrogen atom transfer. The first step is endoenergonic ($\Delta_r G_{step1}$ = 7.5 kcal mol^{-1}), whereas the hydrogen atom transfer is very exoenergetic ($\Delta_r G_{step2}$ = -18.3 kcal mol^{-1}), which turns the first stage of the mechanism an irreversible process.

The second part involves the protonation of a reaction intermediate from which results uric acid and its consequent release. Both steps are exoenergetics ($\Delta_r G_{step3}$ = -11.4 kcal mol^{-1} e $\Delta_r G_{step4}$ = -3.3 kcal mol^{-1}).

The third stage involves the oxidation of the Moco cofactor and the enzymatic turnover. This stage involves a rearrange of protons in the active site of the enzyme with the release of two electrons, followed by the water coordination to the molybdenum cofactor and, finally, the release of two-protons. The energy associated

with this step is endoenergetic ($\Delta_r G$ = 13.8 kcal mol^{-1}) and it is the limiting step of the reaction ($\Delta G^{\ddagger}$ = 14.2 kcal mol^{-1}), which is close to the experimental one ($\Delta G^{\ddagger}$ = 15.72 kcal mol^{-1}).

All the obtained results are consistent with the available experimental data that indicated that Glu802, Arg880 and Glu1261 play a key role in the reaction. This data can now be used to study other mechanism of the enzyme (for example the conversion of hypoxanthine in xanthine) and further be used to develop new drugs to treat uric acid related diseases. Additionally, the importance of computational means was consolidated one again, becoming a stronger approach to test and validate experimental data, as well as to provide new insights and new mechanistic proposals that were still not tested yet.

Keywords

Xanthine Oxidase (XO), xanthine (XAN), uric acid (URC), catalytic mechanism, quantum mechanics, hybrid QM/MM methodologies, ONIOM, density functional theory (DFT), enzymatic catalysis

Resumo

Xantina e ácido úrico são dois intermediários importantes na via catabólica de nucleótidos. No entanto, existem algumas doenças associadas a estes compostos, sendo uma das mais comuns a deposição de ácido úrico nas articulações. Para resolver estes problemas, foram desenvolvidos alguns inibidores que inibem a atividade enzimática da Xantina Oxidase. No entanto, este campo ainda requer muitos avanço científicos dado que o mecanismo catalítico desta enzima ainda é pouco conhecido, o que limita o desenvolvimento de novos fármacos capazes de inibir esta enzima e tratar este tipo de doenças.

Neste trabalho foram utilizadas ferramentas computacionais para estudar o mecanismo catalítico da enzima xantina oxidase. Para este efeito foi construído um modelo da enzima baseado na estrutura cristalográfica com o código PDB 3AMZ. Este modelo foi depois submetido a cálculos teóricos e computacionais usando metodologias QM/MM. A parte QM foi calculada utilizando DFT (B3LYP) com a base de funções 6-31G(d), enquanto que, a parte MM foi calculada por métodos de MM utilizando GAFF e campos de força ff99SB entre outros parâmetros determinados por nós.

O mecanismo determinado é constituído por três fases distintas. A primeira fase envolve a coordenação da xantina ao ião de molibdénio. A segunda fase a formação do ácido úrico e a sua libertação para o solvente. A terceira fase consiste na oxidação do centro ativo e subsequente regeneração da enzima.

A primeira fase envolve dois passos sequenciais, onde ocorre a coordenação da xantina ao ião de molibdénio, e a passagem de um hidrogénio entro o cofactor e o intermediário da reação. O primeiro passo é endoenergónico ($\Delta_r G_{passo1}$ = 7.5 kcal mol^{-1}), enquanto que o segundo passo é muito exoenergónico ($\Delta_r G_{passo2}$ = -18.3 kcal mol^{-1}). O total dos dois passos torna esta primeira fase do mecanismo um processo irreversível.

A segunda fase do mecanismo consiste na formação do ácido úrico e consequente libertação para o solvente. Ambos os passos são exoenergónicos ($\Delta_r G_{passo3}$ = -11.4 kcal mol^{-1} e $\Delta_r G_{passo4}$ = -3.3 kcal mol^{-1}).

A terceira fase do mecanismo envolve a regeneração da enzima. Esta fase inicia-se com um rearranjo de protões no centro ativo do qual resulta a libertação de dois eletrões. De seguida ocorre a coordenação de uma molécula de água ao cofator de molibdénio e, finalmente, a libertação de dois protões. Esta reação é endoenergónica ($\Delta_r G$ = 13.8 kcal mol^{-1}) e a é o passo limitante da reação ($\Delta G^{\ddagger}$ = 14.2 kcal mol^{-1}), que é próximo do determinado experimentalmente ($\Delta G^{\ddagger}$ = 15.72 kcal mol^{-1}).

Todos os resultados obtidos neste trabalho são consistentes com as informações experimentais disponíveis, tanto da cinética, como das mutações, validando resultados relativos ao Glu802, a Arg880 e o Glu1261, ao qual era atribuído um papel importante no mecanismo enzimático. Estas informações podem agora der usadas para estudar outros mecanismos desta enzima (como por exemplo a conversão de hipoxantina a xantina) e também o desenvolvimento de novos fármacos para tratar doenças relacionadas com o ácido úrico. Adicionalmente, a importância da utilização de métodos computacionais em bioquímica foi validada novamente, tornando-se uma forte metodologia para testar e validar informações experimentais, bem como para propor novas teorias que ainda não tenham sido testadas.

Palavras-chave

Xantina Oxidase (XO), xantina (XAN), ácido úrico (URC), mecanismo catalítico, mecânica quântica, métodos híbridos QM/MM, ONIOM, Teoria da Densidade Funcional (DFT), catálise enzimática

Preamble

This dissertation is composed of four major chapters:

A. Introduction

A brief description of Xanthine Oxidase and its general information is presented. In this chapter, it will be described the structure of the enzyme, the available data about mutagenic studies, the biological relevance, diseases, inhibitors and some of the catalytic mechanism theories to date.

B. Theoretical Background

A summarized review of the theoretical methods used during this project is described. Particularly the molecular mechanics, quantum mechanics and the hybrid methodologies.

C. Results and Discussion

The obtained results will be chronologically presented in this chapter. The beginning is about the construction of the QM/MM model and the molecular dynamic simulation. Then, the catalytic mechanism studies will be presented in three distinct parts, showing the obstacles and their resolution, in order to obtain the most accurate results as possible.

D. Conclusions and Future Perspectives

In this chapter, it will be presented the major conclusions about the results of this work, and possible contribution for the advances in the knowledge about Xanthine Oxidase are provided.

E. Bibliography

List of all bibliographic references used along this dissertation. Appearing in order that they are used along the text.

Table of Contents

AGRADECIMENTOS III

ABSTRACT V

RESUMO VII

PREAMBLE IX

TABLE OF CONTENTS XI

LIST OF ABBREVIATIONS XV

I. INTRODUCTION 1

1 Degradation of Purine Nucleotides 3

2 Xanthine Oxidase 4

3 XO's biological role 6

3.1 Diseases related to XO 7

3.1.1 Liver damage 7

3.1.2 Gout and uric acid stone 7

3.1.3 Xanthinuria 7

3.2 Inhibitors 7

3.2.1 Alloputinol 7

3.2.2 6-mercaptopurine 8

3.2.3 Phytic Acid 8

4 Catalytic mechanism 8

4.1 Mutagenic experiments 8

5 Mechanistic studies 9

5.1 Yamaguchi Y. proposal (2007) 9

5.2 Metz and Thiel proposal (2009) 11

II. THEORETICAL BACKGROUND 13

1 Computational Chemistry 15

2 Molecular Mechanics Methods 15

3 Quantum Mechanics Methods 17

3.1 Basis sets 18

4 Hybrid Methods 18

4.1 Hybrid methodologies 19

4.2 ONIOM 19

4.3 Boundary methods 20

4.4 Link atoms approach 21

4.5 Communication between layers 21

4.6 Mechanical embedding 21

4.7 Electrostatic embedding 22

5 In this work 22

III. RESULTS AND DISCUSSION 23

1 Introduction 25

2 Choosing the starting structure. 25

3 Molecular Dynamics (MD) 28

3.1 Parametrization 28

3.2 Protonation state of the residues of the protein 31

3.3 Solvation Stage 31

3.4 Minimization Stage 31

3.5 Equilibration and Production stages 32

4 Analysis of the MD results. 32

4.1 Analysis of the RMSD results. 33

4.2 Analysis of the RDF results 34

5 QM/MM studies 36

5.1 The QM/MM Model 36

5.2 Mechanistic studies 38

5.2.1 Part I – Coordination of substrate to Moco 39

5.2.1.1 Step 1: Nucleophilic attack of XAN to Moco 40
5.2.1.2 Step 2: Hydrogen atom transfer 43
5.2.1.3 Discussion 46
5.2.2 Part II – Protonation and product release 48
5.2.2.1 Step 3: Proton transfer 48
A. Pathway A (Neutral pathway) 49
B. Pathway B (Charged Pathway) 51
C. Pathway C (Semi-Charged pathway) 53
D. Interconversion between Pathway A, B and C 55
5.2.2.2 Step 4: Release of the product of the reaction (URC) 57
A. Pathway A (Neutral pathway) 57
B. Pathway B (Charged Pathway) 59
5.2.2.3 Discussion 61
5.2.3 Part III – Enzymatic Turnover 62
5.2.3.1 Step 5: Oxidation of the Moco 62
5.2.3.2 Step 6: Reaction of Moco with Water 63
A. Pathway A (neutral pathway) 63
B. Pathway B (charged pathway) 63
C. Alternative pathway to pathway B 65
D. Pathway A vs pathway B 66
5.2.3.3 Discussion 67

IV. CONCLUSIONS AND FUTURE PERSPECTIVES 69

1 New proposal for the catalytic mechanism of XO 71
1.1 Experimental data as support information 73
1.1.1 Experimental k_{cat} and irreversibility of the reaction 73
1.1.2 Mutations and the importance of residues 73
1.1.3 X-ray structure 74
1.1.4 Charge distribution 74
1.2 Comparison with previous QM/MM studies 75
2 Future perspectives 76

V. BIBLIOGRAPHY 77

This page was intentionally left blank

List of abbreviations

6-MP	6-mercaptopurine
AMBER	Assisted Model Building with Energy Refinement
AMP	Adenine monophosphate
B3LYP	Becke, three parameters, Lee-Yang-Parr functional
DFT	Density functional theory
FAD	Flavin adenine dinucleotide
FeS	[2Fe-2S] cluster
GAFF	General AMBER Force Field
GMP	Guanine monophosphate
HL	High level
HPA	Hypoxanthine
IM	Intermediate
IMP	Inosine monophosphate
LL	Low Level
MD	Molecular Dynamics
MM	Molecular Mechanics
Moco	Molybdenum cofactor
ONIOM	Our own N-layered integrated molecular orbital molecular mechanics
PDB	Protein Data Bank
QM	Quantum Mechanics
QM/MM	Hybrid method (Quantum Mechanics/Molecular Mechanics)

RDF	Radial distribution functions
RMSd	Root-Mean-Square deviation
RMSf	Root-Mean-Square fluctuations
TS	Transition state
URC	Uric acid
VDW	Van der Walls representation
VMD	Visual Molecular Dynamics software
XAN	Xanthine
XMP	Xanthosine monophosphate
XO	Xanthine Oxidase

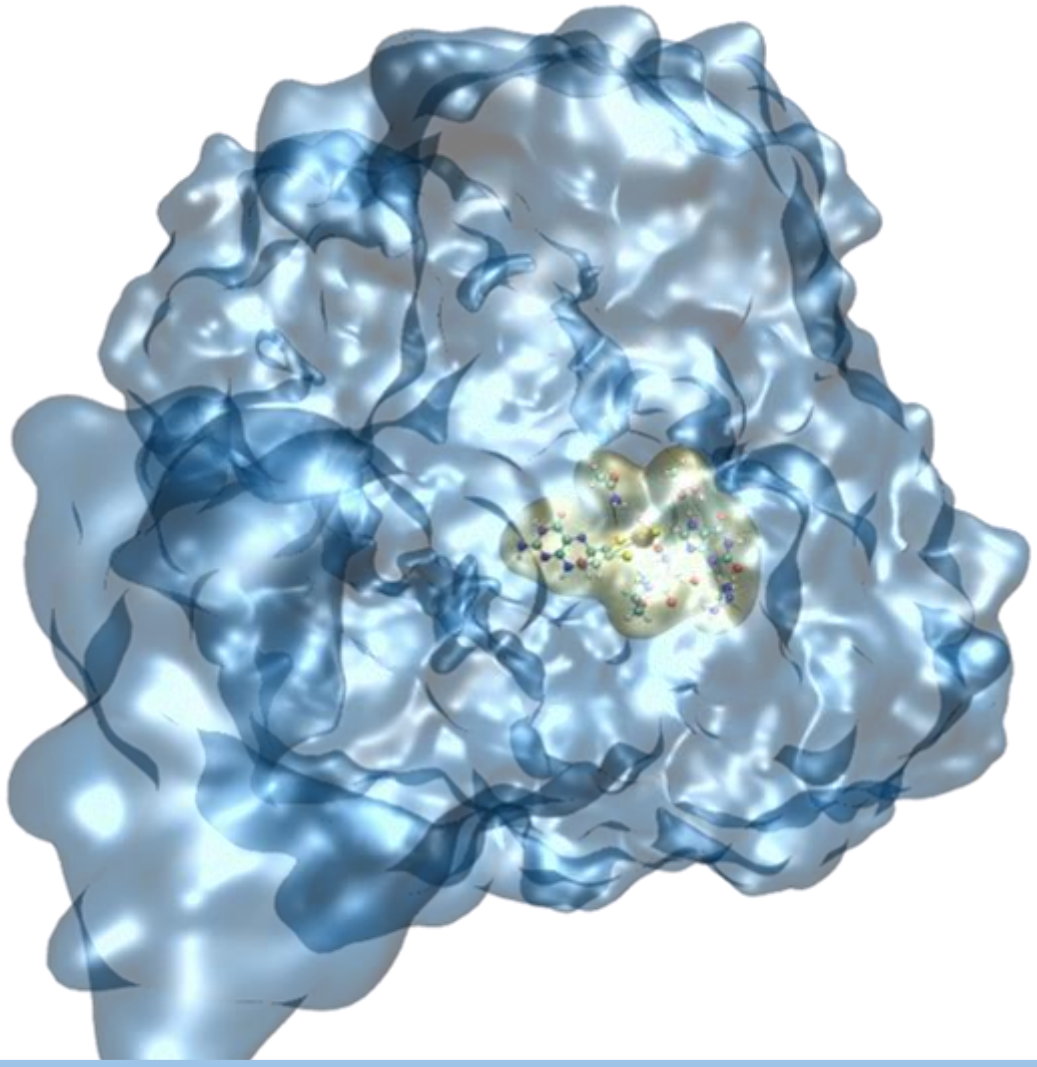

I. Introduction

This page was intentionally left blank

1 Degradation of Purine Nucleotides

Inside the cells, purine ribonucleotides are degradated by specific enzymes in a sequential pathway to ribonucleosides, purine bases, and finally to uric acid (Figure 1).

Adenine monophosphate (AMP), inosine monophosphate (IMP), xanthosine monophosphate (XMP) and guanine monophosphate (GMP) are the starting compounds in the purine degradation. The differences of these ribonucleotides are shown in orange in Figure 1.

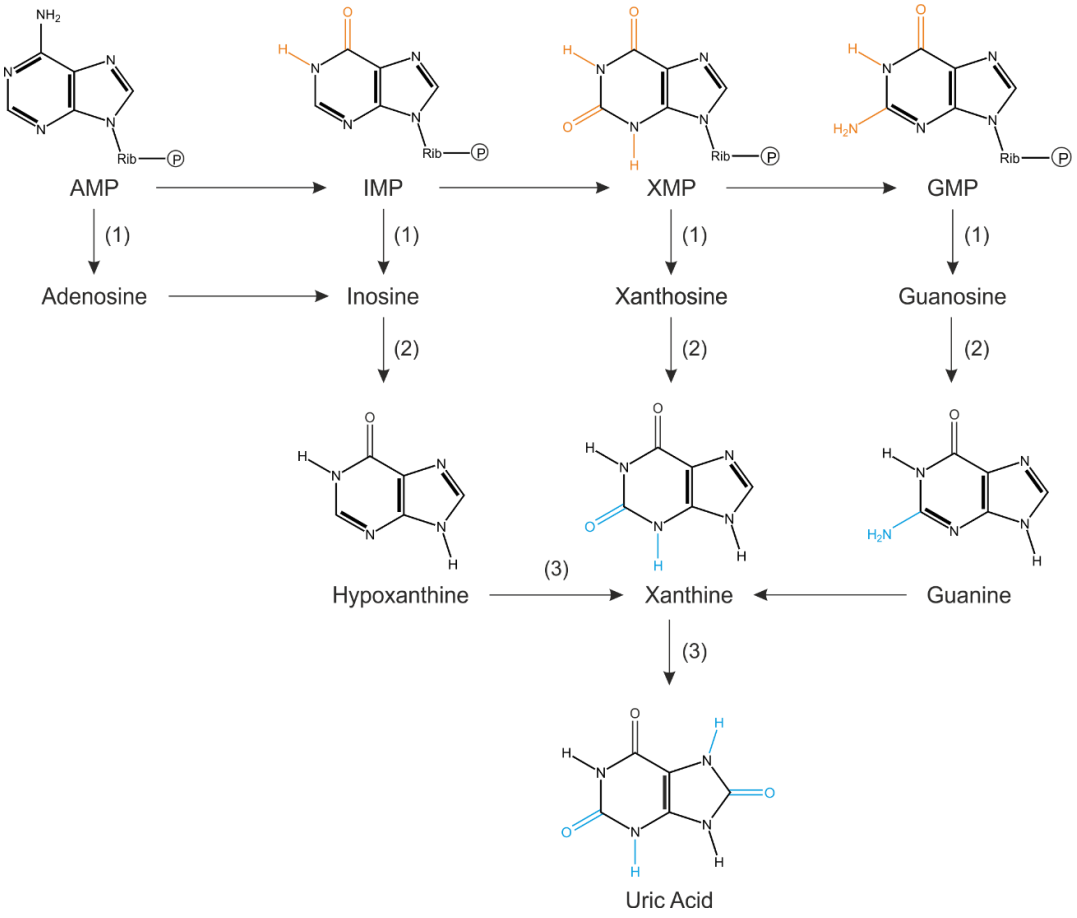

Figure 1 - Purine metabolism pathway.

The first step in this pathway involves the hydrolysis of purine ribonucleotides to ribonucleosides by 5'-nucleotidases (EC 3.1.3.5, 1). The resulting compounds are then converted to purine bases and α-D-ribose-1-phosphate by phosphorolysis catalyzed by

purine nucleoside phosphorylase (EC 2.4.2.1, 2), and one product of this reaction is hypoxanthine. The enzyme xanthine oxidase then catalyzes the conversion of hypoxanthine in xanthine, which is then converted to uric acid by the same enzyme [1].

The uric acid is a toxic compound in high concentrations to the cells. It is released from the cells to the bloodstream and it is excreted from the organism in the kidneys through the urine [2].

2 Xanthine Oxidase

The rate-limiting steps in the degradation of purine nucleotides are catalyzed by the enzyme Xanthine oxidase (XO, E.C. 1.17.3.2): the oxidation of hypoxanthine (HPA) to xanthine (XAN) and xanthine to uric acid (URC). In the course of these reaction are required two water molecules and two oxygen molecules and from which results the release of two molecules of hydrogen peroxide, as it is shown in Figure 2 [3]. It is mainly located in the liver and it is a homo dimer having 1333 residues per chain [4], [5]. XO is extracted from milk and easily purified [6], [7].

It has been estimated experimentally that XO has a reaction rate of 30 s^{-1} at pH8.5 and 25ºC for the conversion of hypoxanthine to xanthine and 18.3 s^{-1} for the conversion of xanthine and uric acid at pH8.5 and 25ºC [3].

Some recent reports also say that XO can take nitrate (NO_3^-) and convert it to nitrite (NO_2^-) and then to nitric oxide (NO•), being able to have an activity similar to nitrato reductase [8]–[12].

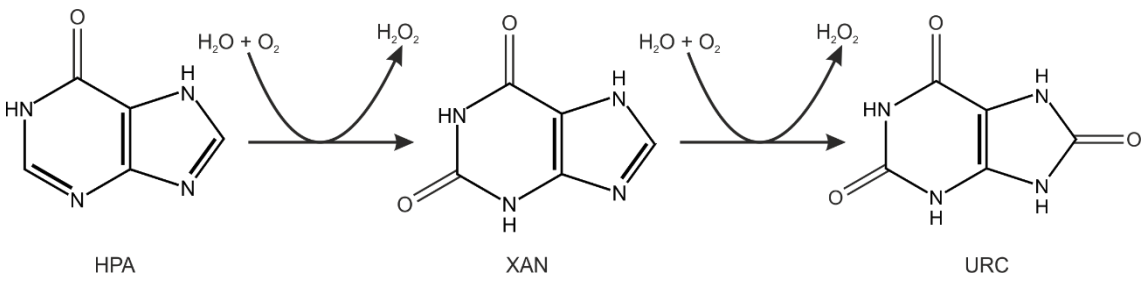

Figure 2 - Hypoxanthine to uric acid oxidation, carried out by XO

XO is mainly produced and located in the cytoplasm of the liver cells [13], [14]. The enzyme is a homodimer that enclosures three redox-active centers that are essential for its catalytic activity [4]. It has two [2Fe-2S] clusters, a flavin adenine dinucleotide (FAD) and a molybdopterin co-factor (Moco) per subunit of the homo-dimer. The Moco is a three-ring structure composed of a pteridine nucleus fused to a pyran ring and attached to the molybdenum through a dithiolene linkage. Eukaryotic enzymes typically contain the molybdopterin cofactor as shown in Figure 3, whereas those from prokaryotic sources contain a dinucleotide of guanine, cytosine, adenine, or hypoxanthine [15]. The Moco is located in the active site of the enzyme and it is directly involved in the catalytic process [3]. The [2Fe-2S] clusters are involved in the electron-transfer pathway that is required to oxidize the Moco cofactor to a FAD molecule during the catalytic process [16], [17] (Figure 3).

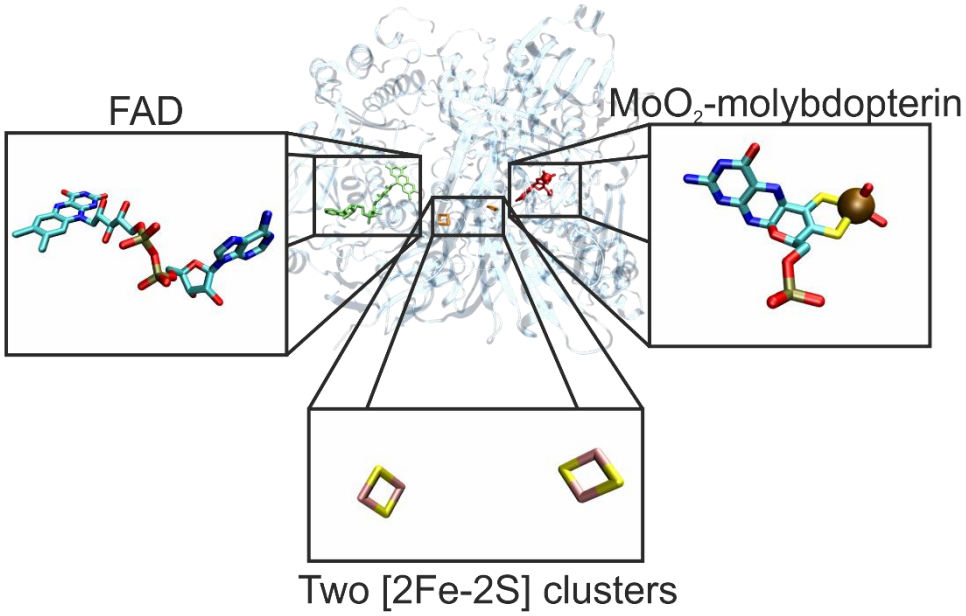

Figure 3 - Representation and location of the cofactors present in each monomer of XO.

In Figure 4 is represented the active site of XO from two different X-ray structures (pdb codes 3NRZ and 3AMZ, respectively), containing the hypoxanthine and xanthine substrates. In the PDB 3AMZ, xanthine is directly bonded to the Mo ion from the Moco, possible intermediate, whereas in the other PDB 3NRZ, hypoxanthine is

flipped vertically in relation to xanthine and it is 2.8Å away from the Mo ion. In both PDBs it is clear that there are several amino acids that stabilized the positions of the substrates in the active site, namely Gln767, Glu802, Glu1261 and Arg880. In addition, there is a conserved water molecule that is forming hydrogen bound with Glu1261 and Arg880 and it is very close to both substrates.

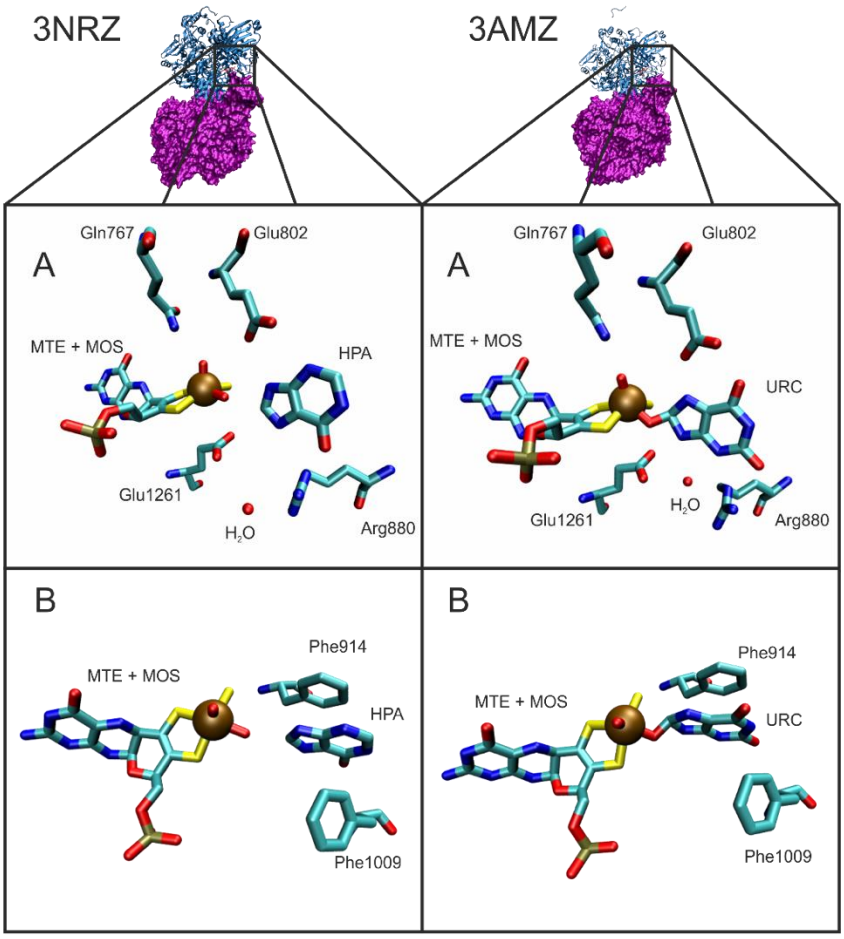

Figure 4 - Representation of XO's amino acid and cofactors in the active center

3 XO's biological role

Since XO is involved in one of the main metabolic pathways in Humans, converting hypoxanthine into xanthine and then to uric acid, it has several diseases associated with it [18]–[20].

3.1 Diseases related to XO

3.1.1 Liver damage

Liver damage can be determined by analyzing the blood for high levels of XO, since most of protein is stocked in the liver and released upon damage [5], [21].

3.1.2 Gout and uric acid stone

Gout is the caused by high levels of uric acid (hyperuricemia), which causes it to precipitate in joints, skin, capillaries and other tissues, forming needle-like crystals and causing pain. Kidney stones also can be formed by formation and deposition of sodium urate crystals [22]–[27].

3.1.3 Xanthinuria

It is a rare genetic disorder where there is a low formation or absence of XO, which leads to high levels of xanthine in blood, causing health problems like renal failure. There are two types for this disease, the type I is caused by mutations in XO gene compromising its activity [28], [29]. The xanthinuria type II is caused by a mechanism failure which inserts the molybdenum cofactor in the enzyme's active center.

3.2 Inhibitors

Several inhibitors targeting XO were developed for the treatment some of the diseases that were described before. Here we provide some examples

3.2.1 Alloputinol

It is the most common inhibitor used in cases of hyperuricemia, it is used to treat gout and formation of some types of kidney stones, also is used to revert some effects of chemotherapy that causes high levels of uric acid. The inhibition occurs since it is an isomer of hypoxanthine (Figure 5) [30], [31].

3.2.2 6-mercaptopurine

Also known as 6-MP, is normally used to treat diverse type of cancers and autoimmune diseases. It is also a hypoxanthine homologue inhibiting XO (Figure 5).

3.2.3 Phytic Acid

Phytic acid is compounds that have been reported to inhibit XO. It is found in abundancy of plants, edible legumes, cereals and oil seeds [32].

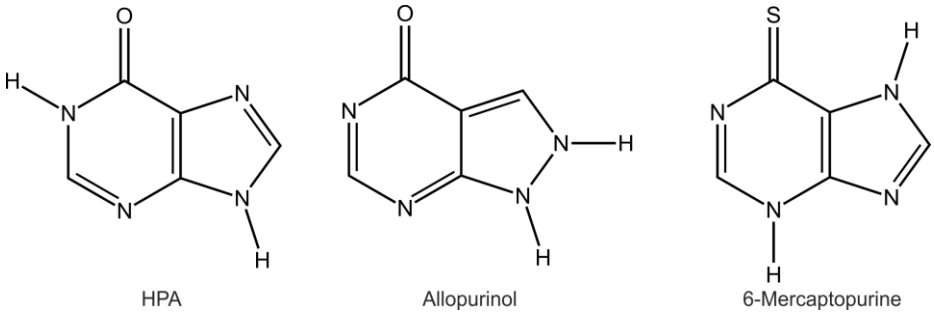

Figure 5 - 2D Structure of HPA compared to two XO inhibitors

4 Catalytic mechanism

Taking into account the importance of XO in the degradation of purines nucleotides and its relation with several diseases, several studies were performed to unravel the catalytic mechanism of this enzyme.

4.1 Mutagenic experiments

During the last 2 decades, several mutations on the active site of XO were conducted aiming to reveal which amino acids residues were more important for the catalytic process.

Choi was one of the first to study XO mechanism using a *R. capsulatus* recombinant. A mutation in Glu1261 for a valine, turned the enzyme completely

inactive. The mutation of Glu802 by a valine show a 100-fold dissociation constant, meaning that this residue has an important role in binding the substrate [33].

Mutation of Glu803 by a valine did not show any activity for hypoxanthine but shown a lower activity for xanthine of 1.4 s^{-1}. In opposite, changing the Arg881 for a methionine, it shown that XO was inactive for xanthine and presented a lower activity for hypoxanthine, about 0.3 s^{-1}. Looking to these results, it is possible to say that Glu803 may be directly involved in the oxidation of hypoxanthine to xanthine and that Arg881 may be involved in turning xanthine in uric acid [3].

5 Mechanistic studies

There are some theories and some testes around XO's mechanism, but there's no consensus in how the mechanism works. One theoretical mechanism was presented by Yamaguchi and colleagues, based on the kinetic data from mutations and observing X-ray structures. While QM and QM/MM approach was carried out by Metz and Thiel. Both of these theories are exposed below.

5.1 Yamaguchi Y. proposal (2007)

Based on the experimental evidences obtained by y Yamaguchi Y. and colleagues in 2007, they predicted that prior to the nucleophilic attack of the substrate to the Mo ion, occurs an activation process involving the proton transfer from the hydroxyl group bonded to the Mo ion to Glu1262 [3].

In this process, it was also proposed that Glu803 would play an active role in guiding and endorse the correct orientation of the substrate in the active site of the enzyme. Once the substrate becomes covalently bonded to the Mo ion, the hydride transfer between the substrate and the sulfido that is bounded to the Mo ion would take place concerted with the passage from the hydrogen in Glu1262 the deprotonated nitrogen of xanthine, momently, returning back after the hydride has been transferred.

Afterwards the substrate would be release from the active site which would be concomitant with the enzymatic turnover.

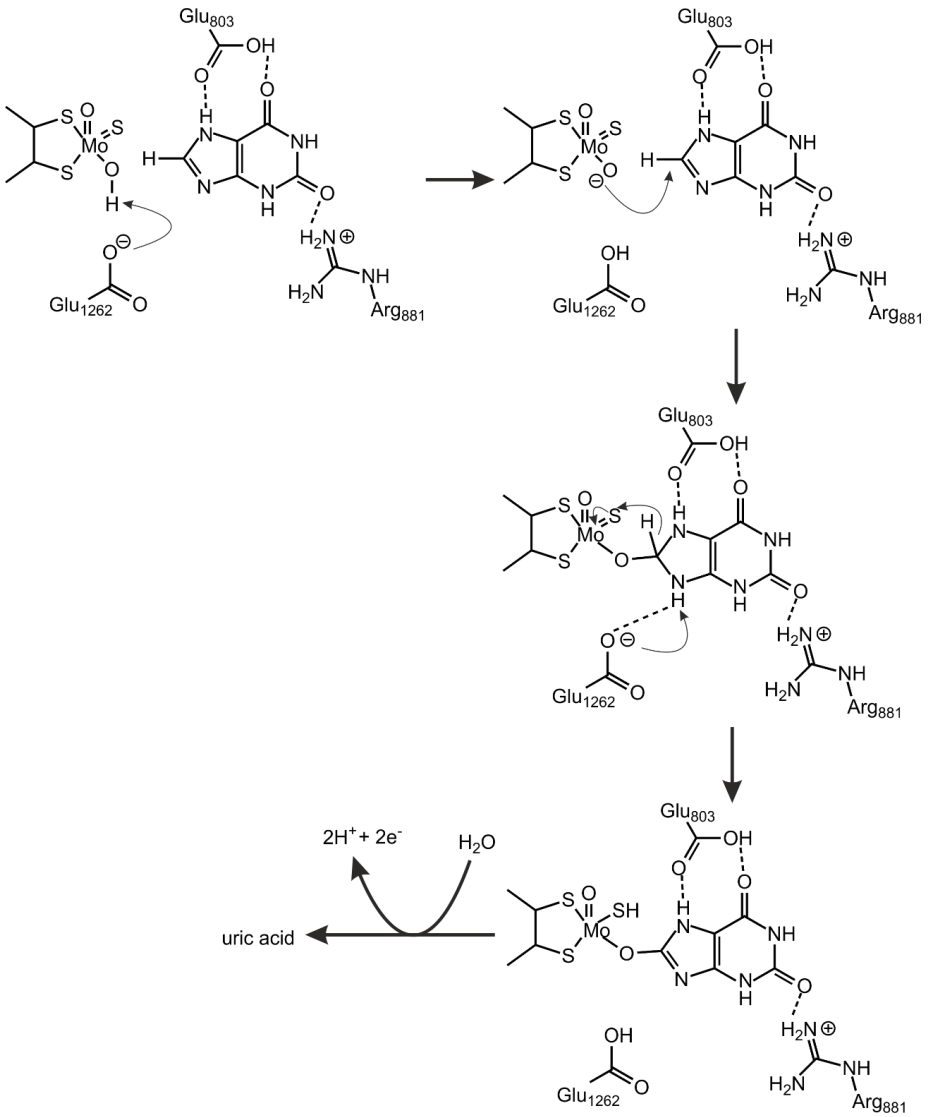

Figure 6 - Representation of a theoretical mechanism proposed by Yamaguchi Y. (2017)

Although this mechanism explains in a simpler manner how the mechanism could be viable it has several flaws. First, it does not explain how the substrate detaches from the Mo ion and how the enzymatic turnover occurs. It is known that this process involves the participation of a water molecule but no details are provided about how this takes place. Secondly, it also does not explain why when Arg881 is mutate by an alanine the enzyme becomes inactive (Figure 6).

5.2 Metz and Thiel proposal (2009)

In 2009, the same mechanism was revisited by Metz and Thiel. In this work they proposed that the catalytic mechanism initiates through the activation of the substrate. This process involves a two-proton transfer, one from xanthine to Glu1261 through a water molecule from which results the formation of a negative charge in the substrate, and one from hydroxyl group bonded to Mo ion to xanthine. Only afterwards occurs the nucleophilic attack of the substrate to the Mo ion and subsequently the hydride transfer from the substrate to the sulfido that is bonded to the Mo ion. The authors presented that this step was the rate-limiting one presenting an activation barrier of 13.1 kcal/mol^{-1} [34], [35] (Figure 7).

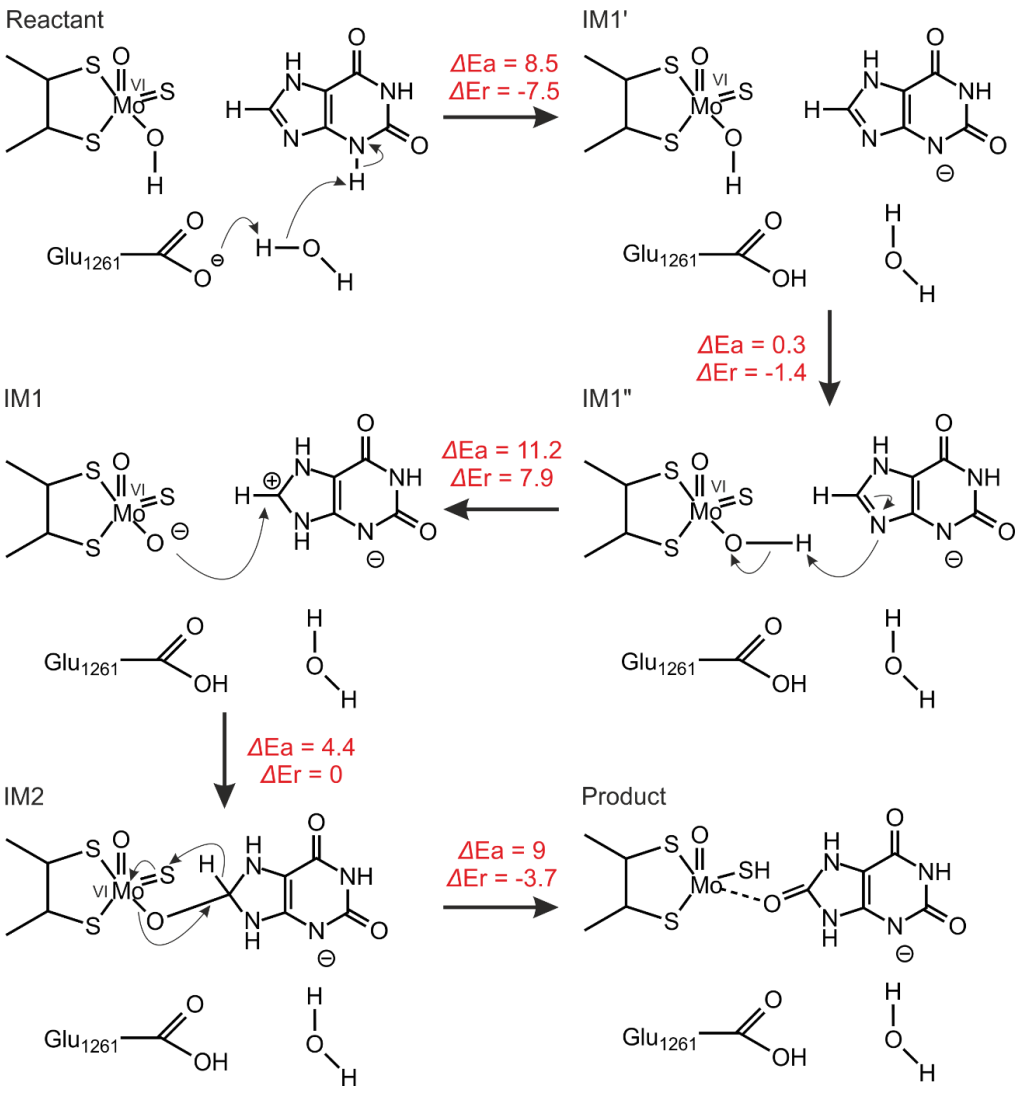

Figure 7 - Representation of mechanism proposed by Metz and Thiel in their QM/MM studies

Again, this mechanism does not explain how the substrate is release from the active site and how the enzymatic turnover takes place. It only provides some insight about the role played by Arg880 in the mechanism, that is proposed to have a key role in neutralizing the negative charge in the substrate. The full energetic profile of the reaction also is a bit far off when compared with the experimental values (15.72 kcal mol^{-1})

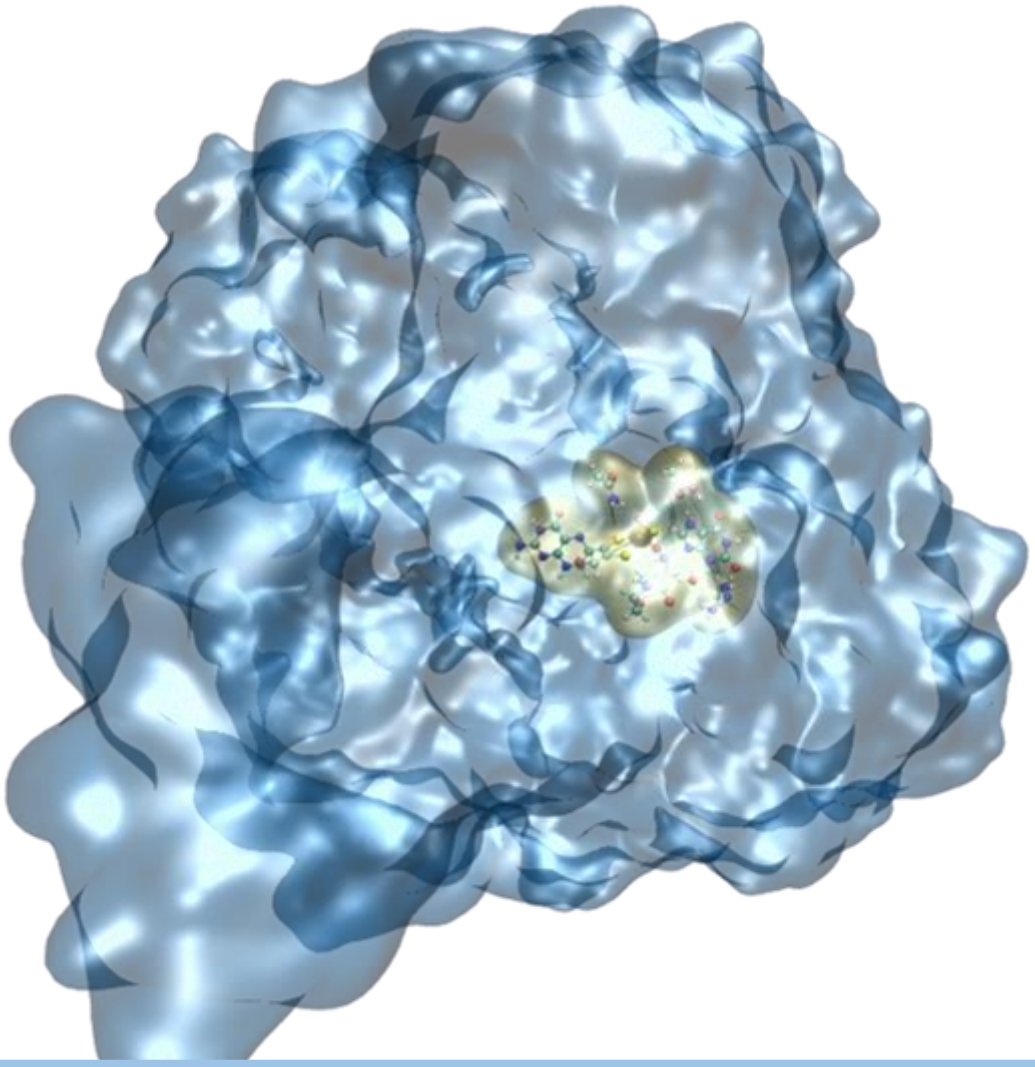

II. Theoretical Background

This page was intentionally left blank

1 Computational Chemistry

Computational chemistry is a branch of chemistry that uses computational simulation to aid in the resolution of chemical problems. It uses theoretical chemistry methods, coded in computer programs, to calculate the structures and properties of molecules and solids, like possible reactions, calculation of free energies, properties of molecules and many more parameters. It is a very important field of research because, while the simulations should support experimental information and connect the vast results, it can disclosure new theories and prove some data that cannot be obtained by experimental means.

There are many computational methods available and the choice of the best one for a particular study depends on many variables like: the type of system that is studied, the number of atoms that compose the model system, accuracy of the calculation, time of the calculation, etc. The fastest methods are the molecular mechanics (MM) that use force fields to calculate energy of a system. The most accurate ones, but also the most time demanding, are the quantum mechanics methods (QM). A brief description of each one of them is provided in the next sections.

2 Molecular Mechanics Methods

Molecule mechanics methods study the connection between atoms using force fields. Each atom is simulated as a particle with a given radius, polarizability and a constant net charge [36].

$$\begin{aligned} E &= E_{covalent} + E_{noncovalent} \\ &= E_{bond} + E_{angle} + E_{dihedral} + E_{electrotatic} + E_{van\ der\ Walls} \end{aligned} \quad (1)$$

Using molecular mechanics, the energy of a molecule (E) can be calculated, for each conformation, by the sum of covalent and noncovalent energetic contributions. The covalent potential energy is calculated by the sum of smaller parameters as bond,

angle and dihedral angles, while noncovalent potential is calculate through the sum of electrostatic and van der Walls interactions (Equation 1) [37].

The bond length potential energy contribution and bond angle potential energy contribution have identical formulas, but with different parameters. They are represented in Equation 2 and 3, respectively [38].

$$E_{bonds} = \sum_{bonds} K_b(b - b_0)^2 \quad (2)$$

$$E_{angles} = \sum_{angles} K_\theta(\theta - \theta_0)^2 \quad (3)$$

Where only two parameters are needed: the force constant (K_b and K_θ) and the equilibrium value (b_0 and θ_0), while the b and θ are the variables.

The potential energy involving dihedrals angles is more complex to calculate since it as a more complex formula and involves a Fourier serie (Equation 4) [38].

$$E_{dihedrals} = \sum_{dihedrals} \sum_{n=1}^{6} K_\phi(1 + \cos(n\phi - \phi_0)) \quad (4)$$

In this equation, the K_ϕ is the force constant, n is the multiplicity, ϕ is the angle variable of the dihedral and, lastly, the ϕ_0 is the equilibrium dihedral's angle.

The non-covalent interactions, which includes the electrostatic and van der Walls energy contributions are calculated through a Coulomb and Lennard Jones potential (Equation 5)[38].

(5)

$$E_{noncovalent} = \sum_{\substack{electrostatic \\ pair\ ij}} \frac{q_i q_j}{4\pi D r_{ij}} + \sum_{\substack{van\ der\ Walls \\ pair\ ij}} \varepsilon_{ij} \left[\left(\frac{r_{ij}^{min}}{r_{ij}} \right)^{12} - 2 \left(\frac{r_{ij}^{min}}{r_{ij}} \right)^{6} \right]$$

Where, for the electrostatic energy, q_i and q_j are the atoms charges, r_{ij} the distance between them and D is a constant, while for van der Walls energy r_{ij}^{min} is the distance between both atoms where the potential energy is minimal and ε_{ij} is the minimal potential [36].

One of the most common software package, used in molecular mechanics, is AMBER (Assisted Model Building with Energy Refinement), which has a vast catalogue of parameters for different bonds, angles and dihedrals to be used with the above equations (ff99SB and GAFF – General Amber Force Field) [39], [40].

3 Quantum Mechanics Methods

In quantum mechanics, it is studied each atom and each subatomic particle individually. In this calculation time-independent Schrödinger equation (Equation 6) is used to calculate the energy of a system.

$$\hat{\mathrm{H}}\Psi = E\Psi \tag{6}$$

This is why quantum mechanics are extremely more exact than MM, but at the same time is more time and computational consuming so it can only be used to study a little more than a hundred atoms simultaneously.

The density functional theory (DFT) is one of the most popular methods used in QM calculations. It calculated the energy of a system taking into account the electron density. However, the calculated energy depends on the functional that is used. One of the most popular ones is B3LYP that was developed by Becke, Lee, Yang and Parr [41]–[44].

3.1 Basis sets

Basis set is a package of mathematical functions used to represent the electronic density in the DFT methods. Quantum chemical calculations use a finite number of basis sets that are used to describe the molecular orbitals of a molecular system.

One of the most common basis set is the 6-31G(d), that contains information from atoms since hydrogen until zinc. For other atoms of the periodic table of the elements, other basis set can be used such as the LanL2dz and the SDD [45].

4 Hybrid Methods

In recent years, hybrid methods have been considered and developed to assign different theoretical levels to different parts of a certain system. Those methods, differ in accuracy and therefore involve different computational costs. For the study of biological systems, like enzymes, it is required to work with a huge number of atoms, normally some thousands of atoms, so QM methods can't be considered and only MM methods can be used. But, MM methods are a problem to study chemical reactions, since they cannot describe the breakage and formation of chemical bonds [46], [47].

So, knowing this, the hybrid methods, commonly known as QM/MM methods divide the model system in two regions. A small part of the model system is studied with QM methods and the remaining part using MM methods. This is helpful when studying enzymes, since the breakage and formation of bonds only occurs in the active center, so it is used QM methods for the active center, and the rest of the enzyme is study through MM. But there needs to be a careful choice of which atoms should be studied using QM, in order to obtain very good results and, at the same time, be possible for computational calculation.

In this work it is used a QM/MM methodology, in order to study the XO catalytic mechanism, using DFT (B3LYP) to describe the active center atoms and the remaining protein and cofactors using AMBER by MM approach.

4.1 Hybrid methodologies

In order to start using the QM/MM methodology, as said above, it is very important to choose wisely the atoms that are included in each of the QM and MM layers. All the atoms that are directly involved in the chemical reaction, are commonly the choice for the high-level layer (HL) and are studied with the most accurate theoretical level (QM). The rest of the protein, water molecules, make the low-level layer (LL), which will be studied with MM methods. The biggest problem of this method is the boundary methods that will be addressed ahead.

The energy calculation is made using two approaches, additive and subtractive methods, in order to correlate the energy calculated in each layer. In this work, the subtractive method is used, so, considering the split system (HL and LL), three calculations describe our total energy ($E_{QM/MM}^{All}$), [48].

$$E_{QM/MM}^{All} = E_{MM}^{ALL} - E_{MM}^{HL} + E_{QM}^{HL} \quad (7)$$

Following Equation 7, the first calculation to be done is the full system using the MM method (E_{MM}^{ALL}). After, only the HL atoms are studied using MM method (E_{MM}^{HL}) and the LL region is calculated subtracting this last energy to the previous one. Finally, the energy of the HL atoms is studied using the QM method (E_{QM}^{HL}) and the result is summed.

4.2 ONIOM

ONIOM (our own *N*-layered integrated molecular orbital molecular orbital molecular mechanics) is one of the most subtractive hybrid methods used, containing the features referred above and some others. Also, ONIOM needs an explicit description of charges and spin multiplicities for each region, which will be described throughout the work for each calculation [49].

For this work, it was created a two-layer system, using DFT method for the HL, with B3LYP functional, and MM approach for the LL (Figure 8). The model contains a bit less than 100 atoms for the HL (yellow region) and approximately 24000 atoms (blue region), and waters around the protein at 2Å of distance (not represented in Figure 8). The model will be explained in more detail in the upcoming chapter.

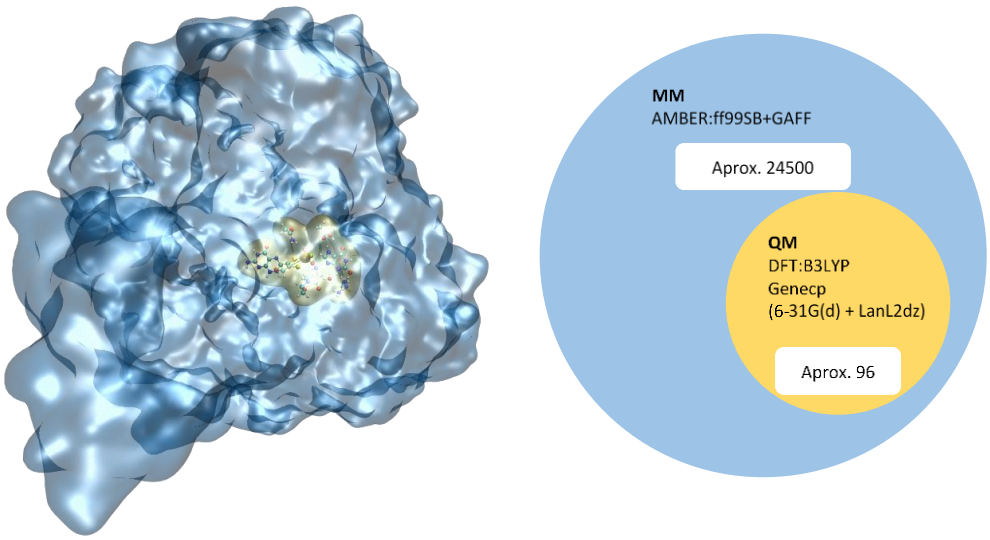

Figure 8 – 3D and 2D representation of QM/MM two-layered model of XO

4.3 Boundary methods

There's some problems relative to the hybrid method, that brings up the atom linkage between atoms in different layers. This problem is more important when the connection between atoms is covalent and not non-bonded interactions. For example, for an amino acid a part can be studied with QM and another with MM but in the end the amino acid need to be studied as a whole [46].

Link atoms approach and the frozen orbital approach were developed in order to overcome these difficulties.

4.4 Link atoms approach

In this work, hydrogen was used as link atoms. These link atoms allow the division of the system in different and calculate the energy of each layer with different theoretical levels of theory [46].

These atoms are added, by Gaussian software [50], though a vector that is oriented by the HL atom configuration. The link atom is placed at a certain typical distance which depends on the involved elements. The energy of these cut bonds will be evaluated by MM method that calculates the energy of both layers together, as a LL [46].

Besides this method's simplicity it can have some geometry and energy errors due to polarization induced by the link atoms in the HL.

4.5 Communication between layers

Another problem related to hybrid methods, as referred previously, is the non-bonded interactions between the atoms, that derive from electrostatic and van der Walls interactions, between the different layers. The mechanical and electrostatic embedding methods are the most used methods.

4.6 Mechanical embedding

This is the simplest method, that permit HL atoms to induce polarization over LL and HL region is calculated using QM without concerning the polarization. After the LL region is calculated by MM method with the polarization caused by HL, induced by through punctual charges.

Some consequences appear due to these approximations. Charges in hybridization states aren't considered for the polarization, but fortunately, Lennard-Jones potential is a short-ranged function that doesn't introduce a very significant error [46].

4.7 Electrostatic embedding

This method induces polarization by the LL region in the HL layer, introducing an additional mono-electronic term to the QM Hamiltonian. Compared to mechanical embedding the LL polarization by the HL atoms isn't considered, but the results tend to be better. The main disadvantage to this approximation is the increase of computational work.

5 In this work

As said briefly above and to summarize, this work will follow some lines from previous works, an QM/MM will be used with the DFT/B3LYP [41]–[44] functional with 6-31G(d)/LanL2dz modified basis set. Gaussian, gaussview and molUP will be used for calculations and some modifications that where needed and visualization and image rendering with VMD [50]–[52].

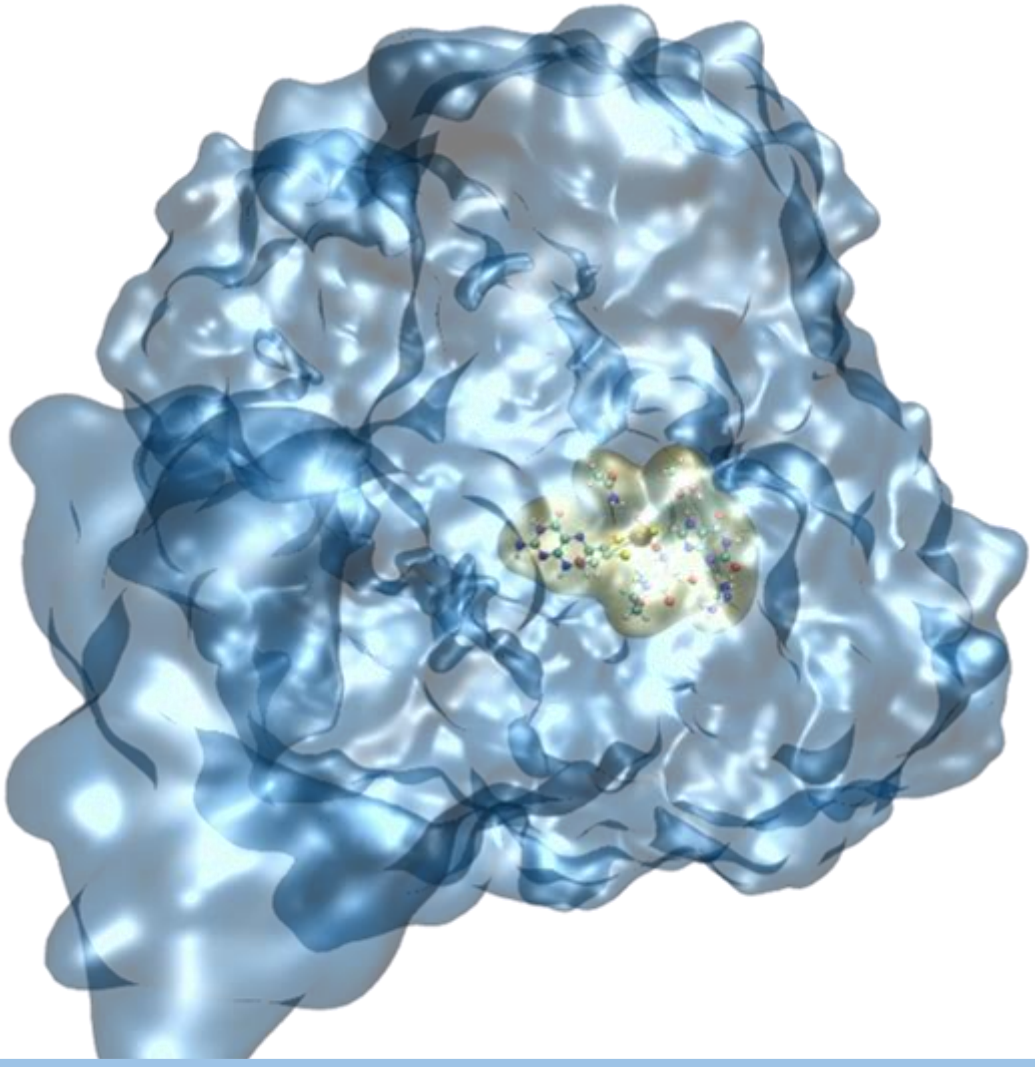

III. Results and Discussion

This page was intentionally left blank

1 Introduction

In this chapter, all the computational results that were done in this thesis to unravel the catalytic mechanism of XO will be presented and discussed. We will start by explaining how the XO model was built. Afterwards, a brief overview about the Molecular Dynamic simulations will be described. Finally, the QM/MM studies regarding several hypothesis about the catalytic mechanism of XO will be presented and discussed. The mechanistic of XO will be separated in three different parts: the first part involves the nucleophilic attack of Xanthine to Moco, the second part the substrate release, and the third part the oxidation of the active site and subsequent enzymatic turnover.

2 Choosing the starting structure.

In the protein databank, only a few structures are available for XO for *Homo sapiens*, however, the resolution of these structure is not very high. Only the structures from XO from *Bos Taurus* have resolution below 2Å and were co-crystallized with several reaction intermediates in the active site of the enzyme (Table 1). These structures are very important for a theoretical and computational studies because they provide important details about a snapshot of the catalytic mechanism.

Table 1 - PDB structures of XO for several organisms available in the protein databank

PDB entry	Species	Resolution	Substrate	Mutations	Reference
2E1Q	*Homo sapiens*	2.6	Salicyclic acid	Glu803Val Arg881Met	[3]
2CKJ	*Homo sapiens*	3.59	-	-	[53]
3UNA	*Bos taurus*	1.9	Salicyclic acid	-	[54]
3UNC	*Bos taurus*	1.65	Salicyclic acid	-	[54]
3AX7	*Bos taurus*	2.34	Salicyclic acid	-	[54]

3AX9	*Bos taurus*	2.3	Salicyclic acid	-	[54]
3NVW	*Bos taurus*	1.6	Guanine	-	[55]
3NVZ	*Bos taurus*	1.6	Idole-3-carbaldehyde	-	[55]
3SR6	*Bos taurus*	2.1	Arsenite	-	[56]
3AMZ	*Bos taurus*	2.1	Uric Acid	-	[57]
3NRZ	*Bos taurus*	1.8	Hypoxanthine	-	[58]
3NS1	*Bos taurus*	2.6	6-mercaptopurine	-	[58]
3BDJ	*Bos taurus*	2	Alloxanthine	-	[59]
3AN1	*Rattus norvegicus*	1.73	Uric Acid	Asp428Ala	[57]
2E3T	*Rattus norvegicus*	2.28	Uric Acid	Trp335Ala Phe336Leu	[60]
1WYG	*Rattus norvegicus*	2.6	Salicyclic acid	Cys535Ala Cys992Arg Cys1324Ser	[61]

In order to evaluate if there are significant differences between the X-ray structures from *Homo Sapiens* and *Bos taurus*, several X-ray structures from both organisms were superimposed. From these analyses, two structures were selected. One from *Homo Sapiens* (PDB code: 2E1Q) and another from *Bos Taurus* that contains the substrate inside the active site (Figure 9). Observing the overlap of both structures, it is possible to see that there are no significant differences between them. This is true either for the overall protein, but also for the conformation of the residues from the active site (RMSD below 1.4Å). Taking these results into account we choose the structure from *Bos Taurus* (PDB code: 3AMZ) to continue the studies for the catalytic mechanism of the enzyme.

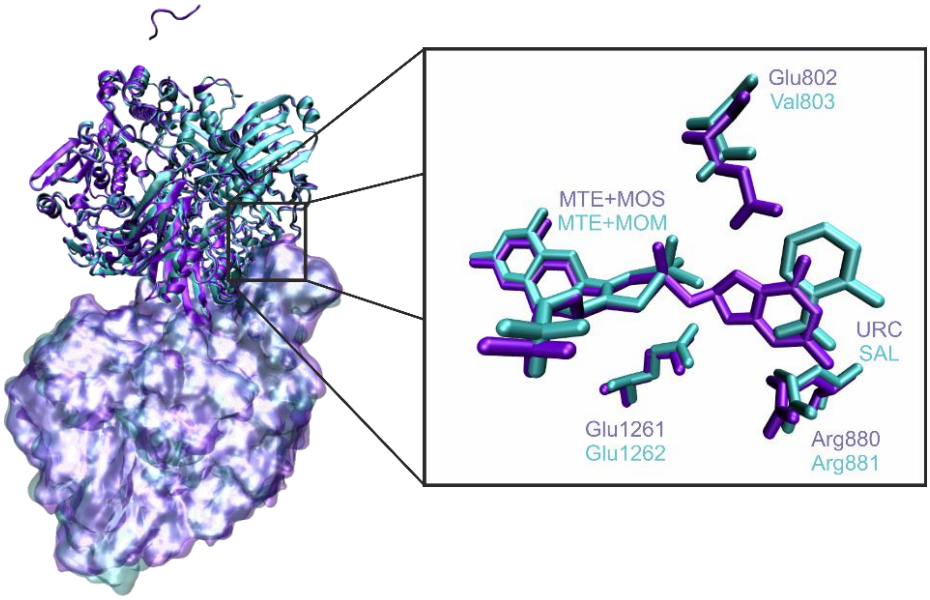

Figure 9 - Comparison between Bos taurus (3AMZ colored in violet) and Homo sapiens (2E1Q colored in cyan) XO, of the full enzyme and active site. Chains A represented in NewCartoon and chains B represented in QuickSurf. (RMSD backbone = 0.391)

Since in the PDB structure 3AMZ, was missing the coordinates of some amino acid structures in the positions 165-190, 529-536 and at the C terminus of the protein, homology modelling techniques were applied. To this end, the SWISS-model software package was used [62], [63]. The sequence alignment used to build the complete model of the XO enzyme using the PDB structure 3AMZ *from Bos Taurus* is shown in Figure 10.

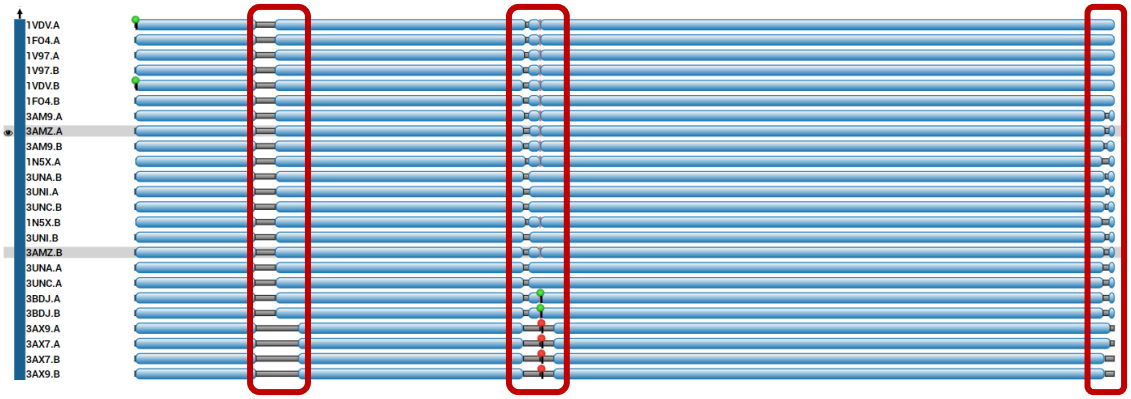

Figure 10 - Comparison between the sequences of XOs PDBs, highlighting in red the missing parts from which no 3D structure is available.

After obtaining the homology model, an overlap was made against 3AMZ PDB in order to copy the coordinates for the cofactors (MoO_2-moblydenopterin, [2Fe-2S] clusters and FAD) and from some water molecules that are close to the active site. The waters copied where the 2106 and 2013 from chain A of 3AMZ PDB, which are close to where the reaction occurs, and the 2151, 1746, 2077, 1356 and 2127 which are close to the phosphate group from the Moco.

3 Molecular Dynamics (MD)

After an adequate preparation of the XO structure, a set of minimizations stages and a molecular dynamic simulations (MD) were performed. These simulations allow to equilibrate the structure that came from homology modelling and get an ensemble of conformations from which we can get hints about the catalytic mechanism. Furthermore, they generate relevant structural information, such as hydrogen atom networks, flexibility of some amino acids, tunnels of water molecules, which can provide important hints and help the study of the catalytic mechanism of an enzyme.

3.1 Parametrization

In order run do the MD simulations it is required that all the amino acid residues and cofactors are correctly parameterized. In this study, it was necessary to parameterized the Moco and the substrate, since they were not available in the AMBER force field ff99SB [38].

During the parameterization, the atomic charges were obtained through an *ab initio* methodology, namely Hartree-Fock, with the 6-31G(d) basis set. Additionally, the ANTECHAMBER program was used to assign the atom typology for the residues that were parameterized. The calculated parameters are described below (Figure 11 and Figure 12; Table 2 and Table 3).

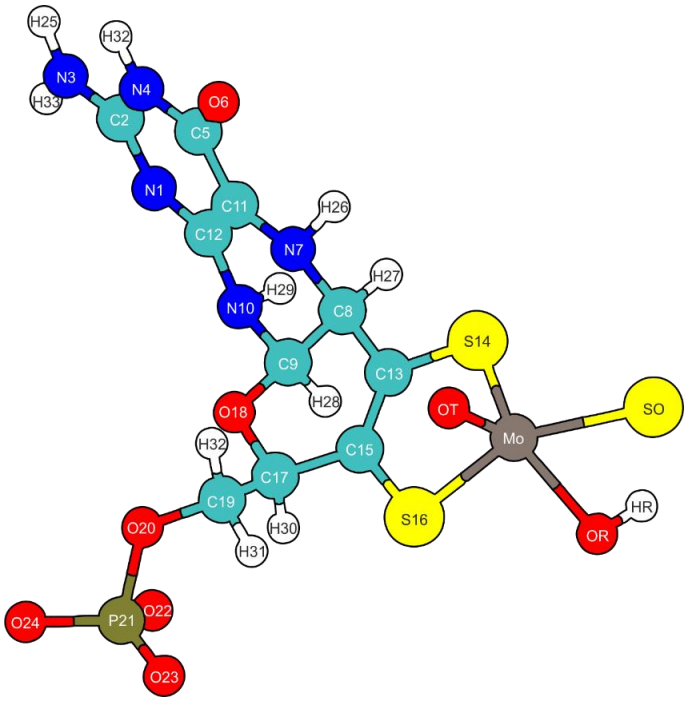

Figure 11 - Moco structure after parameterization, with atoms designation that will be used throughout the work.

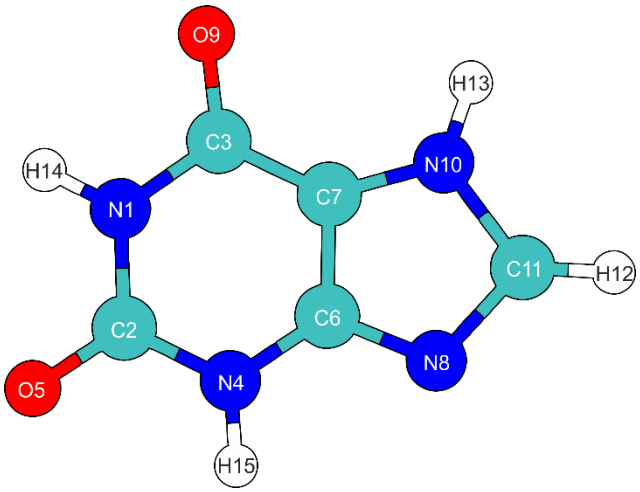

Figure 12 - XAN structure after parameterization, with atoms designation that will be used throughout the work.

Table 2 - Atomic charges (a.u.) assigned to each atom of Moco

Atom	Charge	Atom Type	Atom	Charge	Atom Type
C2	1.005629	cd	HR	0.448976	HR
C5	0.784646	c	Mo	1.200184	MO
C8	0.176439	c3	N1	-0.81613	nc

C9	0.016524	c3	N3	-1.042171	nh
C11	-0.347053	cd	N4	-0.861428	n
C12	0.742392	cc	N7	-0.583624	nh
C13	-0.132639	c2	N10	-0.548134	nh
C15	0.210841	c2	O6	-0.712964	o
C17	0.18774	c3	O18	-0.23956	os
C19	0.180983	c3	O20	-0.598557	os
H28	0.394459	hn	O22	-0.946141	o
H29	0.388656	hn	O23	-0.946141	o
H30	0.073926	h1	O24	-0.946141	o
H31	0.11774	h2	OR	-0.82225	OR
H32	0.42896	hn	OT	-0.501336	OT
H33	0.108421	h1	P21	1.403441	p5
H34	0.004941	h1	S14	-0.483125	S1
H35	0.004941	h1	S16	-0.615269	S2
H38	0.41192	hn	SO	-0.543556	SO
H39	0.394459	hn			

Table 3 - Atomic charges (a.u.) assigned to each atom of XAN

Atom	Charge	Atom Type	Atom	Charge	Atom Type
C2	0.904002	c	H15	0.434529	hn
C3	0.748054	c	N1	-0.75549	n
C6	0.70135	cc	N4	-0.521336	n
C7	-0.183895	cd	N8	-0.664101	nc
C11	0.350387	cd	N10	-0.521336	na
H12	0.135013	h5	O5	-0.624343	o
H13	0.419946	hn	O9	-0.577333	o
H14	0.405918	hn			

The nomenclature of the Cys that belong to the [2Fe-2S] clusters were also changed to CYM. The identification of these residues is: 43, 48, 51 and 73 for one cluster and 113, 116, 148 and 150 for the other one. In addition, the covalent bonds between the Fe atoms of FES to the SG atoms of the CYM cysteines were added using the LEaP program.

3.2 Protonation state of the residues of the protein

To assign the correct protonation state of the residues present in the protein, the software PROPKA was used [64].

The software identified that some amino acid residue should have different *pKa* values in relation to the standard ones, considering the environment where they are located at. One of these residues is Glu802, for which a *pKa* value of 10.34 was calculated. Considering that XO works at a pH of 7, this means that this amino acid residue should be protonated in the active site of the enzyme.

3.3 Solvation Stage

Under physiological conditions, XO is found in the cytoplasm of the cells and therefore surrounded by water molecules. Before the minimizations and molecular dynamic simulation was run, the system was immersed in a box of waters of 12Å using TIP3PBOX program included in the LEaP software [65].

3.4 Minimization Stage

Four minimizations stages where then made using the AMBER software. In the first one, only the water molecules were minimized. In the second minimation stage, only the hydrogen atoms from the protein were set as free. In the third minimization stage, the atoms from the protein backbone were minimized. In the fourth and final minimization stage, the full protein structure, together with the water molecules were fully optimized.

In the end of the minimization stage, no significant changes between the initial X-ray structure and the minimized model were obtained, as it is illustrated in Figure 13.

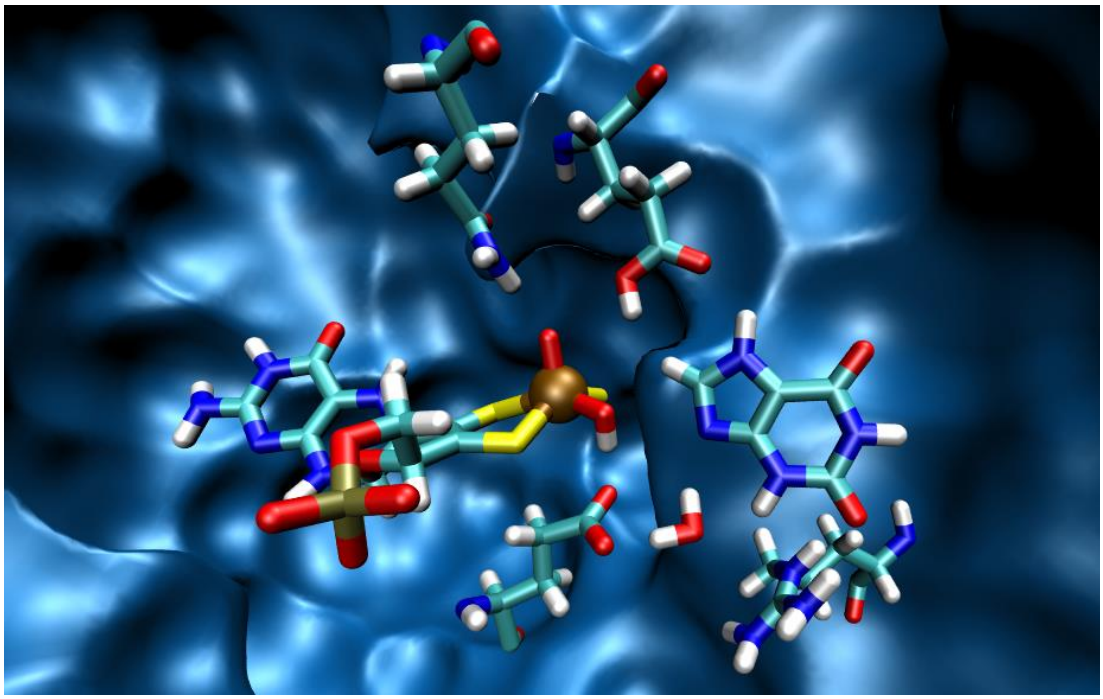

Figure 13 - Active site structure of the XO model after all the four minimizations stages.

3.5 Equilibration and Production stages

After getting the structure minimized, an equilibration was made simulating an increase in the temperature from 0K to 310.15K, in increments of 0.1K. The production was run afterwards and where the temperature was kept fixed and it was carried out for 22ns.

4 Analysis of the MD results.

In order to evaluate the performance of the MD simulation and retrieve some structural information about the structure of XO, a set of parameters were calculated, namely the RMSd and RDF. Each of these parameters will be discussed in the next sections and the conclusions that were retrieved.

4.1 Analysis of the RMSD results.

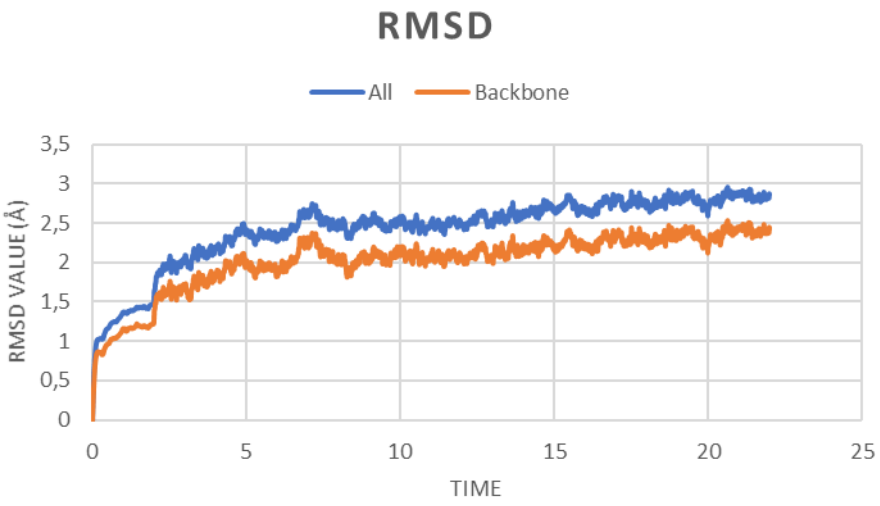

Figure 14 - RMSd obtained from Molecular Dynamics

An RMSd (root mean square deviation) was made in order to evaluate if the XO structure was stabilized during the MD simulation. The results show that after 15 ns the system is equilibrated and minimal variations are observed till the end of the simulation (Figure 14).

Different frames were retrieved after the 15ns of the MD simulation and each structure was analyzed individually. In all of these structures we found that the active site was slightly deformed. Several causes can be pointed out for this to happen, but it seems that this effect was caused due to the presence of negative and positive charges from Glu1261 and Arg880, respectively. The strong ionic interaction between both of them made them to become very close to each other, which in turn move the substrate XAN away from Moco.

These structures were not what we were expecting for since in X-ray structure and on the minimized structure, the substrate, XAN was still very close to Moco. The results that came from the MD simulation is however correct, since it is showing the events before the interaction between the substrate and the Moco takes place.

Facing these results, we choose to use the minimized structure to carry out the QM/MM studies rather than the structures that were retrieved from the MD simulation.

In spite of these results, the outcome obtained from the MD simulation were very interesting, namely the detection of a tunnel of water molecules that is formed nearby the active site of the enzyme.

4.2 Analysis of the RDF results.

From the structures that were retrieved from the MD simulations it was observed an accumulation of water molecules in the bottom region of the active site of the enzyme. In order to understand more clearly how many water molecules could be found in this region of the active site, RDFs calculations were performed around Glu1261 and Arg880 in the MD simulation.

The RDF (radial distribution functions) results for Arg880 show that there are two spheres of water molecules. The first one, at 4Å, contains three water molecules and the second one, at 6Å, contains only one water molecule. After that distance the number of waters exponentially increases, because this region is close to the protein surface and it is exposed to the solvent (Figure 15A).

The RDF for Glu1261 shows a higher concentration of water molecules close to it. It is possible to see five layers of water molecules close to this residue. The first one, appears a little after 3Å and contains one water molecule. Before 4Å another layer of two water molecules is found. Around 6Å and around 7Å it is observed the presence of two other water molecules. Finally, around 9Å a layer of three water molecules is also observed. This last layer of water molecules is already very close to the protein surface (Figure 15B). Although all of these layers water of molecules initially was thought to be dispersed along the protein structure, the MD simulation showed that they were well aligned in the bottom region of the active site, forming a kind of a tunnel, as seen in Figure 16.

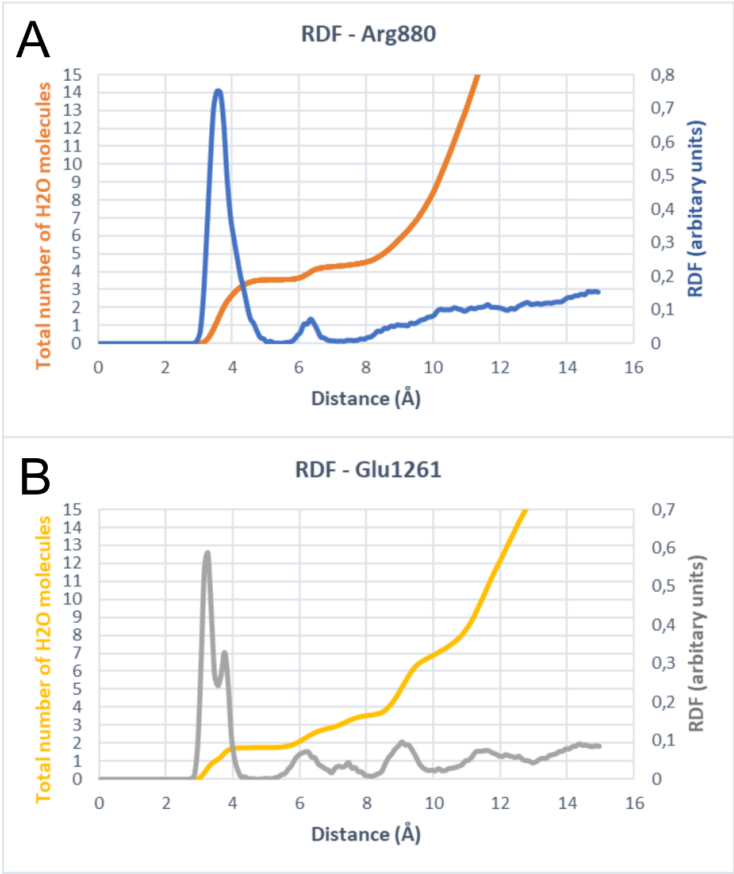

Figure 15 - RDF of Arg880 (A) and RDF of Glu1281 (B)

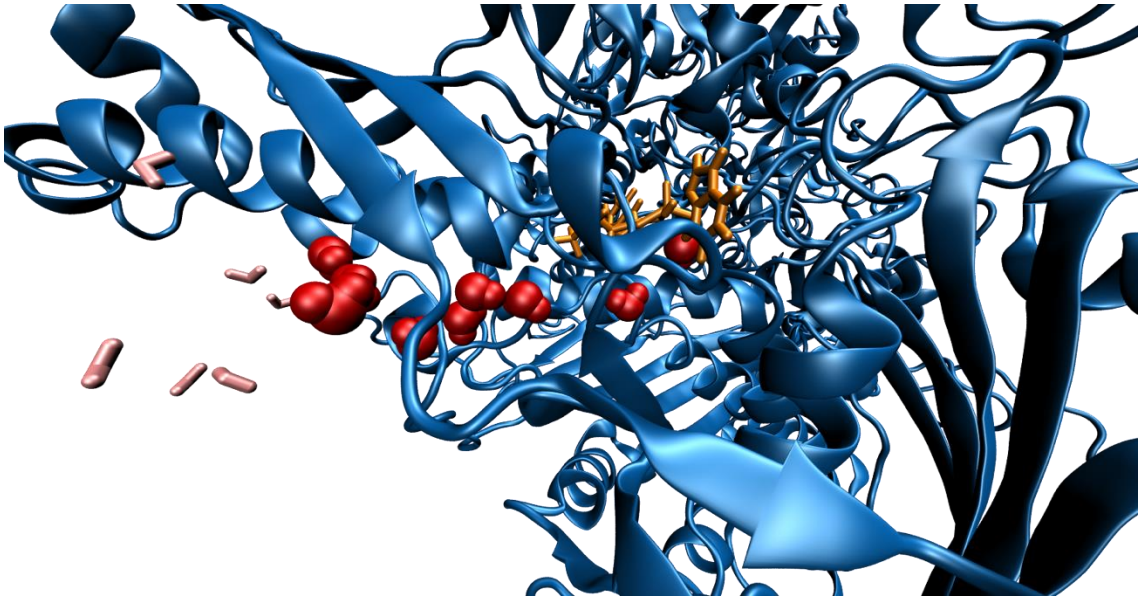

Figure 16 - Water Tunnel found in the bottom region of the active site and very close to Glu1261 and Arg880.

5 QM/MM studies

Since the MD simulation didn't create a trustworthy minimum that agrees with the active site topology of the X-ray structures that are deposited at the protein databank, we built the QM/MM model based on the initial minimization protocol.

5.1 The QM/MM Model

The QM/MM model includes the full protein, the substrate (XAN), the Moco cofactor and a layer of water molecules that surrounds the protein (4.0 Å). The total system is composed by 24100 atoms that were subsequently divided in two layers of atoms and treated with different theoretical levels of theory. The QM layer (also denoted as high layer) includes all the atoms/residues that are involved directly and indirectly in the catalytic process (100 atoms). It includes the Moco, XAN, a water molecule (3366) and the side chains from the residues Gln767, Glu802 and Glu1261 Arg880 and, atoms from the backbone from Ala1079-Ser1080. The MM layer (also denoted as low layer) contains all the remaining atoms (24000 atoms), including the water molecules that surround the protein.

The division between the QM and MM layers was made using hydrogens as link atoms. This truncation was always made in the alpha carbons of the residues that are in the border region between the QM and MM layers, with some exceptions. For example, Glu1261 was truncated in the gamma carbon and Arg880 in its delta carbon. The Moco was also truncated at carbon C19, in order to exclude the phosphate group from the high-layer. This was done because the previous calculations have shown that the phosphate group does not interfere with the electronic structure of the cofactor [34], [35], [66]–[68].

The structure of the QM/MM model was afterward optimized using DFT and the 6-31G(d) basis set in the QM layer and, molecular mechanics and the ff99SB force field in the MM layer. The water molecules that are 15 Å away from the Moco were frozen during the geometry optimizations. This means that the full enzyme is free together

with the enclosed water molecules during the geometry optimizations in the QM/MM model.

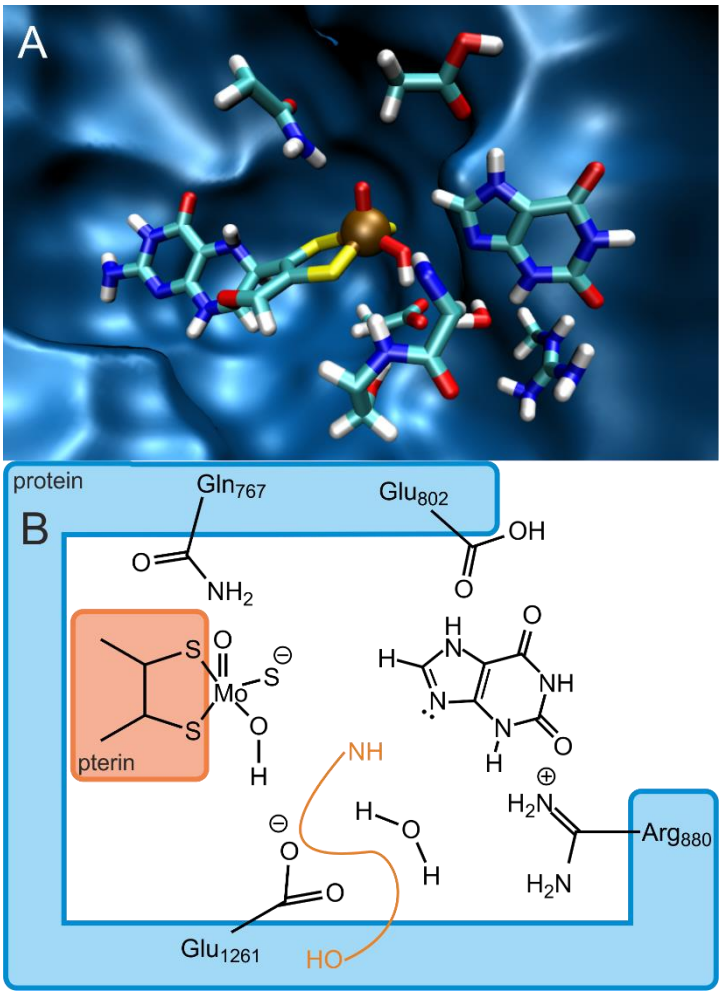

Figure 17 - A - 3D representation of active site after the QM/MM optimization - B - 2D representation of the optimized region of the active site.

The optimized geometry of the QM/MM model is very alike the X-ray structure from which the previous minimization process was performed (pdb code: 3AMZ). The Moco cofactor contains the Mo(VI) ion penta-coordinated to the pterin cofactor, an apical oxygen, an equatorial hydroxyl group and an axial sulfide. The Moco cofactor and the substrate XAN becomes surrounded by a network of hydrogen bonds that stabilizes their position in the active site of the enzyme and allows them to stay in close to each other (Figure 17A). The Moco is stabilized by the hydrogen bonds provided by Gln767 (that interacts with oxygen OT) and by the backbone atoms from Ala1079-Ser1080

(interacts with OR - orange in Figure 17B). The pterin from Moco is further stabilized by several hydrogen bonds provided by the carbonyl group of Gln112, the amino group of Gly797, Phe798 and Gln1194. The phosphate group of the pterin is stabilized by Ser1082 and a chain of water molecules, including WAT2151, Wat2127 and Wat1746. The substrate XAN is stabilized by three hydrogen bonds provided by Glu802, Arg880 and a water molecule. It is also observed a network of hydrogen bonds along the resides located in the bottom region of the active site, involving Glu1261, the water molecule W3366 and Arg880. These interactions stabilize the position of the conserved water molecule inside the active site and endorse the close contact between Glu1261 and Arg880.

5.2 Mechanistic studies

Currently, there is no consensus about the catalytic mechanism of XO. The most detailed studies were carried out by Metz and Thiel in 2009 and 2010 [34], [35] using computational means. However, they do not provide a complete description about the mechanism, neither it agrees with all the available experimental data.

These authors were only able to study the coordination of xanthine to Moco and the proton transfer process. However, no details are given regarding the dissociation of the product of the reaction and the subsequent enzymatic turnover that involves the reaction of Moco with a water molecule. Two models were used in these studies, a QM model and a QM/MM model, that provided very different energetic profiles. The most favorable one was obtained with the QM model and revealed a very exoenergonic process. In the energetic profile of the QM/MM the full process it is shown that the catalytic mechanism could be almost reversible. However, this is not what is found under physiological conditions where an accumulation of uric acid is always observed, revealing therefore that the reversible process should not be possible.

In these studies, the authors also discard the participation of Arg880 in the catalytic mechanism, a residue that upon mutation by Met was shown by Yamaguchi and colleagues to lead to the complete inactivation of the enzyme [3]. The same authors also show that when Glu802 is mutated by a Val, the rate of the reaction

decreases substantially (18.3 s^{-1} in wild type versus 1.4 s^{-1}) [3]. Furthermore, the energetic profile does not agree with the experimental kinetic studies, that predict that the rate-limiting step should have an activation free energy near 15.72 kcal mol^{-1}, but in their mechanism, it is significantly lower (13.1 kcal mol^{-1}).

There are several reasons that can explain the lack of correlation between the mechanism that was studied by Metz and Thiel and the currently available experimental evidences. The mechanism that was followed is perhaps incorrect. The model system (or the high layer of the QM/MM model) did not included all the residues that are required for the catalytic process.

Considering that currently there is no consensus about the catalytic mechanism of XO and many doubts exist regarding the currently available proposals, in this thesis we studied the full mechanism of this enzyme by computational means employing a QM/MM approach.

5.2.1 Part I – Coordination of substrate to Moco

The previous works performed by Metz and Thiel suggest that the initial steps of the catalytic mechanism of XO begins with the activation of the substrate and only afterwards the nucleophilic attack of hypoxanthine to the Mo ion takes place. This reaction involves a proton transfer from XAN, to Glu1261, with the direct participation of one water molecule, W3366. Afterwards occurs a nucleophilic attack from the deprotonated nitrogen N8 of XAN to the proton of the hydroxyl group from Moco. Only after these two steps (activation process), the nucleophilic attack between carbon C11 from XAN to the activated oxygen (OR) from Moco takes place.

We began our study by repeating the same mechanism that was proposed by Metz and Thiel, but using an extended version of the active site in the high layer of the QM/MM model. Our results revealed that such pathway was possible but, as it was found by the authors, it leads to a reaction intermediate that blocks the continuation of the catalytic mechanism.

Facing these results, we look for other proposals for the catalytic mechanism. The one that is going to be described is the one from which we got the best energetic profile and agrees with several experimental results, namely the work performed by Yamaguchi and colleagues [3] that highlighted the active participation of Arg888 during the catalytic process.

5.2.1.1 **Step 1:** Nucleophilic attack of XAN to Moco

The first step of the new mechanistic proposal involves the approximation of carbon C11 from XAN to oxygen OR of Moco, at the same time that occurs a proton transfer from oxygen OR from Moco to Glu1261 (Figure 18).

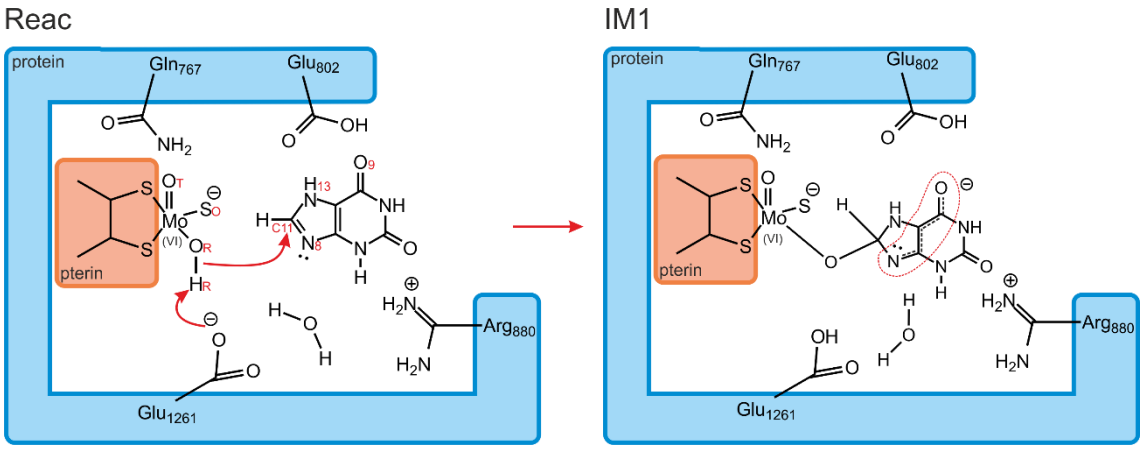

Figure 18 - 2D representation of the reaction's first step, showing the reactant (Reac) and the product (IM1).

In the optimized geometry of the reactant of this reaction (Reac – Figure 18), the Mo(VI) ion adopts a penta-coordinate geometry, with the two sulfur atoms from the pterin ring in the equatorial position (2.5Å and 2.5Å), oxygen OT in the apical position (1.7Å), the sulfide SO in the axial position (2.2Å), and a hydroxyl group at the basal position (1.9Å). The substrate, XAN, adopts a planar configuration and carbon C11 (0.36 a.u.) is 2.6Å away from the oxygen OR (-0.60 a.u.) that belongs to the hydroxyl group that is coordinated to the Mo ion. XAN is stabilized by three hydrogen bonds provided

by Glu802 ($B_{Glu802\text{-}H13}$=1.7Å), Arg880 ($B_{Arg880\text{-}O5}$=1.8Å) and from the water molecule, Wat3366 ($B_{wat\text{-}H15}$=1.9Å).

The main difference between the previous optimized QM/MM geometry and the reactant of this step is the position of Glu802, that goes from an equatorial to an axial position, favoring by the way the approximation of XAN to the Moco. We estimated this conformational rearrangement by theoretical means and it requires 3.0 kcal mol^{-1}.

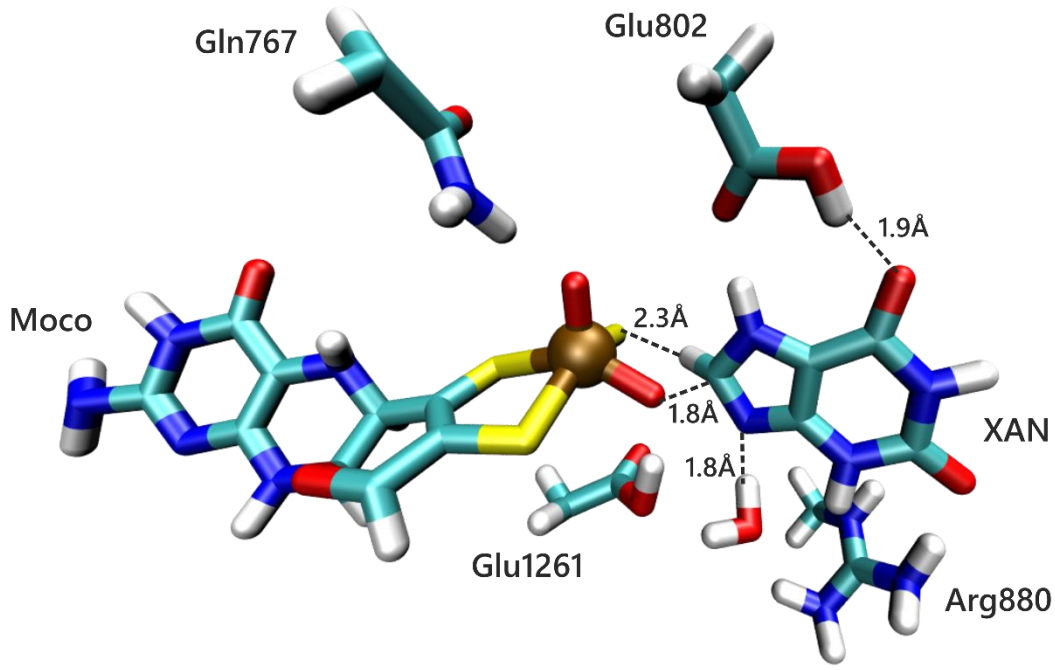

Figure 19 – Transition state of the first step of the catalytic mechanism of XO (TS1). In the image are highlighted some important distances between the residues from the active site of the enzyme, the cofactor and the substrate.

The transition state of the first step (TS1 – Figure 19) is characterized by an imaginary frequency of 275i cm^{-1}. In TS1, the distance between Glu1261 and the proton HR from the hydroxyl group of Moco increases, favoring by this way an accumulation of the charge around oxygen OR (-0.73 a.u. versus -0.60 a.u. in the Reac). This effect promotes the proximity between this atom and carbon C11 of XAN (1.8Å in TS1 versus 2.6Å in Reac) promoting by this way the nucleophilic attack of the Moco cofactor to XAN.

Glu802 plays an important role in TS1 stabilizing the position of XAN in relation to Moco. It undergoes a slight rotation that endorses the formation of two hydrogen bonds with oxygen O9 ($B_{Glu802\text{-}O9}$=1.9Å) and hydrogen H13 ($B_{Glu802\text{-}H13}$=1.7Å) from XAN.

In TS1, it is also observed a conformation rearrangement of the water molecule Wat3366, that no longer establishes a hydrogen bond with hydrogen H15 from XAN but becomes aligned with nitrogen N8 ($B_{wat\text{-}N8}$=1.8Å).

In the product of this reaction, (IM1 – Figure 26), XAN becomes covalently bonded to Moco ($B_{XAN\text{-}C11\text{-}Moco\text{-}OR}$=1.5Å) and carbon C11 adopts a tetrahedral configuration. The network of hydrogen bonds around the active site that were described in TS1 keep up in the product of the reaction, stabilizing by this way the product of the first step. The charge that in the reactants was concentrate on Glu1261, now becomes lodged at XAN and spread between nitrogen N8 and oxygen O9 (Figure 20, IM1 highlighted in red).

This reaction has a free activation energy ($\Delta G^{\ddagger}$) of 11.6 kcal mol^{-1} and the reaction is endoenergonic ($\Delta_r G$) in 7.5 kcal mol^{-1}.

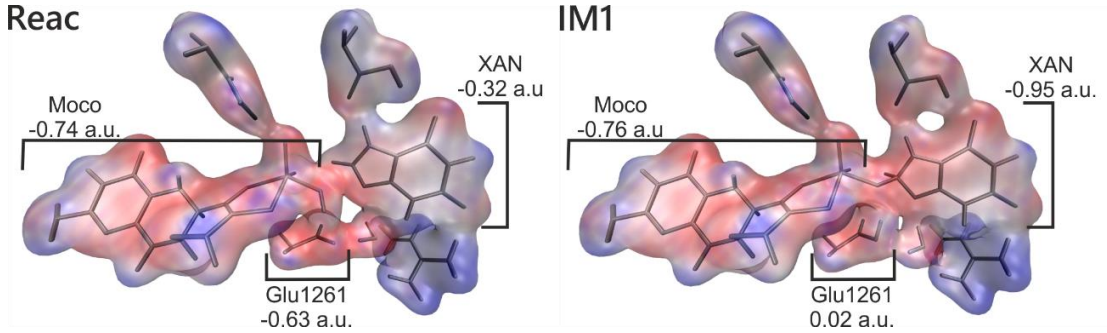

Figure 20 - Electrostatic potential, for step 1, of the reactant and product of the reaction using the high-layer of the QM/MM model. The isosurfaces were calculated using gaussian09. Blue regions represent the positive charged atoms and in red the regions where the negative charges atoms are located at.

It is worth mentioning that during the reaction, the observed charge transfer from Glu1261 to XAN is stabilized by the conjugated pi system of XAN that is in turn supported by the hydrogen bonds provided by Glu802. This effect can be seen in Figure 20, where the region of XAN is less charged (less red) in Reac than in IM1. This also

reveals that in the product of the reaction, the negative charge is located in the substrate rather than in the pterin as firstly thought.

These results go in line with the experimental result obtained by Yamaguchi and colleagues, that have shown that when Glu802 is mutated to a Valine the reaction occurs but becomes too slow. This occurs due to the lack of stabilization of the resonance structure that is essential for the charge transfer that needs to occur in this step.

5.2.1.2 **Step 2:** Hydrogen atom transfer

The second step of the catalytic mechanism of XO, involves the hydrogen atom transfer from XAN to the sulfido that is coordinated to the Mo ion (Figure 21).

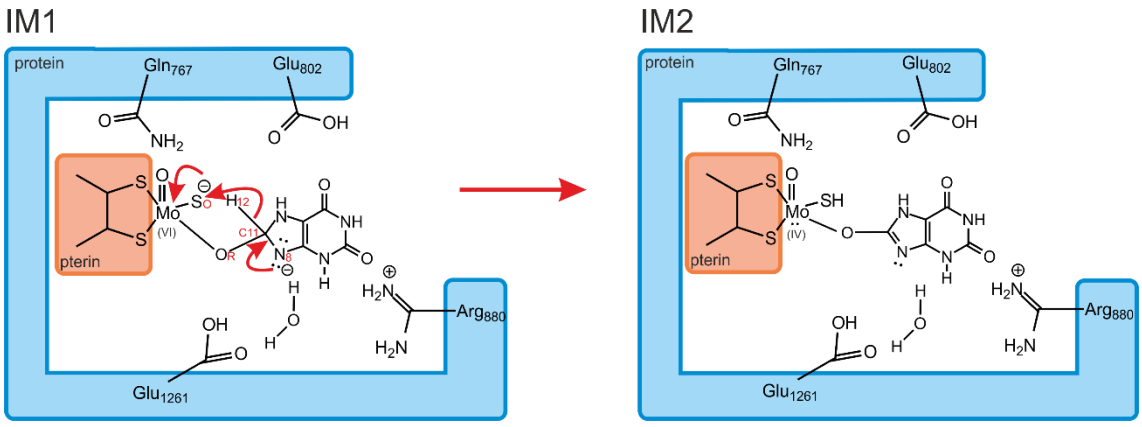

Figure 21 - 2D representation of the reaction's second step, showing the reactant (IM1), the product (IM2).

The optimized geometry of the reactant of the second step shown no significant differences in relation to the product of the first step (IM1 – Figure 29), either in the orientation of XAN and Moco molecules or even on the network of hydrogen bonds in the active site. The Moco continues to be covalently bonded to carbon C11 of XAN (1.5Å) and four hydrogen bonds promoted by Glu802, Arg880 and Wat3366, continue to stabilize and holding XAN in same position on the active site of the enzyme.

Hydrogen H12 from XAN is located at 2.3 Å from the sulfide SO that is coordinated to the Mo ion.

The negative charge that results from the first step of the mechanism continues to be lodged at XAN (-0.95 a.u.). The charge in Moco remains constant (-0.74 a.u.) and concentrated at the sulfide SO that is coordinated to the Mo ion (-0.23 a.u.).

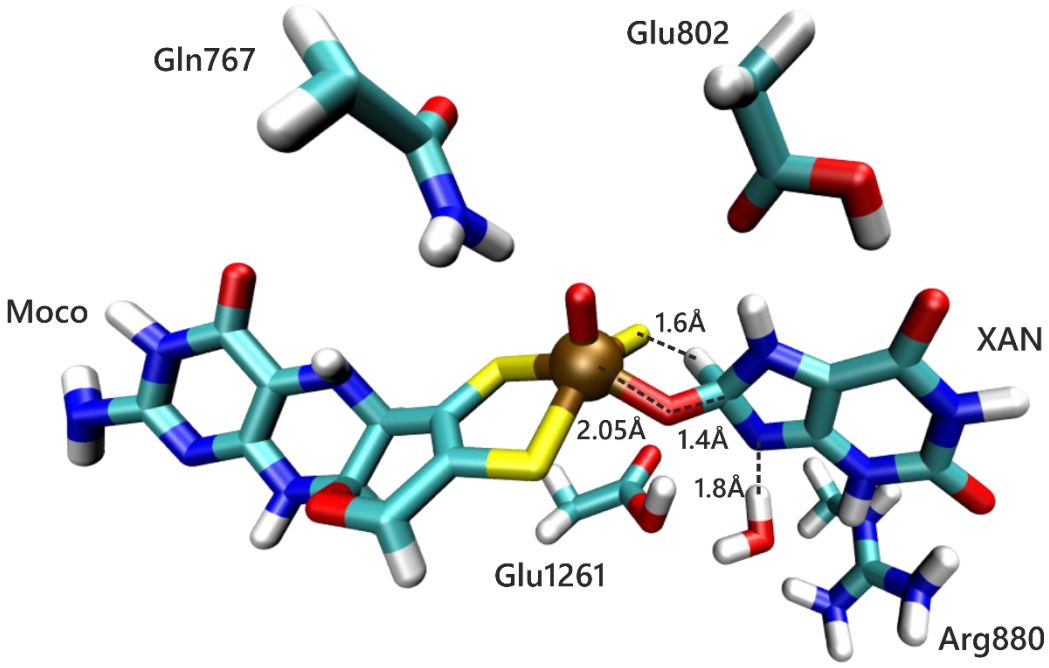

Figure 22 - Transition state of the second step of the catalytic mechanism of XO (TS2). In the image are highlighted some important distances between the residues from the active site of the enzyme, the cofactor and the substrate.

The transition state of the second step (TS2 – Figure 30) is characterized by one imaginary frequency at 1028.7i cm^{-1}. Hydrogen H12 (0.06 a.u.) is now closer to the sulfido SO (-0.23 a.u.) (1.6Å versus 2.3Å in IM1), at the same time that the distance between oxygen OR and the Mo ion slightly increases from 2.0Å in IM1 to 2.05Å and the distance between the OR and C11 from XAN decreases from 1.5Å to 1.4Å.

A lot of speculation and discussion subsists in this step. It is not known if hydrogen H12 is transferred to carbon C11 as a hydride, a hydrogen or a proton. The computational calculation shows that in the transition state of this step (TS2), H12 has a charge of -0.01 a.u., indicating that it is transferred to the sulfide SO atom as a

hydrogen atom. Between the IM1 and TS2 minima, there are also no significant changes between the charged of the sulfido (-0.27 a.u. versus -0.23, respectively).

In the product of the second step (IM2 – Figure 29), hydrogen H12 (-0.01 a.u.) is now covalently bonded to sulfur SO (1.4Å versus 2.3Å in the reactants) that is coordinated to the Mo ion (-0.27 a.u.). Carbon C11 from XAN adopts a fully planar sp2 geometry (tetrahedral in IM1) and remains covalently bonded to oxygen OR that is coordinated to the Mo ion. Comparing to the reactant of this step, the distance between these two atoms decreased from 1.5Å to 1.3Å. This bond distance is commonly found in carbonyl group. However, in this case we cannot say that the reaction intermediate in IM2 has already disconnected from Moco, since the Mo ion is still very close to the oxygen OR (2.2Å).

In the product of this this step, it is observed a charge transfer from XAN to Moco while the hydrogen atom transfer is completed. This means that only in this step we observe the reduction of the Mo ion from Mo(VI) to Mo(IV) and the oxidation of XAN. This effect can be seen looking at the total charged of the Moco that goes from -0.76 a.u. in the IM1 to -1.16 a.u. in IM2, as it is illustrated in Figure 23.

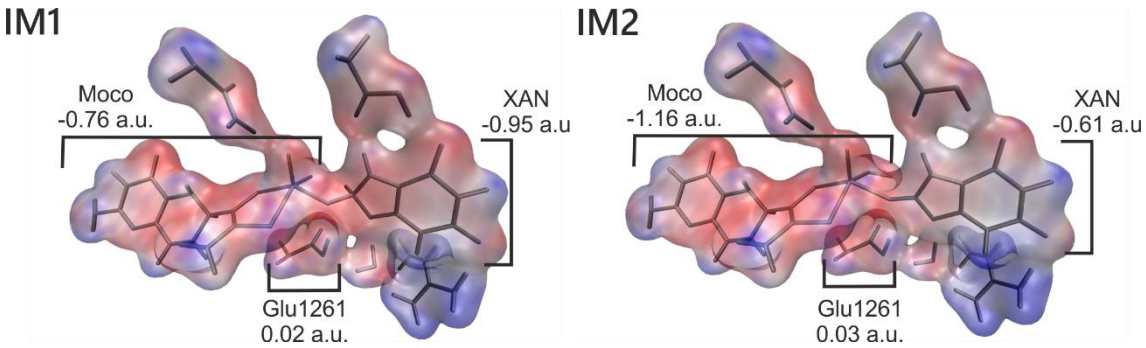

Figure 23 - Electrostatic potential, for step 2, of the reactant and product of the reaction using the high-layer of the QM/MM model. The isosurfaces were calculated using gaussian09. Blue regions represent the positive charged atoms and in red the regions where the negative charges atoms are located at.

In the same structure, it is also observed a new organization of some hydrogen bonds. The hydrogen bond provided by the water molecule Wat3366 and was stabilizing the negative charge of nitrogen N8 of XAN in the reactants has now increased from 1.7Å to 1.8Å. The same effect is also observed between the hydrogen bond

between XAN and Glu802 increasing from 1.9Å to 2Å. This happens due to the charge transfer from the XAN to Moco that no longer demands a great stabilization of XAN. This effect helps to endorse the release of the product of the reaction that will occur in the next steps.

This step has a very small free activation energy ($\Delta G^{\ddagger}$) of 3.9 kcal mol^{-1} and the reaction is exoenergonic ($\Delta_r G$) in -18.3 kcal mol^{-1}.

5.2.1.3 Discussion

The first part of the catalytic mechanism of XO involves the substrate binding to Moco and a hydrogen atom transfer, from which results a reaction intermediate that is very close to the product of the full reaction.

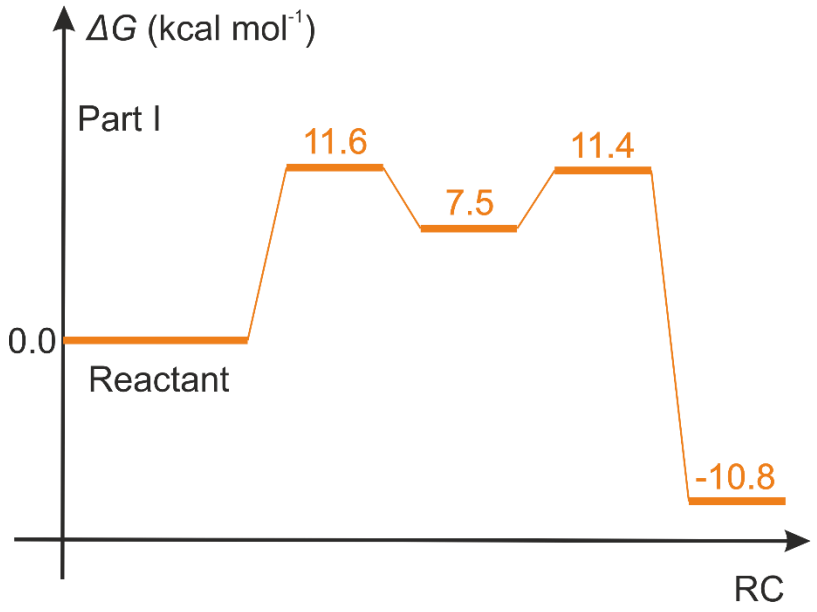

Figure 24 – Free Energetic Profile of the first two steps of the catalytic mechanism of XO.

During these two steps there is a charge transfer from Glu1261 to XAN and afterwards from XAN to Moco. This means that the Mo cofactor only becomes reduced to Mo(IV) after the second step of the catalytic process.

The energetic profile of the first two steps is displayed in Figure 24. The overall reaction is exoenergonic in 10.8 kcal mol^{-1}. The first is endoenergonic, but the activation energy is below the experimental k_{cat} (15.72 kcal mol^{-1}).

These results show that after these two steps the mechanism is not reversible, since it would require an activation energy above 22 kcal mol^{-1} which would difficulty occur at physiological conditions. This agrees with the experimental observations, from which it has been observed that the formation of xanthine from the uric acid is not possible, due to the diverse of diseases associated to the excess of uric acid.

The results obtained with these two steps also allow to justify the importance of Glu802 and Glu1261 in the catalytic mechanism. Glu802 allows the correct orientation of XAN in the active site and allows the stabilization of the negative charge that is formed in the reaction intermediate. Glu1261 assists the coordination of Xan to Moco.

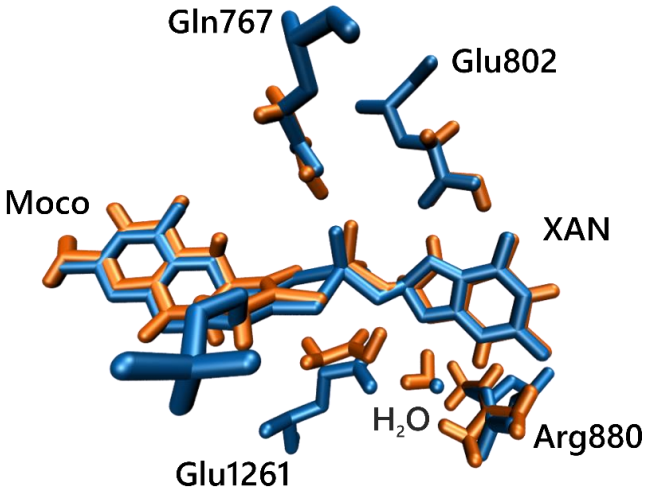

Figure 25 - Comparison between 3AMZ (blue) and QM/MM model (IM1) used in this work (orange). RMSD for whole protein backbone is 1.14Å

The product of the first step (IM1) of the proposed catalytic mechanism can be almost superimposed to the X-ray structure with the PDB code 3AMZ. The RMSD between both structures is very small (1.14Å) (Figure 25). This result is very important since it resembles a reaction intermediate that was obtained by X-ray crystallography [57].

5.2.2 Part II – Protonation and product release

The second part of the catalytic mechanism of XO involves the formation of the product of the reaction, uric acid (URC), and its subsequent release from the active site to the solvent.

Initially, it was suggested that the release of URC was a concerted step, i.e., while the covalent bond between the Mo ion and oxygen OR is broken, the release of URC would take place. The theoretical results have however shown that this could not be possible, since the calculated energetic profiles for the simulated reaction were always above 25 kcal mol^{-1} and no transition state could be located.

Our initial results have shown that the release of the URC would only be possible after the protonation of XAN. This can be achieved by different mechanistic proposals that are described in the following sections (step 3). Only afterwards, the release of the product of the reaction takes place (step 4).

5.2.2.1 Step 3: Proton transfer

There are three different mechanistic proposals can be drawn for the proton transfer, accordingly to Figure 26:

- Pathway A: The proton transfer from Arg880 to nitrogen N8 from XAN, through Wat3366.
- Pathway B: The proton transfer from Glu1261 to nitrogen N8 from XAN directly.
- Pathway C: Intramolecular proton transfer between nitrogen N8 and N4 from XAN, through Wat3366.

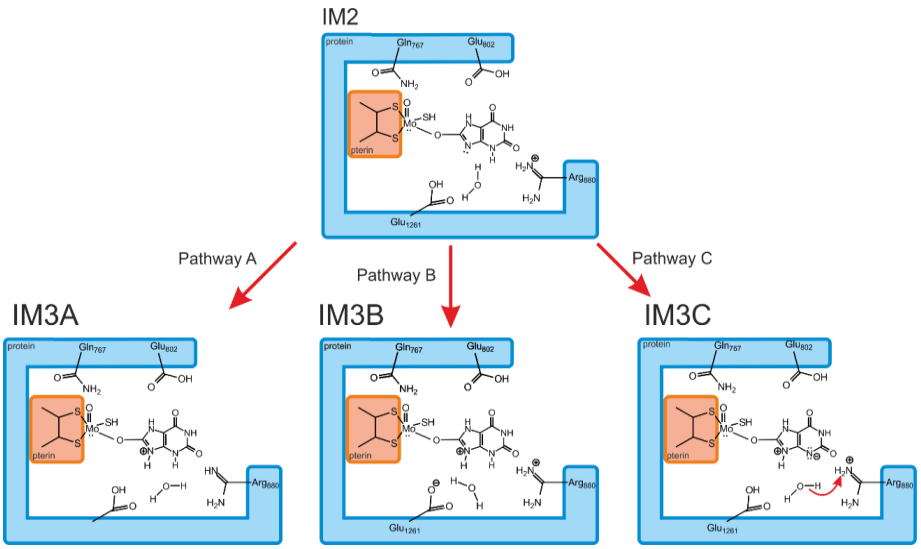

Figure 26 – Diagram of possible outcomes of proton transfer in step 3

Each of these mechanistic proposals interferes with the bottom region of the active site and have different mechanistic outcomes. Hypothesis A leads to the formation of neutral Glu1261-Wat3366-Arg880 triad, hypothesis B a charged catalytic triad and, hypothesis C a semi-charged triad. Each of these proposals are described below.

A. Pathway A (Neutral pathway)

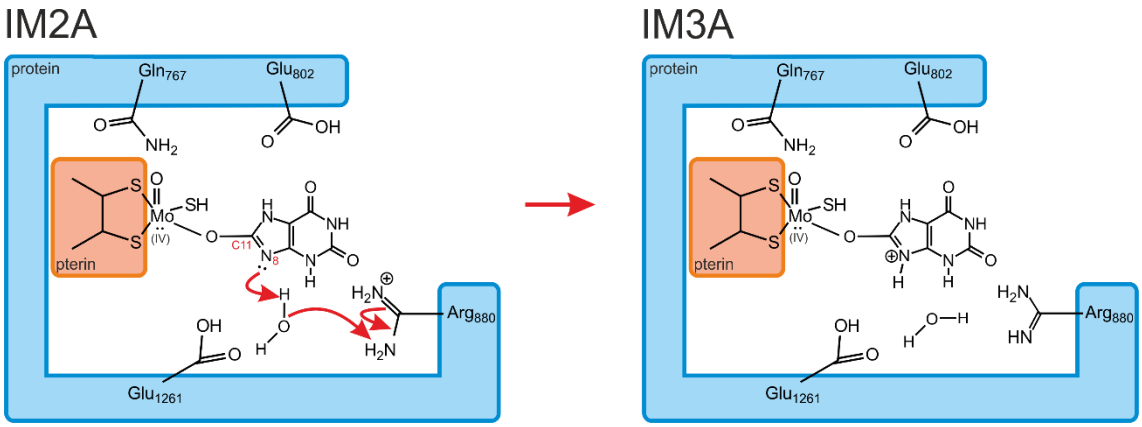

Figure 27 - 2D representation of the reaction's third step (neutral pathway), showing the reactant (IM2A) and the product (IM3A).

Hypotheses A involves the proton transfer from Arg880 to nitrogen N8 from XAN through Wat3366 (Figure 27). Since in the end of this reaction Glu1261 and ARG880 become neutral, this mechanism is also called the neutral pathway.

In the reactant of this step (IM2A – Figure 35), XAN continues to be stabilized by four hydrogen bonds endorse by Arg880, Wat3366 and Glu802. The water molecule, Wat3366, is well aligned between Arg880 (2Å) and nitrogen N8 of XAN (1.9Å) to promote the intermolecular proton transfer. The charge continues to be lodged at the Moco cofactor (-1.16 a.u.) and XAN (-0.55 a.u.).

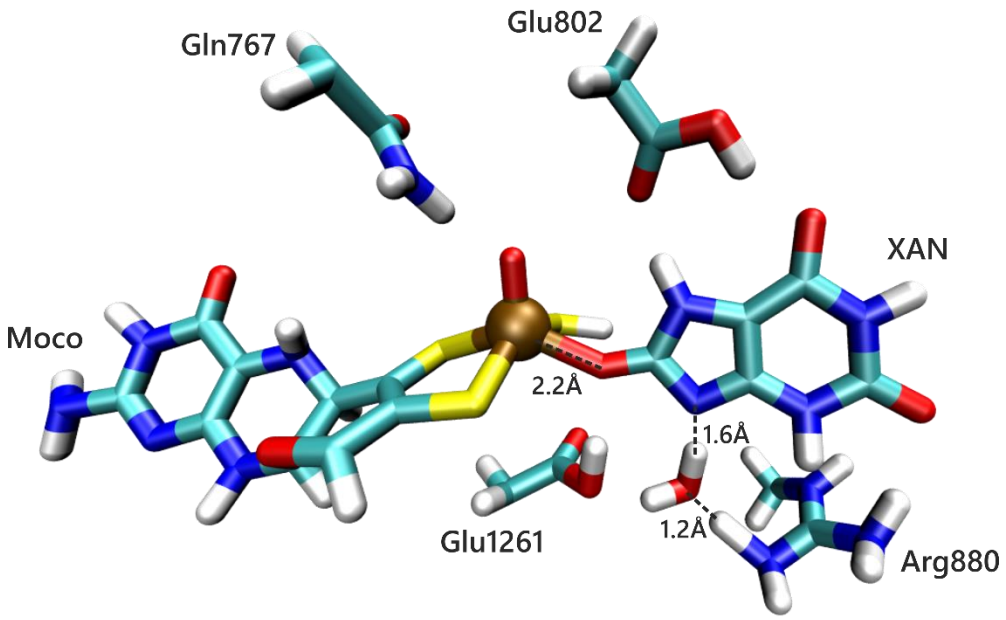

Figure 28 - Transition state of the third of the catalytic mechanism of XO, pathway A (TS3A). In the image are highlighted some important distances between the residues from the active site of the enzyme, the cofactor and the substrate.

The transition state of pathway A (TS3A – Figure 28) is characterized by one imaginary frequency at -591 cm^{-1}. In this structure, one of the hydrogen atoms from the water molecule is already half the way towards nitrogen N8 from XAN. One of the protons from Arg880 is also already very close to the oxygen from the water molecule (1.2Å in TS3A versus 2Å in IM2A). It is also observed a small conformational

rearrangement of Arg880, that in the TS no longer interacts with oxygen O5 from XAN (1.9Å in IM2A to 2.2Å in TS3A).

In the product of this reaction (IM3A – Figure 27), the proton transfer from Arg880 to XAN is complete forming URC. However, it does not dissociate from the Mo ion (2.2Å in IM3A). This happens because of the positive charge that is generate at nitrogen N8 and it is in resonance with carbon C11 from XAN. In the end of this step Arg880 becomes neutral (0.00 a.u. in IM3A versus 0.55 a.u. in IM2A).

This step has a free activation energy ($\Delta G^{\ddagger}$) of 3.9 kcal mol^{-1} and the reaction is exoenergonic ($\Delta_r G$) in -11.4 kcal mol^{-1}.

B. Pathway B (Charged Pathway)

Hypothesis B also leads to the formation of the uric acid but using a different mechanism. In this case the protonation occurs directly from Glu1261 to nitrogen N8 from XAN and does not require the participation of the water molecule. This step is also called the charged pathway because in the end of the process Glu1261 becomes negatively and Arg880 remains positively charged.

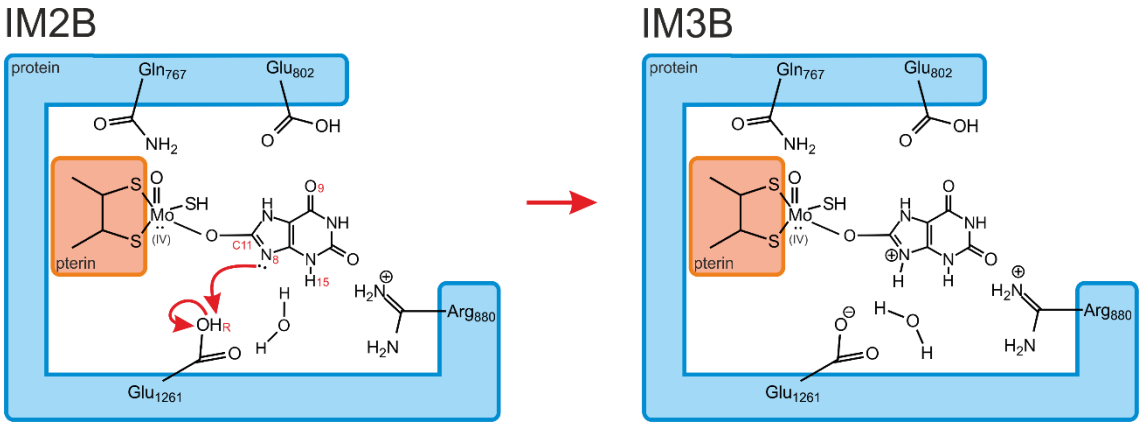

Figure 29 - 2D representation of the reaction's third step (charged pathway), showing the reactant (IM2B) and the product (IM3B).

In the reactant of pathway B (IM2B – Figure 29) one of the oxygens from Glu1261 is very close to nitrogen N8 from XAN and interact with it by a short hydrogen bond ($B_{Glu1261\text{-}N8}$=1.8Å). In this reaction, the water molecule Wat3366 continues to interact with Glu1261 ($B_{wat\text{-}Glu1261}$=1.8Å) through a hydrogen bond, but no longer though the hydroxyl group but instead through the other oxygen atom. It is also observed that the hydroxyl group from Glus802 no longer has a hydrogen bond with O9 from XAN (2Å in IM2 versus 2.9Å in IM2B). All the other hydrogen bonds remained the equal to what was observed in the product of step 2.

The transition state of pathway B (TS3B – Figure 30) is characterized by an imaginary frequency at 826.6i cm^{-1}. The proton HR from Glu1261 is already half the way and very close to nitrogen N8 from XAN (1.3Å). At the same time, it is also observed the formation of a new hydrogen bound between the water molecule, Wat3366 and hydrogen H15 from XAN ($B_{H15\text{-}wat}$=1.9Å).

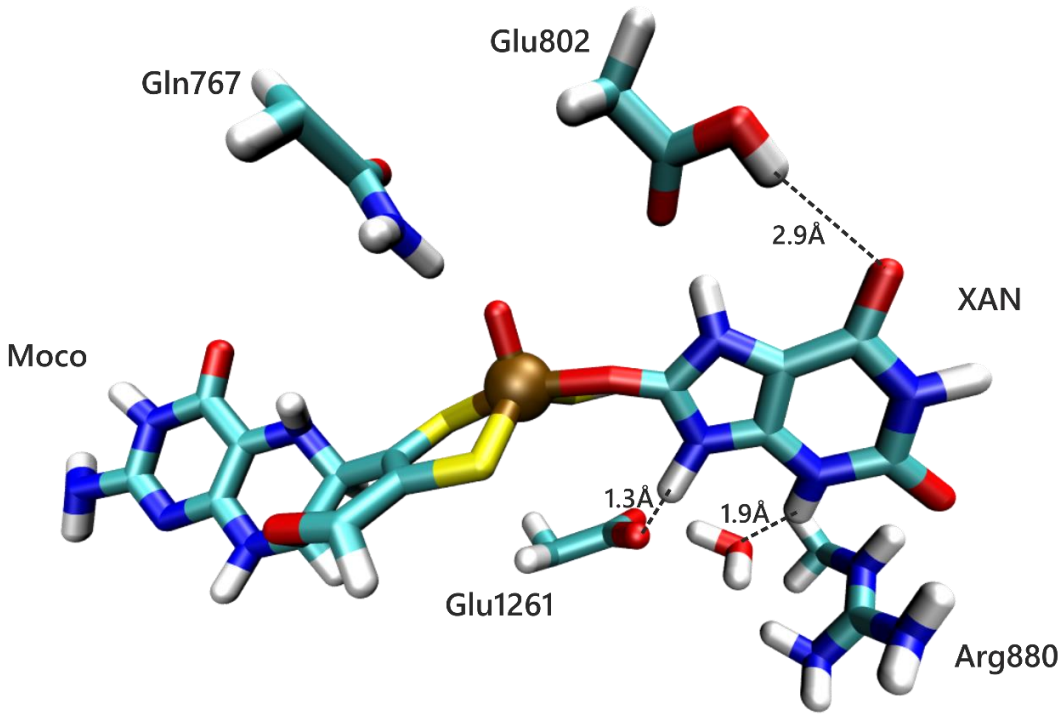

Figure 30 - Transition state of the third of the catalytic mechanism of XO, pathway B (TS3B). In the image are highlighted some important distances between the residues from the active site of the enzyme, the cofactor and the substrate.

In the product of this reaction (IM3B – Figure 29) the proton HR from Glu1261 (-0.54 a.u. in IM3B versus -0.06 in IM2B) is now covalently bonded to nitrogen N8 from XAN (1.1Å, versus 1.7 Å in the reactants) from which results URC (-0.13 a.u. versus -0.60 a.u. in IM2B). Similarly, to what was found in the mechanism from pathway A, URC continues to be coordinated to the Mo ion, and the positive charge generated in nitrogen N8 has a resonance with carbon C11 from XAN. Glu1261 becomes negatively charged (-0.57 a.u.) and Arg880 remains positively charged (0.81 a.u.) as in the reactant. In the end of the reaction, the water molecule continues to interact very closely with hydrogen H15 of URC ($B_{H15\text{-}wat}$=1.8Å).

This step has a free activation energy ($\Delta G^{\ddagger}$) of 1.8 kcal mol^{-1} and the reaction is endoenergonic in ($\Delta_r G$) 2.6 kcal mol^{-1}. The fact that the reaction free energy has a higher value than the activation free energy can be attributed to the error that is inherent to the DFT used in the high layer of the QM/MM calculation and it is estimated to accounts for 3 kcal/mol. Considering the energies involved in this step we can say that is should be very fast and almost thermo-neutral.

C. Pathway C (Semi-Charged pathway)

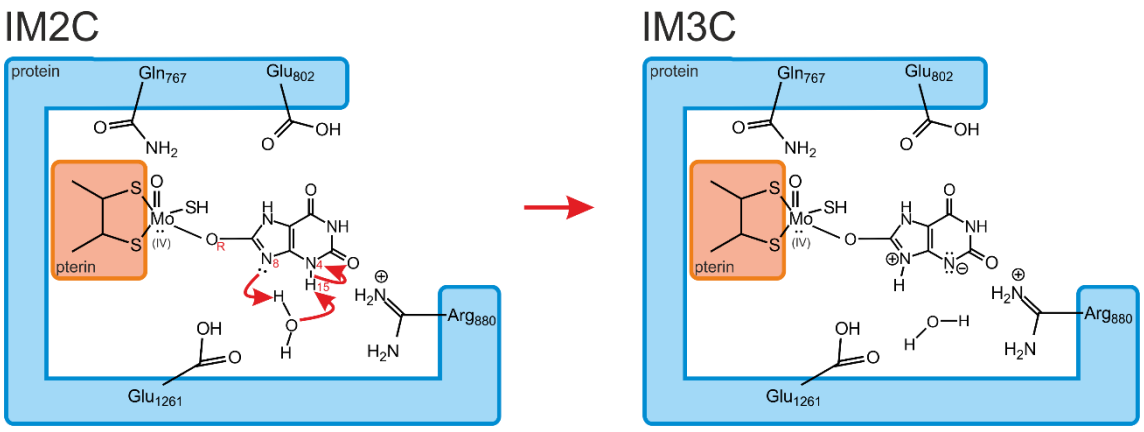

Figure 31 - 2D representation of the reaction's third step (semi-charged), showing the reactant (IM2C) and the product (IM3C).

Hypothesis C involves a semi-charged mechanism. It involves the intra molecular proton transfer between nitrogen N4 to nitrogen N8 of XAN, through the water molecule, Wat3366, and does not require the participation of either Glu1261 or Arg880.

In the reactant of pathway C (IM2C – Figure 31), the position of the water molecule Wat3366 is stabilized by a hydrogen bond provided by another water molecule that is located very close to the active site, Wat3273 ($B_{wat-wat}$=1.8Å). This new position allows the water molecule Wat3366 to interact very closely with hydrogen H15 and nitrogen N4 of XAN (2Å and 1Å, respectively). In this new rearrangement Glu1261 no longer establishes a hydrogen bond with oxygen OR from XAN ($B_{Glu1261-OR}$=2Å) and now is making a hydrogen bond with nitrogen N8 of XAN ($B_{Glu1261-N8}$=2Å).

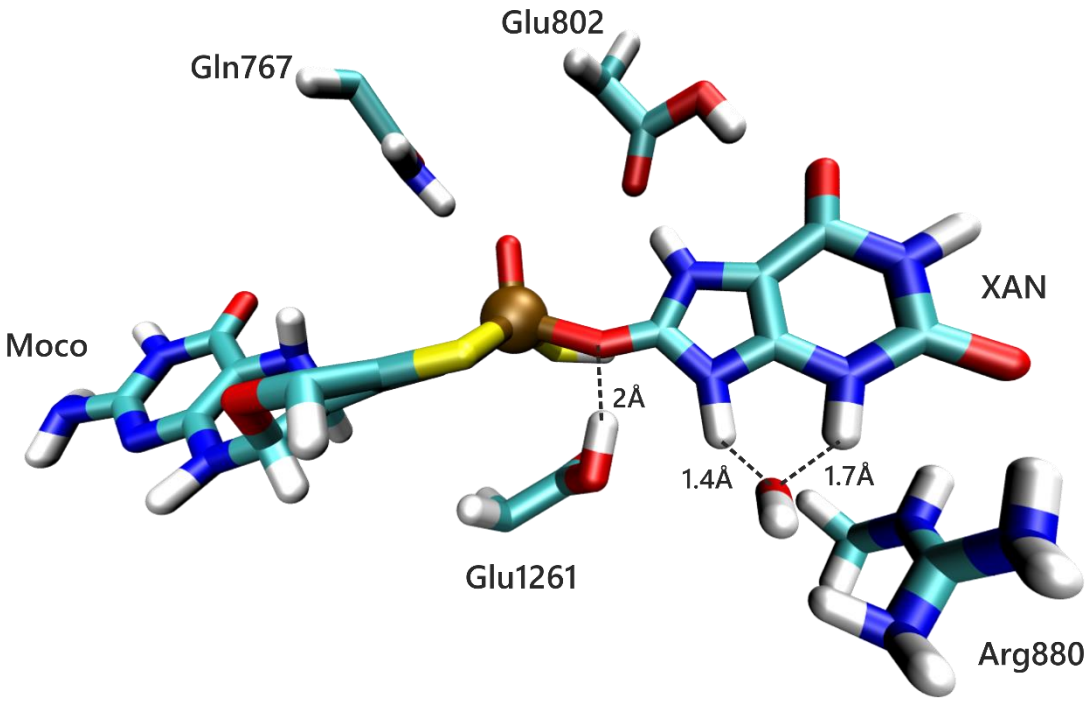

Figure 32 - Transition state of the third of the catalytic mechanism of XO, pathway C (TS3C). In the image are highlighted some important distances between the residues from the active site of the enzyme, the cofactor and the substrate.

The transition state of pathway C (TS3C – Figure 32) is characterized by an imaginary frequency at 680.7i cm^{-1}. Here, the hydroxyl group from Glu1261 undergoes a conformational rearrangement and now interacts with oxygen OR of XAN ($B_{Glu1261-OR}$=2Å). The water molecule already lost its proton to nitrogen N8, at a distance of 1.4Å, but at the same time hydrogen H15 from XAN (0.38 a.u.) started to get closer to the oxygen (-0.87 a.u.) from water molecule (1.7Å in TS3C versus 2Å in the IM2C).

In the product of this reaction (IM3C – Figure 31), the proton H15 from XAN has already passed onto the oxygen from the water molecule Wat3366, but maintains the hydrogen bond interaction with nitrogen N4 from XAN (B_{wat-N4}=1.8Å). The pathway is called the semi-charged pathway because Arg880 remains positively charged (0.78 a.u), whereas the charge of Glu1261 remains neutral (0.03 a.u.).

Pathway C has the highest activation energy of all the described pathways ($\Delta G^{\ddagger}$ = 11.2 kcal mol^{-1}) although the reaction is the highest exoenergonic ($\Delta_r G$) with -17.2 kcal mol^{-1}. This final structure is very similar to what was obtained in the mechanism of Metz and Thiel.

D. Interconversion between Pathway A, B and C

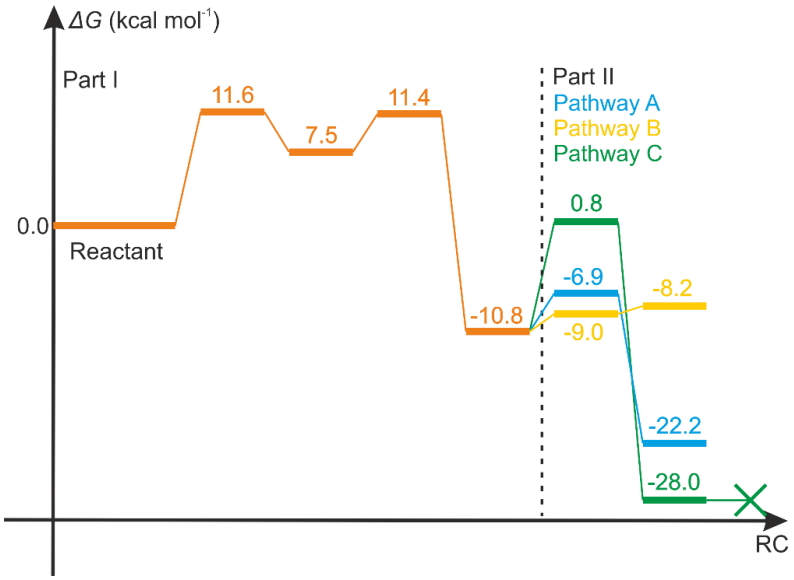

Figure 33 - Energies from all step 3 pathways

The energetic profiles of all the pathways that were studied revealed that the most favorable mechanisms are the ones from pathways A and C from the thermodynamic point of view. Pathway B is more favorable from the kinetic point of view. At this point is very difficult to analyze which of the pathways should be more favorable since any of them can occur under physiological conditions.

Since all the products of each pathway lead to the formation of the same reaction intermediate, i.e. the uric acid covalently bonded to the Mo ion, and only differ in the protonation state of the residues located in the bottom of the active site, Glu1261 and Arg880, we also investigated if these minima could be interconverted among them (IM3A, IM3B and IM3C).

The conversion between IM3C to IM3A involved the proton transfer from Arg880 to the nitrogen N4 from XAN. This reaction is slightly endothermic (ΔE_r = 1.9 kcal mol^{-1}) but it requires a high energy of activation (ΔE_a = 19.2 kcal mol^{-1}).

The conversion between IM3B in IM3A, required the proton transfer through the water molecule, from Glu1261 to Arg880. We observed that the final product of this reaction ends up falling in the product of IM3C (Figure 34). This reaction requires a small activation energy of (ΔE_a = 1.2 kcal mol^{-1}) and the reaction is very exothermic (ΔE_r = -10.9 kcal mol^{-1}).

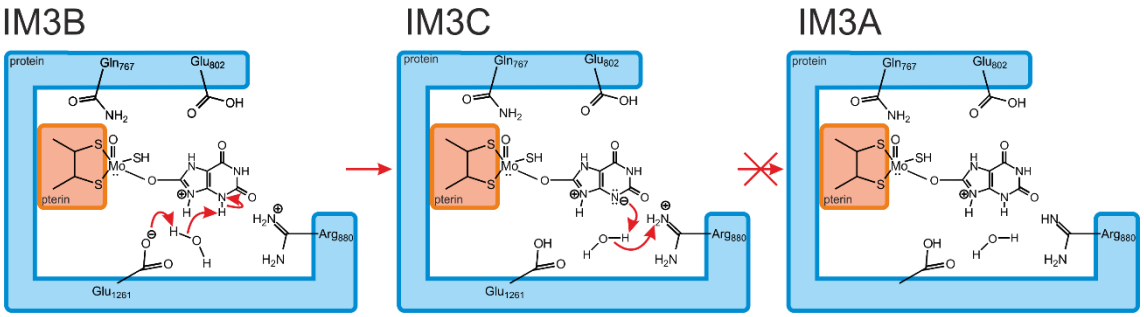

Figure 34 - Diagram of the conversion of IM3B to IM3C and in IM3A

These results indicate therefore that only pathways A and B can lead to the continuation of the mechanism and the ones that will be used to continue the study of the catalytic mechanism. The product of the reaction of pathway C is very similar to the minimum that was obtained by Metz and thiel and from which the release of URC was found to be not possible, similarly to what was found be us.

In pathway A we can again see the importance of Arg880 in the mechanism. This goes in line with the results of Yamaguchi and colleagues and indicates that Arg880

does not only plays an active role in binding of XAN to the Mo ion but also in the formation of uric acid.

5.2.2.2 **Step 4:** Release of the product of the reaction (URC)

In the previous step, it was found that the formation of the uric acid is not concomitant with its release from the active site. The previous calculations show that after the formation of this molecule, it still remains connected to the Mo ion and an additional step is required to complete this reaction.

Since in the last step it was found that only pathways A and B are the most favorable ones, we studied the release of URC in both scenarios. Each of these reactions are described below.

A. Pathway A (Neutral pathway)

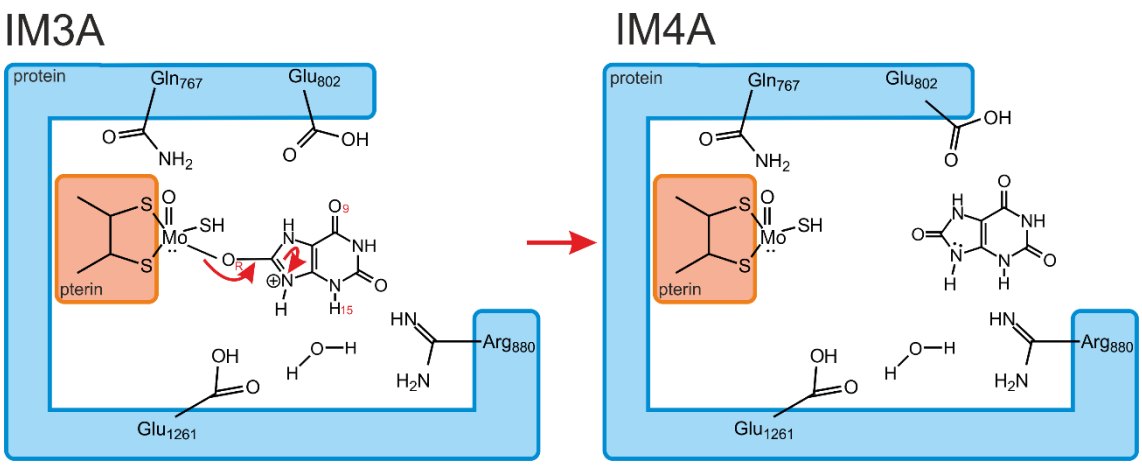

Figure 35 - 2D representation of the reaction's fourth step (neutral pathway), showing the reactant (IM3A) and the product (IM4A).

In pathway A, both Glu1261 and Arg880 are in the neutral state. The release of URC was tested by increasing the distance between Mo (0.38 a.u.) and the oxygen OR (-0.48 a.u.) from URC. There are no differences between the reactant of this step and the

product of the last step of the same pathway (IM3A) (Figure 35). The network of hydrogen bonds around the active site remain unaltered.

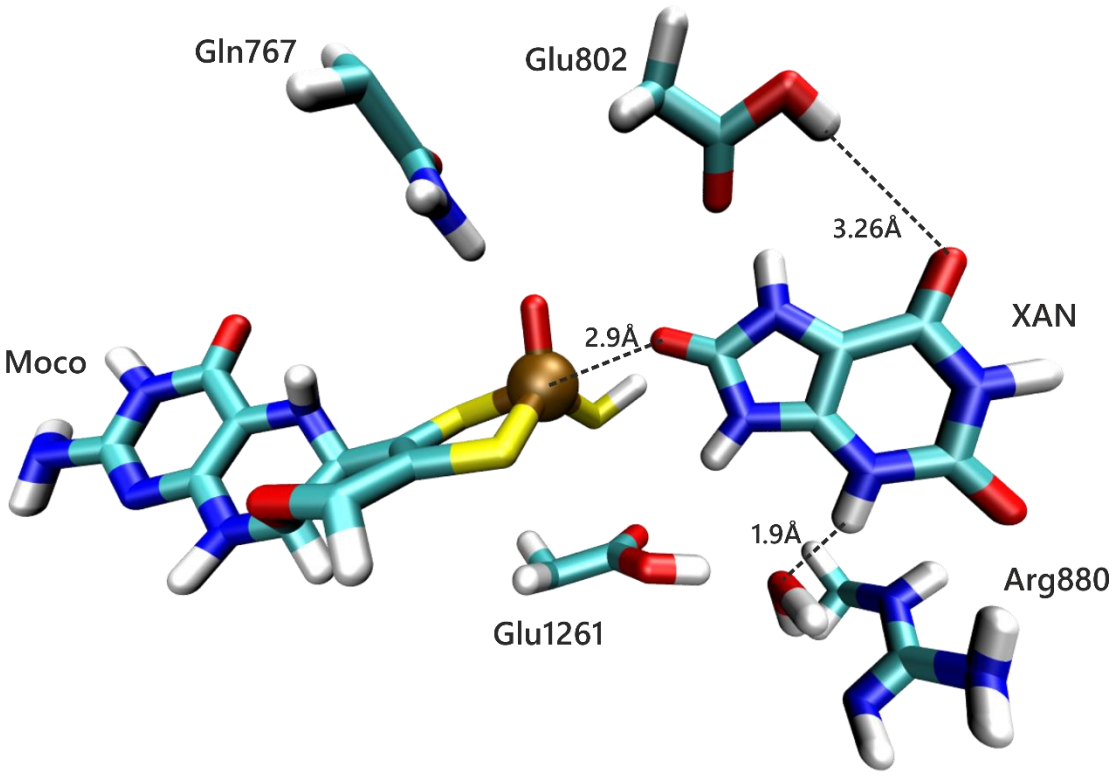

Figure 36 - Transition state of the fourth of the catalytic mechanism of XO, pathway A (TS4A). In the image are highlighted some important distances between the residues from the active site of the enzyme, the cofactor and the substrate.

In the transition state of this pathway (TS4A – Figure 36), the distance between Mo and oxygen OR from URC increased from 2.1Å in IM3A to 2.9Å. This endorses conformational change in Glu802 that no longer interacts with oxygen O9 from URC by a hydrogen bond. Instead, the water molecule Wat3366 starts to interact with hydrogen H15 from URC by a hydrogen bond ($B_{H15\text{-}wat}$=1.9Å).

In the product of this reaction (IM4A – Figure 35) the bond between to Mo ion and oxygen OR from URC is cleaved and they become apart in 3.7Å. The cleavage of this bond is helped by Glu802 that exchange between an axial conformation to an equatorial conformation.

This reaction has an activation energy of (ΔE_a) of 7.2 kcal mol^{-1} and a reaction energy of (ΔE_r) of -3.3 kcal mol^{-1}.

B. Pathway B (Charged Pathway)

In pathway B, Glu1261 and Arg880 are negatively and positively charged, respectively.

In this pathway, the cleavage of URC is not obtained in a single step as it was found in pathway A. Instead, two sequential steps were obtained. In the first step, there is a conformational rearrangement of Glu802, that is almost a thermoneutral process. Only afterwards takes place the release of URC.

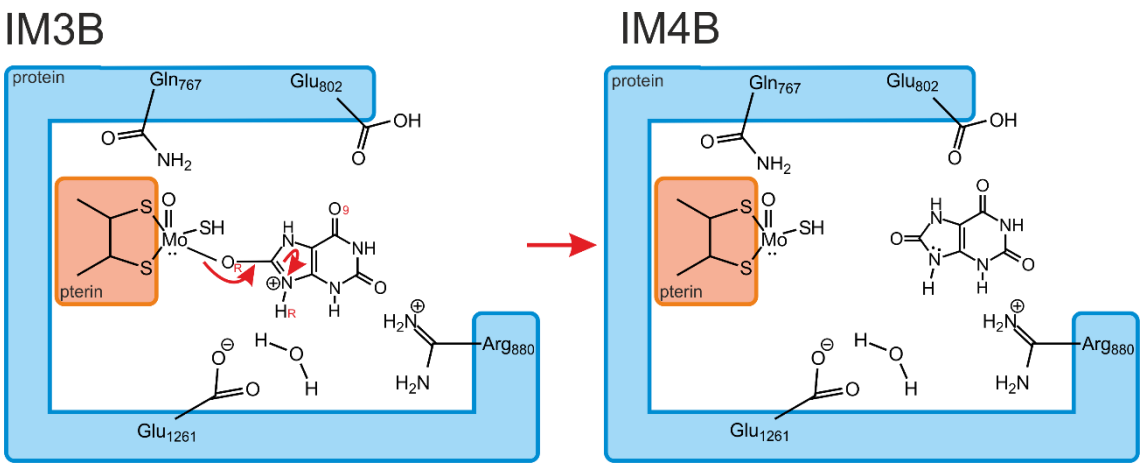

Figure 37 - 2D representation of the reaction's fourth step (charged pathway), showing the reactant (IM3B) and the product (IM4B).

In the reactant of this step (IM3B - Figure 37) is very similar to the product of the previous step. The only difference is the absence of one hydrogen bond between the hydroxyl group of Glu802 with oxygen O9 from URC.

In the transition state of this step (TS4B – Figure 38), the distance between Mo ion and oxygen OR from URC increased from 2.2Å to 3.2Å. Relative to the hydrogen

bonds, only one significant change is observed. Hydrogen HR from URC no longer interacts with Glu1261, as it was found in the reactants (2.1Å versus 1.7Å in IM3B).

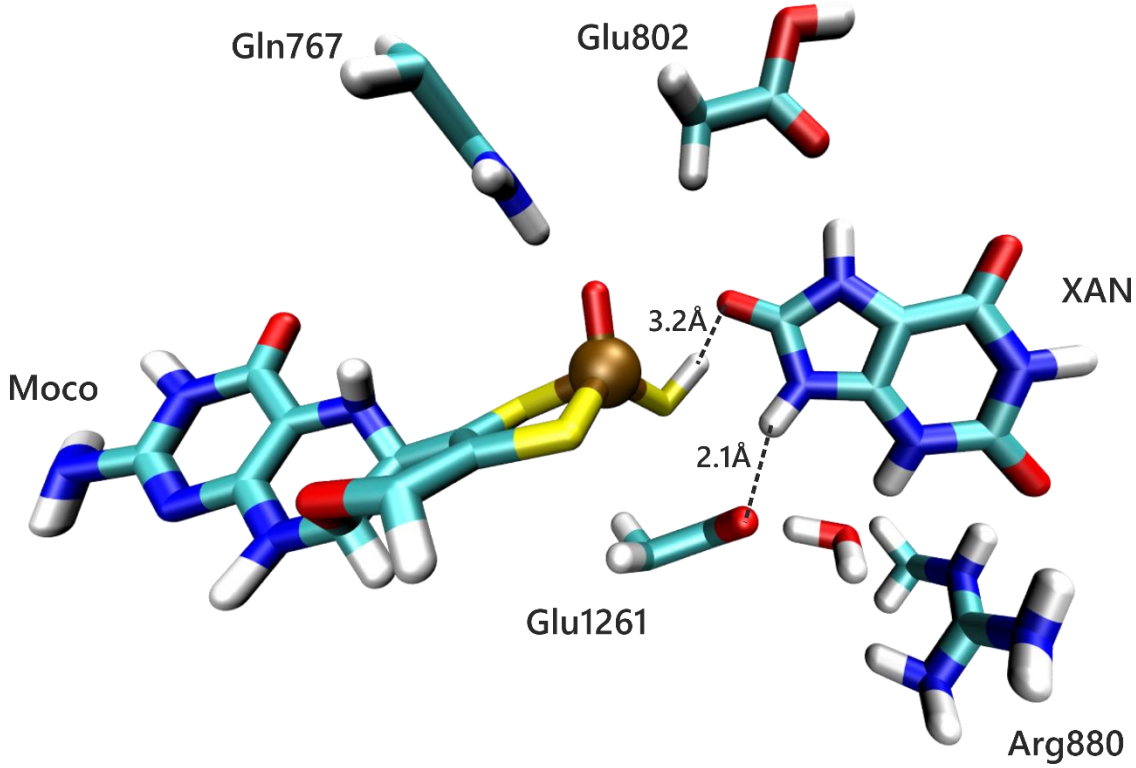

Figure 38 - Transition state of the fourth of the catalytic mechanism of XO, pathway B (TS4B). In the image are highlighted some important distances between the residues from the active site of the enzyme, the cofactor and the substrate.

In the product of this step (IM4B – Figure 37) the distance between Mo and OR from URC increases to 3.5Å, notably this release is harder due to the charged residues, than in pathway A (3.5Å versus 3.7Å in pathway A).

This step has an activation energy (ΔE_a) of 7.6 kcal mol^{-1} and a reaction energy (ΔE_r) of 4 kcal mol^{-1}.

5.2.2.3 Discussion

Looking to the energies of both pathways for step 4 (Figure 39), it is easy to notice that only one of the two has an exothermic reaction, which is the pathway A. However, one can notice that both pathways have similar activation energies.

The release of URC from the charged pathway requires a higher activation energy, probably due to the fact that the amino acid Glu1261 and Arg880 charges attract more the product to the active site, whereas when they are found in the neutral the release is easier.

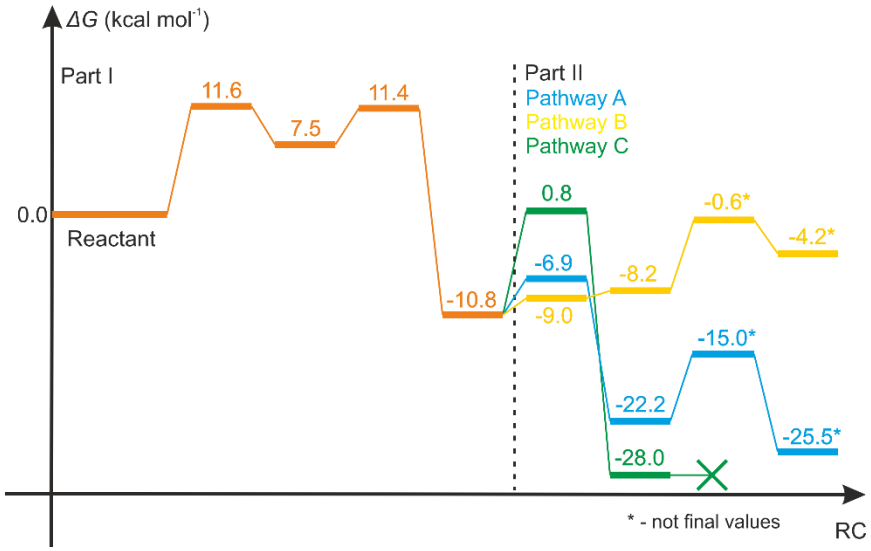

Figure 39 - Energy chart from the pathways used in step 4

In pathway A the distance between the Mo ion and oxygen OR from URC is of 2.1Å in IM3A and 3.7Å in IM4A, while the pathway B these distances are 2.2Å in IM3B and 3.5Å in IM4B. This value indicates that in pathway B, the distance from Moco and URC is shorter, but this may be due to the charges in the active site (Glu1261 and Arg880) that when optimizing the structure came closer to these residues, this may also be why the reaction is endoenergonic. Relativity to pathway A, the product optimized further away from the Moco center because there are no charges in the residues from

the active site, which contribute for a favorable release that is proved by the reaction energy values obtained (-3.3 kcal mol^{-1})

5.2.3 Part III – Enzymatic Turnover

Once URC leaves the active site, the Moco contains a reduced Mo(IV) ion. The bottom region of the active site continues to be composed by the catalytic triad formed by Glu1261, Wat3366 and Arg880 that are interconnected by hydrogen bonds.

The next step of the catalytic mechanism involves the oxidation of the active site, the reaction of Moco with a water molecule and subsequent enzymatic turnover.

Facing the results from the previous step, and even though, the best pathway from step 4 was IM4A, both models from the previous step (IM4A and IM4B) were used for study the enzymatic turnover.

Also, since there is no consensus if the oxidation of the active site occurs after or prior to the reaction of the water molecule, both situations were also studied.

5.2.3.1 Step 5: Oxidation of the Moco

The theoretical calculations have shown that the water molecule can only react with the Mo ion when the Moco is oxidized (MO(VI)). The approximation of the water molecule to Mo(IV) is characterized by an exponential increase in the energy where no transition state can be identified. These results occur whenever pathway A (neutral) or pathway B (charged) is followed.

This result indicates that, prior to the reaction of the water molecule, two electrons must exit Moco through the FeS centers and reach FAD. Only afterwards the catalytic mechanism can continue.

5.2.3.2 Step 6: Reaction of Moco with Water

The reaction of the water molecule was studied with Mo(VI) and in the two pathways that results from the previous steps. In pathway A, the Glu1261 and Arg880 are in a neutral state, in pathway B these to residues are negatively and positively charged, respectively.

A. Pathway A (neutral pathway)

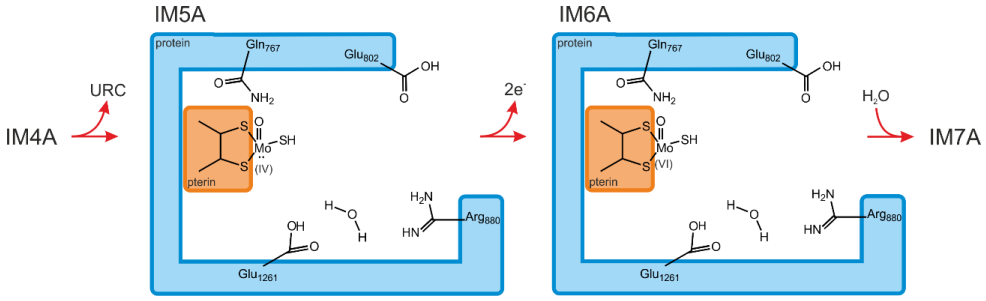

Figure 40 - Representation of URC and electrons release and the entrance of solvent in the active site (H_2O) for pathway A

After the release of URC to the solvent and the Moco (Figure 40) has been oxidised, the water molecule enters the active site, and becomes lodged close to the Mo ion. The position of the water molecule is stabilized by Glu1261 that established a hydrogen bond with it. However, with this model we were not able to react the water molecule with the Mo ion. This happens because Glu1261 is protonated and therefore could not activate the water molecule to favor that reaction.

B. Pathway B (charged pathway)

In this model Glu1261 is not protonated and therefore it can help the nucleophilic attack of the water molecule to the Mo ion. The computational calculation has shown however, that in the reactant of this reaction there is an almost spontaneous

transfer of the proton of the sulfido to Glu1261 (Figure 41). The water molecule continues to be close to the Mo ion (2.3Å) and is stabilized by the Glu1261 by a hydrogen bond ($B_{wat\text{-}Glu1261}$=1.9Å) (Figure 42, IM7B). In spite of this reaction, this model allows the water molecule to become covalently bonded to the Mo ion. This happens because at the same time that the water molecules get closer to the Mo ion the proton from Glu1261 migrates again to the sulfido.

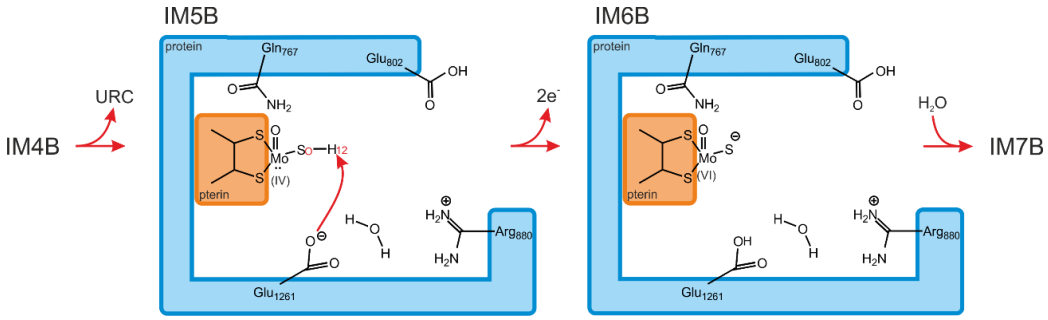

Figure 41 - Representation of URC and electrons release and the entrance of solvent in the active site (H_2O) for pathway B

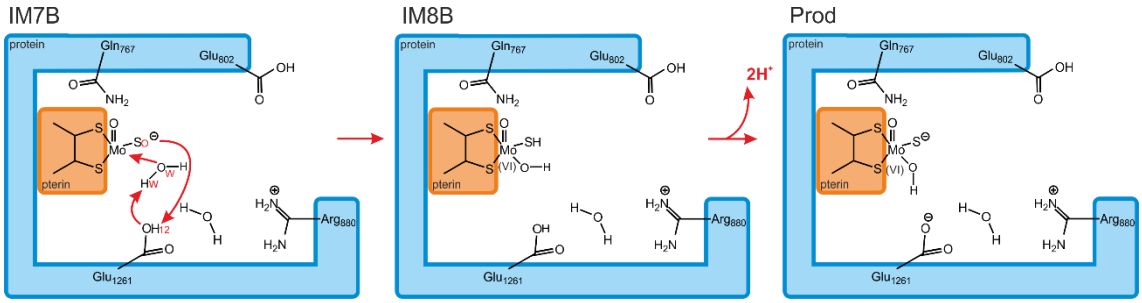

Figure 42 - 2D representation of the reaction's fourth step (charged pathway), showing the reactant (IM7B) and the product (IM8B) and the regenerate active site (Prod).

The transition state of this step (TS8B – Figure 43) was isolated with an imaginary frequency of 700.1i cm^{-1}. The distance between Mo ion and the oxygen OW slightly decreased to 2.2Å. Here, the distance between the proton from the new water molecule HW, is a lot closer to Glu1261 (1.2Å versus 1.9Å in IM7B) and at the same time, the proton H12 from the sulfido is already very close to one of the oxygens of Glu1261 (1.4Å in IM4Bm versus 2.3Å in the reactants).

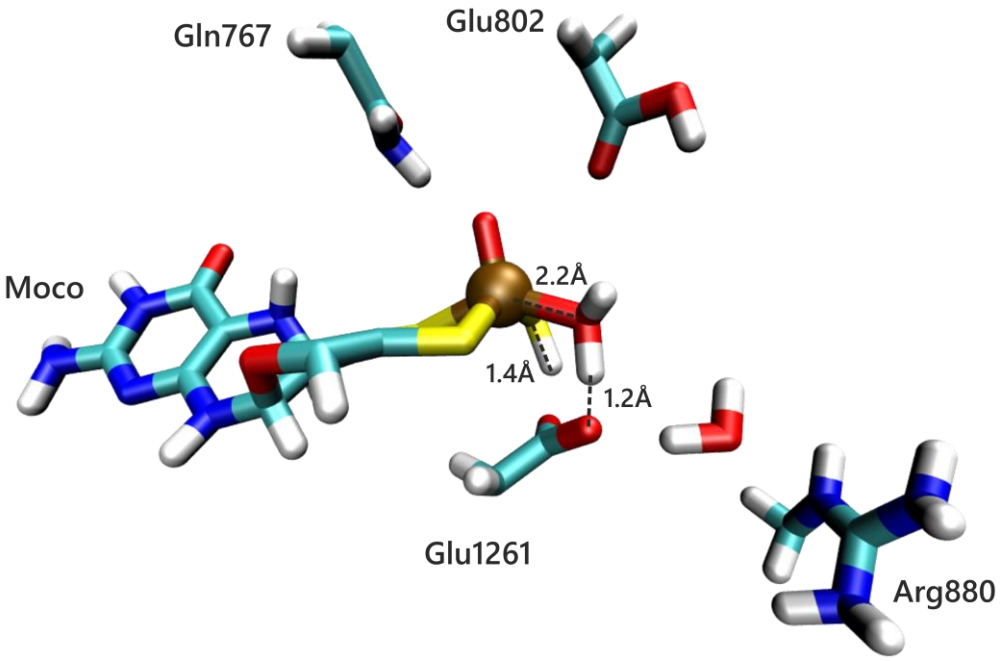

Figure 43 - Transition state of the water turnover of the catalytic mechanism of XO, pathway B (TS8B). In the image are highlighted some important distances between the residues from the active site of the enzyme, the cofactor and the substrate.

In the product of this step (IM8B – Figure 42), the hydroxyl group is bonded with Mo ion (2.1Å versus 2.3Å in IM7B) and the proton transfer that start to happening in TS8B have now been completed. The proton HW is now connected to Glu1261 (1Å) and the sulfido SO has become again protonated (1.4Å).

After this step two protons will be loss to the solvent (proton HW and H12), regenerating the XO's active site for a new cycle (Prod – Figure 42).

C. Alternative pathway to pathway B

Above we saw that, the proton H12 was connected to the sulfido SO in IM5B but at IM6B it is bonded to Glu1261 (Figure 44), before the water molecule connects with the Mo ion. However, the same proton goes back to the sulfide SO after the water molecule becomes coordinated to the Mo ion. This ping-pong mechanism is spontaneous and therefore we believe that the two protons are not released simultaneously but they are release in a stepwise fashion. In Figure 44, it is represented the Pathway B and its alternative pathway (IM8T and IM9T).

The energies from this alternative pathway are being studied in order to compare if one pathway is more favorable than the other, from the kinetic and thermodynamic point of view.

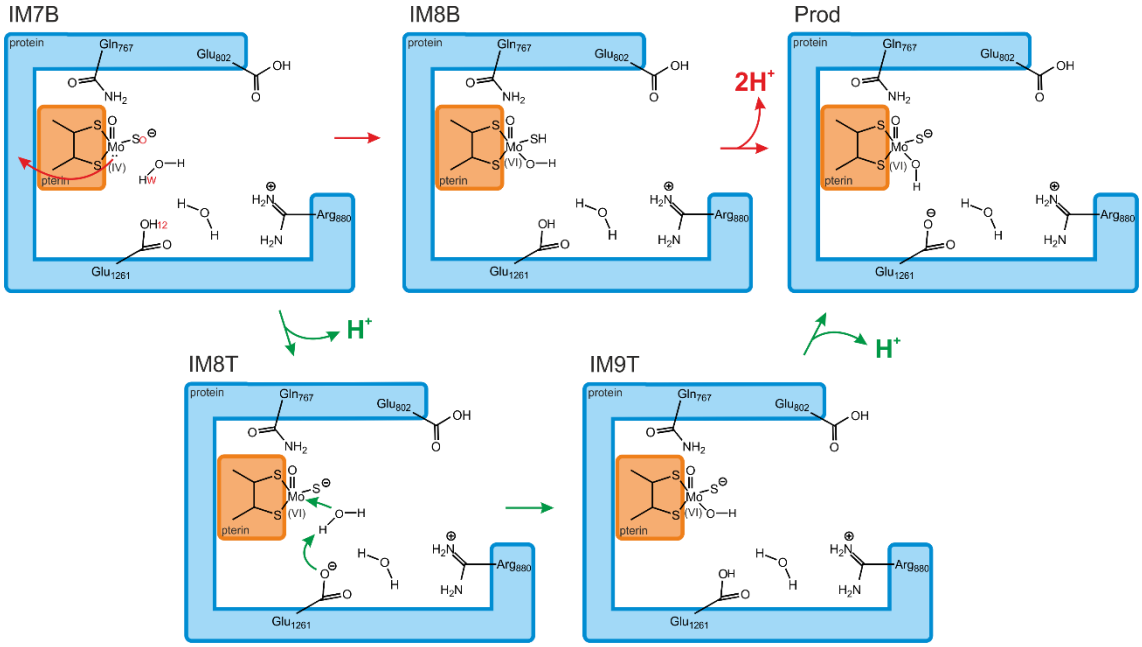

Figure 44 – Comparison of pathway B (red arrows) and the alternative mechanism (green arrows)

D. Pathway A vs pathway B

The previous mechanism also gave some insight about the pathway A. If a proton trade occurs from Glu1261 to Arg880, through the conserved water molecule, or if since we will have several water molecules in the active site they could deprotonate the Glu1261 and protonate the Arg880, it would fall in the same structure as IM5B. This would permit pathway A, that is more exothermic, become possible until the water molecules enter the active site.

Also, as said in the initial part of the discussion, there is a water tunnel at the bottom of the active site nearby Glu1261 and Arg880. So, when the URC is still leaving, the water molecules cannot enter through the active site tunnel, but the ones from the water tunnel can follow through. But, looking for the IM4A and IM4B structures (Figure 45) it can be noticed that the Glu1261 and Arg880 function like a gate. If both of them

are charged (Pathway B) the water molecule is stuck between them due to high electrostatic environment that is created and therefore closes the gate. When these two residues are in a neutral state, (Pathway A) the water molecules can easily flow through to the active site and then as referred if the water molecules deprotonate Glu1261 and protonate Arg880, they will close the gate and the turnover with the water molecule can occur.

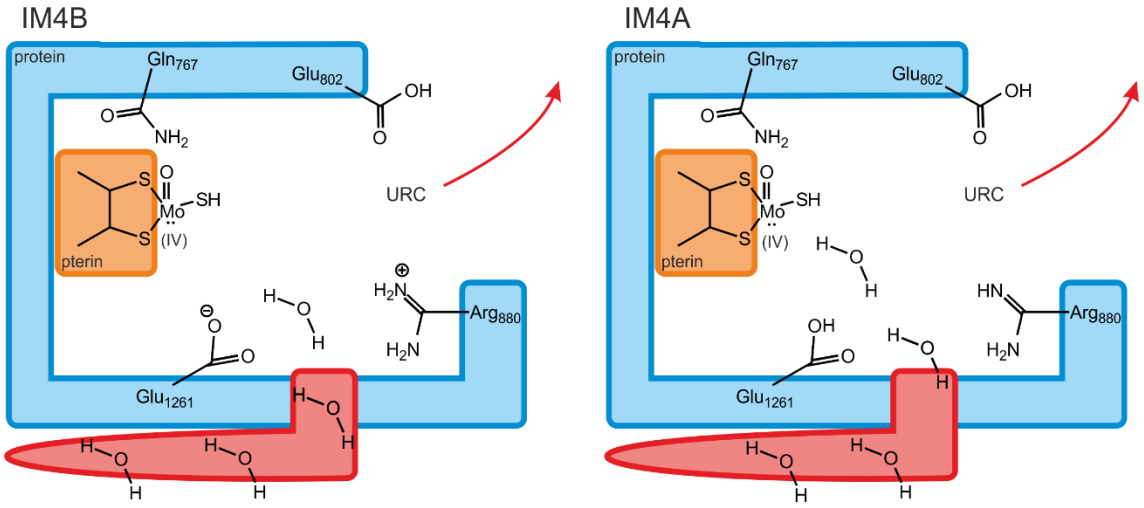

Figure 45 - Representation of the water tunnel gate working with Glu1261 and Arg880

5.2.3.3 Discussion

The enzymatic turnover only occurs with Mo (VI) and, for the coordination of the water to bond the Mo ion, the Glu1261 must be deprotonated.

Since the electron transfer and proton losses are kinetically fast reaction, they are not near close to the limiting step and will not be accounted for.

So, after adding the energies from the Part III to our previous energy profile (Figure 46) it is possible to see that the pathway A is more favorable than the pathway B, having a reaction energy of -11.7 kcal mol^{-1} versus 9.6 kcal mol^{-1}, respectively. Also, the pathway A is supported by the implication that Arg880 is very important for the reaction and that the enzymatic turnover may be faster due to the entrance of water through the water tunnel.

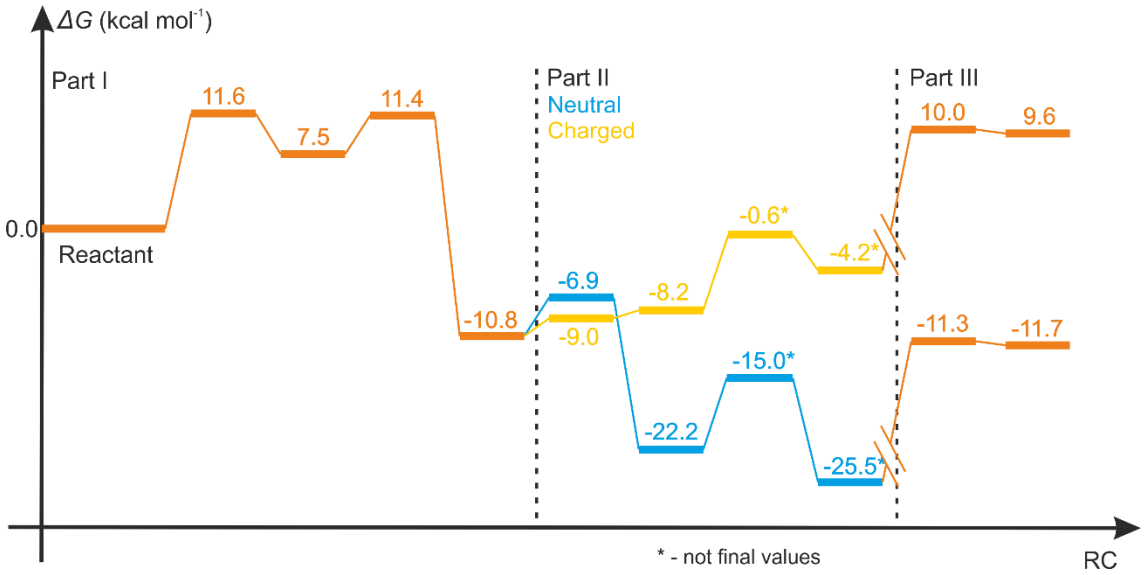

Figure 46 - Energetic profile with enzymatic turnover for all possible pathways

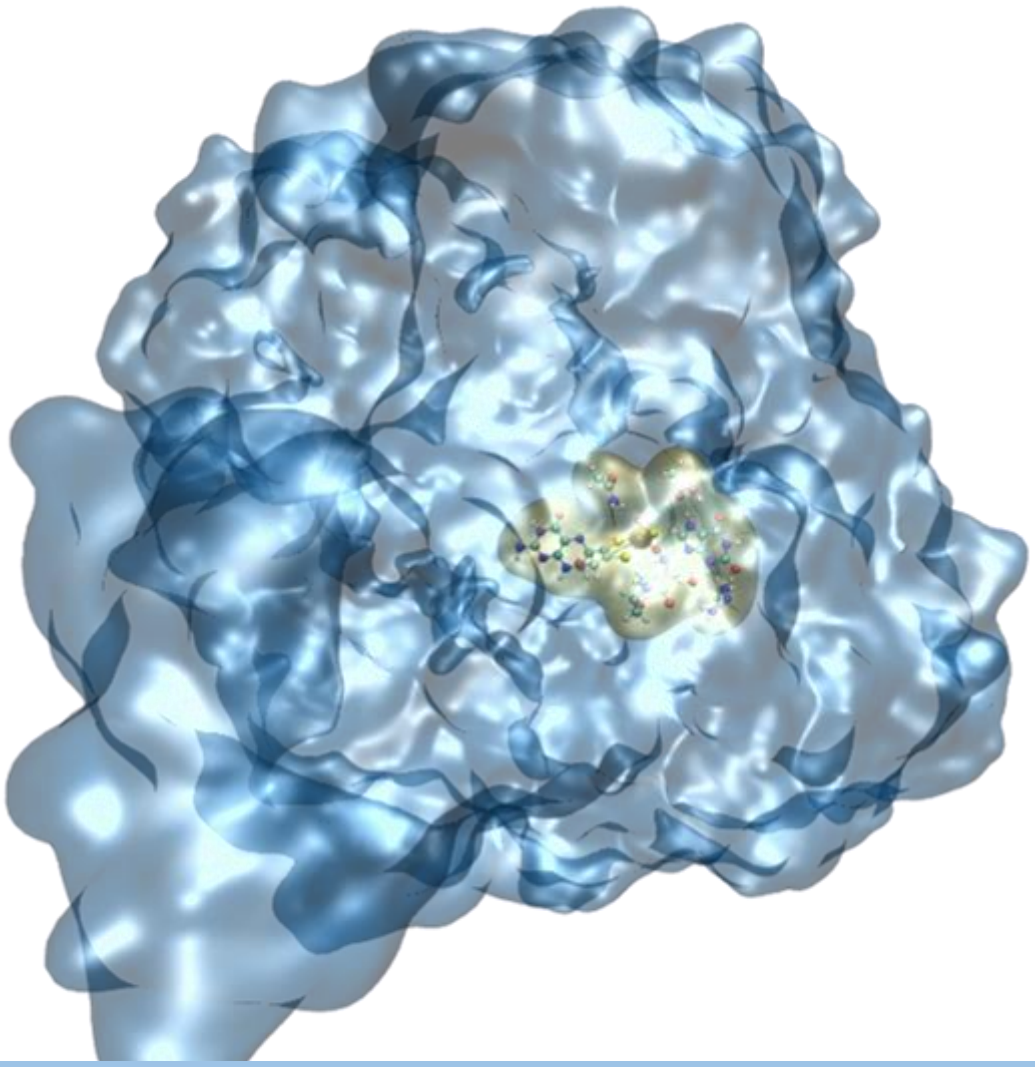

IV. Conclusions and Future Perspectives

This page was intentionally left blank

1 New proposal for the catalytic mechanism of XO

The theoretical and computational calculation developed in this work allowed to gather a new proposal about the catalytic mechanism of XO that is in agreement with several experimental data.

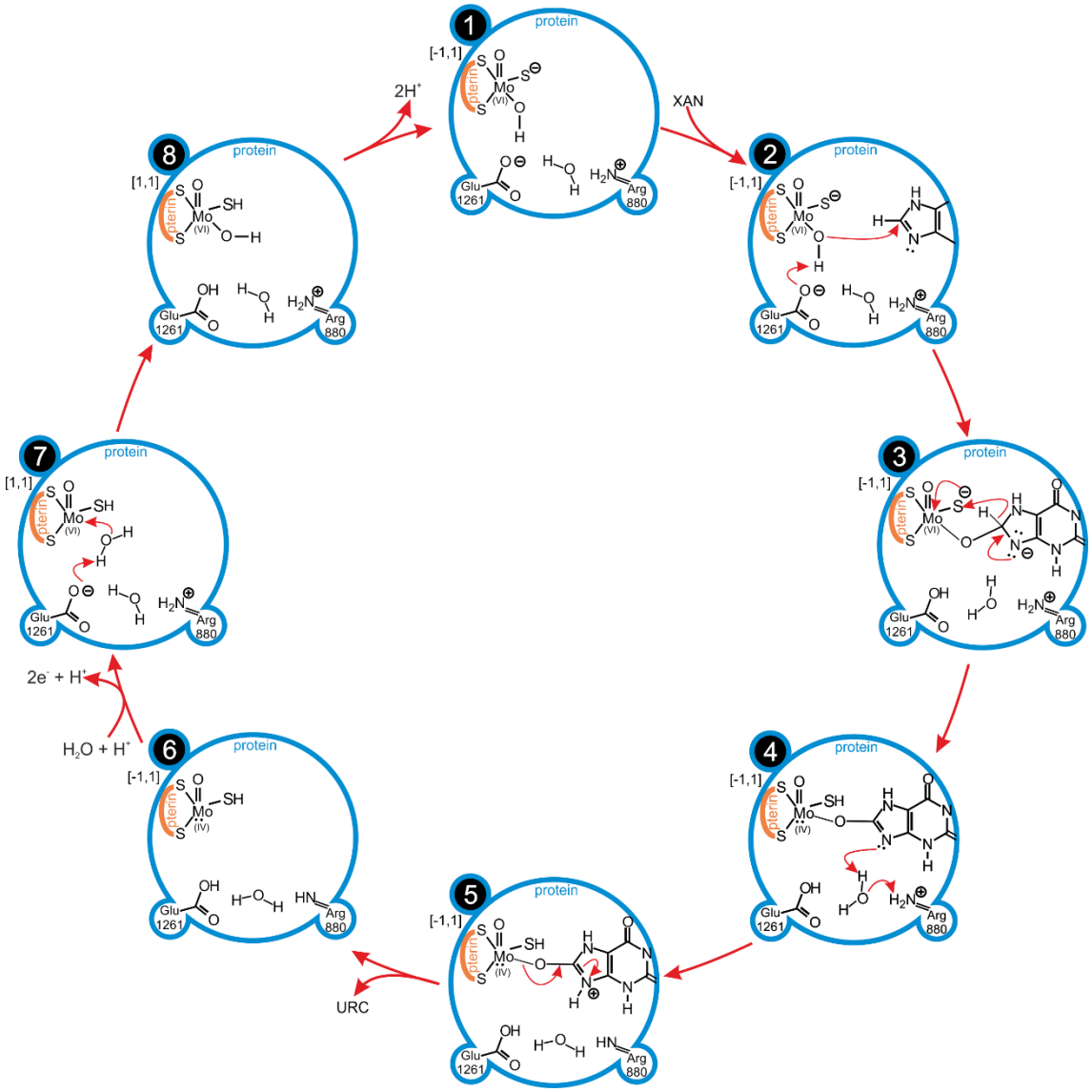

Figure 47 - Proposed mechanism full cycle. Each structure is an intermediate of the reaction, with representation of the Mo ion oxidation state and the charge and spin of each intermediate.

In the new proposal the mechanism starts with the entrance of the substrate in the active site (Figure 47 – 1 to 2) that is populated with a molybdenum cofactor. The

first step starts with the coordination of the substrate to the Mo(VI) ion (2 to 3 – Mo(VI)) which is then followed by a hydrogen transfer (3 to 4 – Mo(IV)). After the protonation of the reaction intermediate take place (4 to 5 – Mo(IV)), uric acid is formed and released (5 to 6 – (MoIV)). At this point the active site is not yet regenerated. But, before the enzymatic turnover can take place, two electrons leave the Moco to FeS and FAD and the deprotonation of Glu1261 occurs (6 to 7). The Mo ion then reacts with a water molecule and the enzymatic is obtained (7 to 8 – Mo(VI)) after the active site loses two protons (8 to 1).

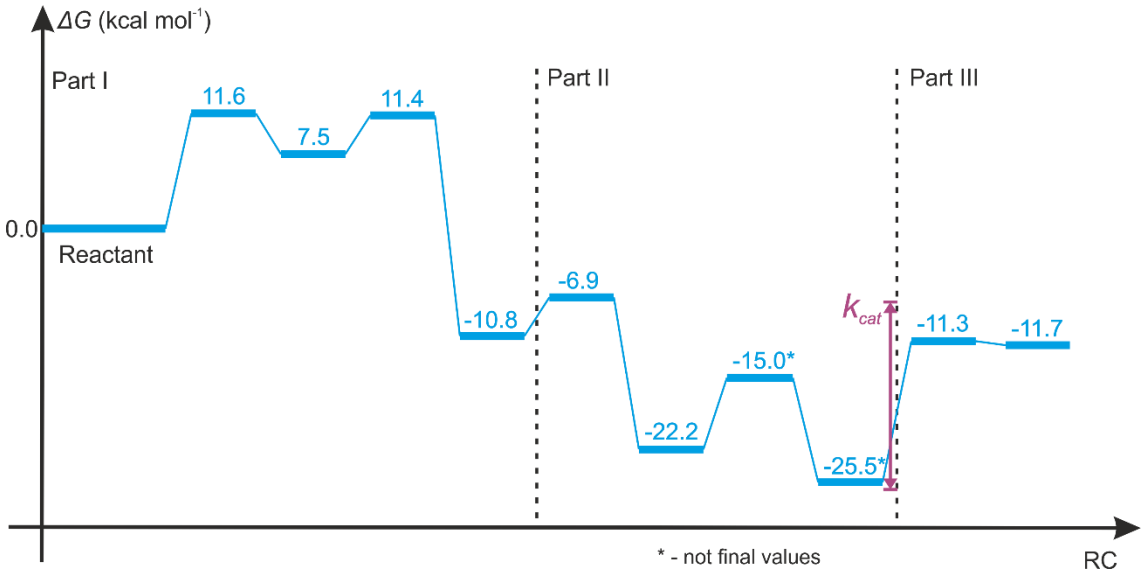

Figure 48 - Final energy chart for the whole reaction, with k_{cat} associted with the limiting step

The energetic profile of this new proposal is displayed in Figure 48.The coordination of XAN to Moco (Figure 48 – Part I and II) is an endoenergonic step. (Figure 47 – 2 to 3). From there every single step is exoenergonic till the release of URC, having a total energy of conversion of -25.5 kcal mol^{-1}. On part III, the enzymatic turnover again a endoenergonic step. It has an activation barrier of 14.2 kcal mol^{-1} and it is the rate-limiting step of the full mechanism.

1.1 Experimental data as support information

1.1.1 Experimental k_{cat} and irreversibility of the reaction

As said above, our limiting step is the enzymatic turnover is the reaction of the oxidized Moco with the water molecule, which is close to the experimental energy barrier of 15.72 kcal mol^{-1}.

Although k_{cat} from the XAN to URC is very different to the HPA to XAN (18.3 s^{-1} versus 30 s^{-1}, respectively), the limiting step has similar energies values (15.72 kcal mol^{-1} versus 15.43 kcal mol^{-1}, at 25°C), with only a difference of 0.3 kcal mol^{-1}. So, this may be supporting our limiting step, the enzymatic turnover, which is a step common to both mechanisms. However, more computational studies need to be done to the mechanism of conversion of HPA to XAN to confirm this assumption.

The computational have also shown that the coordination of XAN to Moco is an irreversible step. This also goes in line with the available experimental data since the enzyme cannot catalyse the conversion of uric acid in xanthine.

1.1.2 Mutations and the importance of residues

Our mechanism proposal supports several mutagenic experiments that were conducted in the last decade by several researchers. Glu1261 was found to have an important role in holding and releasing protons (Figure 47 – 2 to 3 and 7 to 8), that may stabilize the reaction making hydrogen bonds with the oxygen from Moco that when it is converted into XAN.

Glu802 also plays an important role during the reaction. First, it orients the substrate to the Moco, and stabilizes the position of XAN in the active site. In addition, it stabilizes the negative charge that is generated during the catalytic mechanism. These results shown for the first time the key role played by this residue on the mechanism. These evidences are in agreement with the mutagenic experiments, that have shown

that when Glu802 is mutated by a valine the enzyme becomes less efficient (k_{cat} of 18.3 s^{-1} WT versus 1.4 s^{-1} mutated).

Finally, it is also supported by the data from the previous authors, who say that Arg880 is crucial for the reaction (k_{cat} of 18.3 s^{-1} WT versus not occurring when mutated). Our mechanism proposal shows that this residue has an active role in the proton transfer that is required to form URC (Figure 47 – 4 to 5). This means therefore that if this residue is not available, the mechanism would stop in this step and no uric acid should be detected experimentally.

Glu1261 and Arg880 may also, function as a gate for the water tunnel in order to get the enzymatic turnover faster, while the URC is still being released.

1.1.3 X-ray structure

The x-ray structure (pdb: 3AMZ) that was optimized with the carbon involved in sp^3, after the nucleophilic attack, which validated our model in the end of step one. But since this step is reversible, it would be hard to crystalize. But upon a close look to the x-ray data it is possible to see that the carbon is in sp^2 configuration, that is after the irreversible step, being more possible to crystalize. Although, we can't say for sure if the structure is our IM2 or IM3A due to the proton positions.

1.1.4 Charge distribution

The charge distribution, as said above, in the first step is stored in XAN. Only afterwards the negative charge is transferred to the Moco from which the reduction of the Mo ion (Mo(VI) to Mo(IV)) takes place. In this process the pterins play an important role in asylum the excess of negative charge around the Mo ion.

This ability of the pterin to hold the excess of negative charge can be seen on Figure 49.

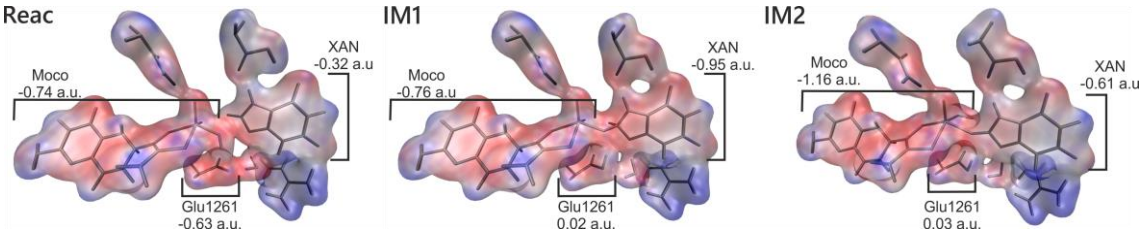

Figure 49 - Electrostatic potential, for step 1 and 2, of the reactant and product of each reaction using the high-layer of the QM/MM model. The isosurfaces were calculated using gaussian09. Blue regions represent the positive charged atoms and in red the regions where the negative charges atoms are located at.

1.2 Comparison with previous QM/MM studies

Although the work from Metz and Thiel gave great insight about the reactant position relativity to the Moco, they didn't complete the mechanism, missing the product release and enzymatic turnover.

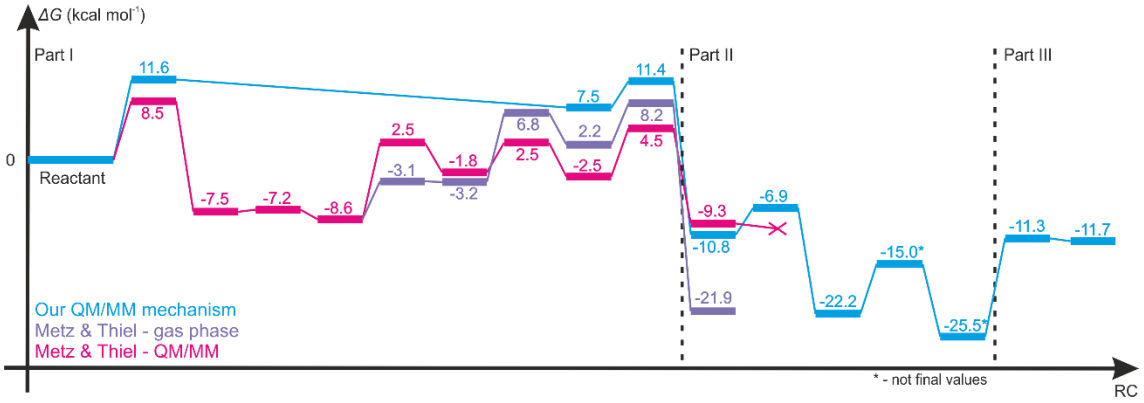

Figure 50 - Our proposed mechanism's energy values in comparison with the one carried by Metz and Thiel in 2009

The mechanism proposed in this work for the catalytic mechanism of XO is very different from the previous computational studies that were made in this area. While the one that was proposed by Metz and Thiel involves an activation of the substrate, that involves two proton transfers and only afterwards the coordination to the Mo ion and the proton/hydride transfer occurs, in the new proposal this activation mechanism

is not necessary. We with less steps, we were able to arrive to an equivalent minimum that was obtained by the same authors, with a lower energy (-10.8 kcal mol^{-1} versus -9.3 kcal mol^{-1} obtained by Metz and Thiel), as seen in Figure 50.

In the mechanism proposed by Metz and Thiel they were not able to release uric acid from the Moco. In the new proposal, this step is possible. A possible reason for this fact is the absence of the initial activation of the substrate that in the new proposal only occurs afterwards. This effect increases the charge around the Moco and enhances the dissociation of uric acid. Also, the biggest energetic difference in their work is 13.1 kcal mol^{-1}, corresponding from the proton transfer that is required to activate the enzyme. In the new proposal the rate limiting step involves the reaction of the water molecule with the Moco and requires 14.2 kcal mol^{-1}. This value is now much closer to the experimental k_{cat} than the energies proposed by Mets and Thiel.

2 Future perspectives

This mechanism gave us great insight about the mechanism from which XO catalysis the conversion of xanthine to uric acid. This new proposal is in agreement with several experimental observations which the previous proposals were insufficient to justify them. These results can now be used to study the conversion of HPA to XAN or study the recent reports about the nitrate reductase activity, or even to study the inhibitory mechanism of several drugs, such as Allopurinol. This information can then be used to develop new inhibitors targeting XO.

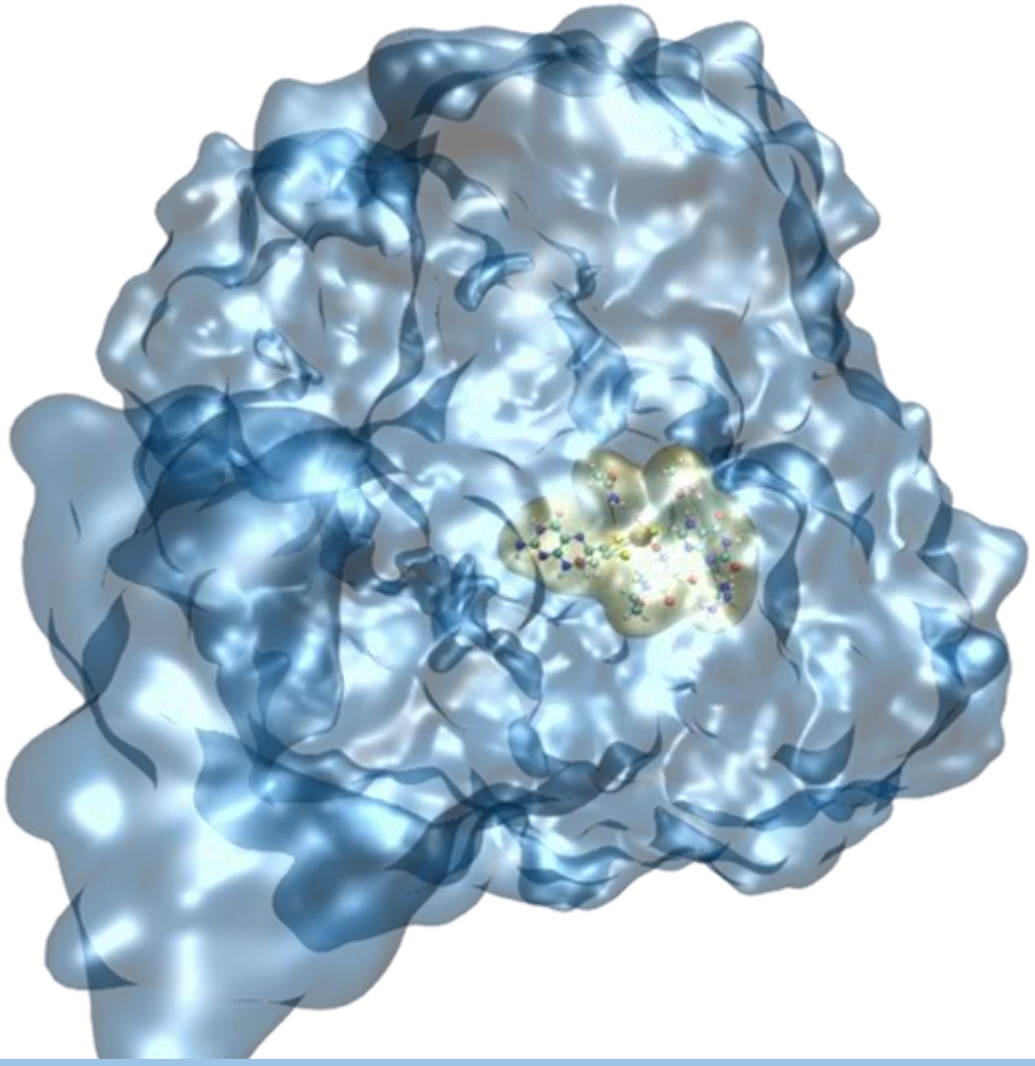

V. Bibliography

This page was intentionally left blank

[1] B. A. Moffatt and H. Ashihara, "Purine and Pyrimidine Nucleotide Synthesis and Metabolism," *Arab. B.*, vol. 1, p. e0018, 2002.

[2] I. A. Bobulescu and O. W. Moe, "Renal Transport of Uric Acid: Evolving Concepts and Uncertainties," *Advances in Chronic Kidney Disease*, vol. 19, no. 6. pp. 358–371, 2012.

[3] Y. Yamaguchi, T. Matsumura, K. Ichida, K. Okamoto, and T. Nishino, "Human xanthine oxidase changes its substrate specificity to aldehyde oxidase type upon mutation of amino acid residues in the active site: Roles of active site residues in binding and activation of purine substrate," *J. Biochem.*, vol. 141, no. 4, pp. 513–524, 2007.

[4] M. Saksela and K. O. Raivio, "Cloning and expression in vitro of human xanthine dehydrogenase/oxidase," *Biochem. J.*, vol. 315, no. 1, pp. 235–239, 1996.

[5] C. A. Pritsos, "Cellular distribution, metabolism and regulation of the xanthine oxidoreductase enzyme system," *Chem. Biol. Interact.*, vol. 129, no. 1–2, pp. 195–208, 2000.

[6] J. P. Zikakis, M. A. Dressel, and M. R. Silver, "Bovine, caprine, and human milk xanthine oxidases: isolation, purification, and characterization," *Instrumental analysis of foods / edited by George Charalambous, George Inglett*. New York : Academic Press, 1983., 1983.

[7] S. Kalra, M. K. Paul, H. Balaram, and A. K. Mukhopadhyay, "Application of HPLC to study the kinetics of a branched bi-enzyme system consisting of hypoxanthine-guanine phosphoribosyltransferase and xanthine oxidase-an important biochemical system to evaluate the efficiency of the anticancer drug 6-mercaptopurine i," *J. Chromatogr. B Anal. Technol. Biomed. Life Sci.*, vol. 850, no. 1–2, pp. 7–14, 2007.

[8] N. M. F. S. A. Cerqueira *et al.*, "The effect of the sixth sulfur ligand in the catalytic mechanism of periplasmic nitrate reductase," *J. Comput. Chem.*, vol. 30, no. 15, pp. 2466–2484, Nov. 2009.

[9] L. B. Maia, V. Pereira, L. Mira, and J. J. G. Moura, "Nitrite Reductase Activity of Rat and Human Xanthine Oxidase, Xanthine Dehydrogenase, and Aldehyde Oxidase: Evaluation of Their Contribution to NO Formation *in Vivo*," *Biochemistry*, vol. 54, no. 3, pp. 685–710, Jan. 2015.

[10] L. B. Maia and J. J. G. Moura, "Nitrite reduction by molybdoenzymes: a new class of nitric oxide-forming nitrite reductases," *JBIC J. Biol. Inorg. Chem.*, vol. 20, no. 2, pp. 403–433,

Mar. 2015.

[11] Z. Zhang, D. Naughton, P. G. Winyard, N. Benjamin, D. R. Blake, and M. C. Symons, "Generation of nitric oxide by a nitrite reductase activity of xanthine oxidase: a potential pathway for nitric oxide formation in the absence of nitric oxide synthase activity.," *Biochem. Biophys. Res. Commun.*, vol. 249, no. 3, pp. 767–772, Aug. 1998.

[12] H. Li, A. Samouilov, X. Liu, and J. L. Zweier, "Characterization of the magnitude and kinetics of xanthine oxidase-catalyzed nitrite reduction. Evaluation of its role in nitric oxide generation in anoxic tissues.," *J. Biol. Chem.*, vol. 276, no. 27, pp. 24482–24489, Jul. 2001.

[13] Y. Hellsten-Westing, B. Norman, P. D. Balsom, and B. Sjödin, "Decreased resting levels of adenine nucleotides in human skeletal muscle after high-intensity training.," *J. Appl. Physiol.*, vol. 74, no. 5, pp. 2523–8, 1993.

[14] D. J. Palmer, V. C. Kelly, A. M. Smit, S. Kuy, C. G. Knight, and G. J. Cooper, "Human colostrum: Identification of minor proteins in the aqueous phase by proteomics," *Proteomics*, vol. 6, no. 7, pp. 2208–2216, 2006.

[15] R. Hille, "The Mononuclear Molybdenum Enzymes†," 1996.

[16] D. Collison, C. D. Garner, and J. A. Joule, "The structure and mode of action of the cofactor of the oxomolybdoenzymes," *Chem. Soc. Rev.*, vol. 25, no. 1, p. 25, 1996.

[17] W. H. Campbell, "Nitrate Reductase Biochemistry Comes of Age.," *Plant Physiol.*, vol. 111, no. 2, pp. 355–361, 1996.

[18] X. J. Wang *et al.*, "[Molecular docking analysis of xanthine oxidase inhibition by constituents of cichory]," *Zhongguo Zhong Yao Za Zhi*, vol. 40, no. 19, pp. 3818–3825, 2015.

[19] M. Umamaheswari, A. Madeswaran, and K. Asokkumar, "Virtual Screening Analysis and In-vitro Xanthine Oxidase Inhibitory Activity of Some Commercially Available Flavonoids.," *Iran. J. Pharm. Res. IJPR*, vol. 12, no. 3, pp. 317–23, 2013.

[20] J. Yan, G. Zhang, Y. Hu, and Y. Ma, "Effect of luteolin on xanthine oxidase: Inhibition kinetics and interaction mechanism merging with docking simulation," *Food Chem.*, vol. 141, no. 4, pp. 2766–2773, 2013.

[21] M. G. Battelli *et al.*, "Serum xanthine oxidase in human liver disease.," *Am. J.*

Gastroenterol., vol. 96, no. 4, pp. 1194–9, 2001.

[22] P. Richette and T. Bardin, "Gout," *The Lancet*, vol. 375, no. 9711. pp. 318–328, 2010.

[23] D. Brule, G. Sarwar, and L. Savoie, "Changes in serum and urinary uric acid levels in normal human subjects fed purine-rich foods containing different amounts of adenine and hypoxanthine.," *J. Am. Coll. Nutr.*, vol. 11, no. 3, pp. 353–358, Jun. 1992.

[24] C. M. RAMSDELL and W. N. KELLEY, "The Clinical Significance of Hypouricemia," *Ann. Intern. Med.*, vol. 78, no. 2, pp. 239–242, Feb. 1973.

[25] L. X. Chen and H. R. Schumacher, "Gout: an evidence-based review.," *J. Clin. Rheumatol.*, vol. 14, no. 5 Suppl, pp. S55-62, Oct. 2008.

[26] T. Iwanaga, D. Kobayashi, M. Hirayama, T. Maeda, and I. Tamai, "Involvement of uric acid transporter in increased renal clearance of the xanthine oxidase inhibitor oxypurinol induced by a uricosuric agent, benzbromarone," *Drug Metab. Dispos.*, vol. 33, no. 12, pp. 1791–1795, 2005.

[27] M. A. Becker *et al.*, "Febuxostat, a novel nonpurine selective inhibitor of xanthine oxidase: A twenty-eight-day, multicenter, phase II, randomized, double-blind, placebo-controlled, dose-response clinical trial examining safety and efficacy in patients with gout," *Arthritis Rheum.*, vol. 52, no. 3, pp. 916–923, 2005.

[28] K. Ichida, Y. Amaya, N. Kamatani, T. Nishino, T. Hosoya, and O. Sakai, "Identification of two mutations in human xanthine dehydrogenase gene responsible for classical type I xanthinuria.," *J. Clin. Invest.*, vol. 99, no. 10, pp. 2391–7, 1997.

[29] N. Sakamoto *et al.*, "Identification of a new point mutation in the human xanthine dehydrogenase gene responsible for a case of classical type I xanthinuria," *Hum. Genet.*, vol. 108, no. 4, pp. 279–283, 2001.

[30] P. Pacher, A. Nivorozhkin, and C. Szabó, "Therapeutic effects of xanthine oxidase inhibitors: renaissance half a century after the discovery of allopurinol.," *Pharmacol. Rev.*, vol. 58, no. 1, pp. 87–114, Mar. 2006.

[31] R. V. Smalley, A. Guaspari, S. Haase-Statz, S. A. Anderson, D. Cederberg, and J. A. Hohneker, "Allopurinol: Intravenous Use for Prevention and Treatment of Hyperuricemia," *J. Clin. Oncol.*, vol. 18, no. 8, pp. 1758–1763, Apr. 2000.

[32] S. Muraoka and T. Miura, "Inhibition of xanthine oxidase by phytic acid and its

antioxidative action.," *Life Sci.*, vol. 74, no. 13, pp. 1691–700, Feb. 2004.

[33] E.-Y. Choi, A. L. Stockert, S. Leimkühler, and R. Hille, "Studies on the mechanism of action of xanthine oxidase," *J. Inorg. Biochem.*, vol. 98, no. 5, pp. 841–848, May 2004.

[34] S. Metz and W. Thiel, "QM/MM studies of xanthine oxidase: Variations of cofactor, substrate, and active-site Glu802," *J. Phys. Chem. B*, vol. 114, no. 3, pp. 1506–1517, 2010.

[35] S. Metz and W. Thiel, "A Combined QM/MM Study on the Reductive Half-Reaction of Xanthine Oxidase: Substrate Orientation and Mechanism," *J. Am. Chem. Soc.*, vol. 131, no. 41, pp. 14885–14902, Oct. 2009.

[36] K. Vanommeslaeghe, O. Guvench, and A. D. MacKerell, "Molecular mechanics.," *Curr. Pharm. Des.*, vol. 20, no. 20, pp. 3281–92, 2014.

[37] S. A. Adcock and J. A. McCammon, "Molecular Dynamics: Survey of Methods for Simulating the Activity of Proteins," *Chem. Rev.*, vol. 106, no. 5, pp. 1589–1615, May 2006.

[38] V. Hornak, R. Abel, A. Okur, B. Strockbine, A. Roitberg, and C. Simmerling, "Comparison of multiple Amber force fields and development of improved protein backbone parameters," *Proteins Struct. Funct. Bioinforma.*, vol. 65, no. 3, pp. 712–725, Nov. 2006.

[39] D. A. Case *et al.*, "The Amber biomolecular simulation programs.," *J. Comput. Chem.*, vol. 26, no. 16, pp. 1668–88, Dec. 2005.

[40] P. E. M. Lopes, O. Guvench, A. D. MacKerell, and Jr., "Current status of protein force fields for molecular dynamics simulations.," *Methods Mol. Biol.*, vol. 1215, pp. 47–71, 2015.

[41] T. van Mourik, M. Bühl, and M.-P. Gaigeot, "Density functional theory across chemistry, physics and biology.," *Philos. Trans. A. Math. Phys. Eng. Sci.*, vol. 372, no. 2011, p. 20120488, Mar. 2014.

[42] M. Herrera, R. M. Serra, and I. D'Amico, "DFT-inspired methods for quantum thermodynamics," *Sci. Rep.*, vol. 7, no. 1, p. 4655, Dec. 2017.

[43] C. Lee, W. Yang, and R. G. Parr, "Development of the Colle-Salvetti correlation-energy formula into a functional of the electron density," *Phys. Rev. B*, vol. 37, no. 2, pp. 785–789, Jan. 1988.

[44] A. D. Becke, “Density-functional thermochemistry. III. The role of exact exchange,” *J. Chem. Phys.*, vol. 98, no. 7, p. 5648, 1993.

[45] Y. Yang, M. N. Weaver, K. M. Merz, and Jr, “Assessment of the "6-31+G** + LANL2DZ" mixed basis set coupled with density functional theory methods and the effective core potential: prediction of heats of formation and ionization potentials for first-row-transition-metal complexes.,” *J. Phys. Chem. A*, vol. 113, no. 36, pp. 9843–51, Sep. 2009.

[46] C. J. Cramer, *Essentials of computational chemistry : theories and models*. Wiley, 2013.

[47] F. Jensen, *Introduction to computational chemistry*. .

[48] D. C. Young, *Computational chemistry : a practical guide for applying techniques to real world problems*. Wiley, 2001.

[49] S. Dapprich, I. Komáromi, K. S. Byun, K. Morokuma, and M. J. Frisch, “A new ONIOM implementation in Gaussian98. Part I. The calculation of energies, gradients, vibrational frequencies and electric field derivatives,” *J. Mol. Struct. THEOCHEM*, vol. 461–462, pp. 1–21, Apr. 1999.

[50] D. J. Frisch, M. J.; Trucks, G.W.; Schlegel, H. B.; Scuseria, G. E.; Robb, M. A.; Cheeseman, J. R.; Scalmani, G.; Barone, V.;Mennucci, B.; Petersson, G. A.; Nakatsuji, H.; Caricato, M.; Li, X.; Hratchian, H. P.; Izmaylov, A. F.; Bloino, J.; Zheng, G.; Sonnenber, “Gaussian 09,” *Gaussian, Inc. Wallingford CT*, pp. 2–3, 2009.

[51] W. Humphrey, A. Dalke, and K. Schulten, “VMD: Visual molecular dynamics,” *J. Mol. Graph.*, vol. 14, no. 1, pp. 33–38, 1996.

[52] R. Dennington, T. Keith, and J. Millam, “GaussView, Version 5.,” *Semichem Inc. , Shawnee Mission, KS*. p. Semichem Inc, 2009.

[53] J. M. Perez-Canadillas, “Grabbing the message: structural basis of mRNA 3’UTR recognition by Hrp1.,” *EMBO J.*, vol. 25, no. 13, pp. 3167–3178, Jul. 2006.

[54] H. Ishikita, B. T. Eger, K. Okamoto, T. Nishino, and E. F. Pai, “Protein conformational gating of enzymatic activity in xanthine oxidoreductase.,” *J. Am. Chem. Soc.*, vol. 134, no. 2, pp. 999–1009, Jan. 2012.

[55] H. Cao, J. Hall, and R. Hille, “Substrate orientation and specificity in xanthine oxidase: crystal structures of the enzyme in complex with indole-3-acetaldehyde and guanine.,”

Biochemistry, vol. 53, no. 3, pp. 533–541, Jan. 2014.

[56] H. Cao, J. Hall, and R. Hille, "X-ray crystal structure of arsenite-inhibited xanthine oxidase: mu-sulfido,mu-oxo double bridge between molybdenum and arsenic in the active site.," *J. Am. Chem. Soc.*, vol. 133, no. 32, pp. 12414–12417, Aug. 2011.

[57] K. Okamoto, Y. Kawaguchi, B. T. Eger, E. F. Pai, and T. Nishino, "Crystal structures of urate bound form of xanthine oxidoreductase: substrate orientation and structure of the key reaction intermediate.," *J. Am. Chem. Soc.*, vol. 132, no. 48, pp. 17080–17083, Dec. 2010.

[58] H. Cao, J. M. Pauff, and R. Hille, "Substrate orientation and catalytic specificity in the action of xanthine oxidase: the sequential hydroxylation of hypoxanthine to uric acid.," *J. Biol. Chem.*, vol. 285, no. 36, pp. 28044–28053, Sep. 2010.

[59] K. Okamoto, B. T. Eger, T. Nishino, E. F. Pai, and T. Nishino, "Mechanism of inhibition of xanthine oxidoreductase by allopurinol: crystal structure of reduced bovine milk xanthine oxidoreductase bound with oxipurinol.," *Nucleosides. Nucleotides Nucleic Acids*, vol. 27, no. 6, pp. 888–893, Jun. 2008.

[60] R. Asai *et al.*, "Two mutations convert mammalian xanthine oxidoreductase to highly superoxide-productive xanthine oxidase.," *J. Biochem.*, vol. 141, no. 4, pp. 525–534, Apr. 2007.

[61] T. Nishino *et al.*, "Mechanism of the conversion of xanthine dehydrogenase to xanthine oxidase: identification of the two cysteine disulfide bonds and crystal structure of a non-convertible rat liver xanthine dehydrogenase mutant.," *J. Biol. Chem.*, vol. 280, no. 26, pp. 24888–24894, Jul. 2005.

[62] L. Bordoli, F. Kiefer, K. Arnold, P. Benkert, J. Battey, and T. Schwede, "Protein structure homology modeling using SWISS-MODEL workspace," *Nat. Protoc.*, vol. 4, no. 1, pp. 1–13, Dec. 2008.

[63] K. Arnold, L. Bordoli, J. Kopp, and T. Schwede, "The SWISS-MODEL workspace: a web-based environment for protein structure homology modelling," *Bioinformatics*, vol. 22, no. 2, pp. 195–201, Jan. 2006.

[64] T. J. Dolinsky, J. E. Nielsen, J. A. McCammon, and N. A. Baker, "PDB2PQR: an automated pipeline for the setup of Poisson-Boltzmann electrostatics calculations," *Nucleic Acids Res.*, vol. 32, no. Web Server, pp. W665–W667, Jul. 2004.

[65] M. W. Mahoney and W. L. Jorgensen, “A five-site model for liquid water and the reproduction of the density anomaly by rigid, nonpolarizable potential functions,” *http://scitationinfo.org/p/1XPS-389/jcpspotlight*, May 2000.

[66] J. Li and U. Ryde, “Comparison of the Active-Site Design of Molybdenum Oxo-Transfer Enzymes by Quantum Mechanical Calculations,” *Inorg. Chem.*, vol. 53, no. 22, pp. 11913–11924, Nov. 2014.

[67] N. M. F. S. A. Cerqueira, P. A. Fernandes, P. J. Gonzalez, J. J. G. Moura, and M. J. Ramos, “The Sulfur Shift: An Activation Mechanism for Periplasmic Nitrate Reductase and Formate Dehydrogenase,” *Inorg. Chem.*, vol. 52, no. 19, pp. 10766–10772, Oct. 2013.

[68] N. M. F. S. A. Cerqueira, B. Pakhira, and S. Sarkar, “Theoretical studies on mechanisms of some Mo enzymes,” *JBIC J. Biol. Inorg. Chem.*, vol. 20, no. 2, pp. 323–335, Mar. 2015.